NONLINEAR AND FAR-FROM-EQUILIBRIUM DYNAMICS OF OPTICAL PULSES IN FIBER OSCILLATORS

A DISSERTATION SUBMITTED TO
THE GRADUATE SCHOOL OF ENGINEERING AND SCIENCE
OF BILKENT UNIVERSITY
IN PARTIAL FULFILLMENT OF THE REQUIREMENTS FOR
THE DEGREE OF
DOCTOR OF PHILOSOPHY
IN
PHYSICS

By
Tesfay Gebremedhin Teamir
August 2017

Nonlinear and far-from-equilibrium dynamics of optical pulses in fiber oscillators

By Tesfay Gebremedhin Teamir

August 2017

We certify that we have read this dissertation and that in our opinion it is fully adequate, in scope and in quality, as a dissertation for the degree of Doctor of Philosophy.

Fatih Ömer Ilday(Advisor)

Hakan Altan

Oğuz Gülseren

Mehmet Özgür Oktel

Mehmet Emre Taşgın

Approved for the Graduate School of Engineering and Science:

Ezhan Karaşan
Director of the Graduate School

ABSTRACT

NONLINEAR AND FAR-FROM-EQUILIBRIUM DYNAMICS OF OPTICAL PULSES IN FIBER OSCILLATORS

Tesfay Gebremedhin Teamir
Ph.D. in Physics
Advisor: Fatih Ömer Ilday
August 2017

Fundamentals of mode locking of lasers have been extensively studied and well established for the last three decades. However, it continues to be an intensely studied field. The continued interest is, in part, due to the scientific and technological applications enabled by the generation of ultrashort pulses of light using mode-locking. There is also a deeper reason for the interest. Despite decades of effort, there is still no encompassing theory of mode-locking that applies to the broad range of dynamics displayed by modern mode-locked lasers, in particular, fiber lasers. Mode-locking is a collective phenomenon that arises from the nonlinear interactions between thousands of optical modes supported by a laser cavity, which is typically initiated from laser noise in the cavity. In addition to many unanswered questions from a nonlinear dynamics perspective, there has been limited progress from the point of the thermodynamics, even though mode-locking corresponds to a far-from-equilibrium steady state of a laser.

The central premise of this thesis is that mode-locked lasers are invaluable as experimental platforms not only for nonlinear phenomena, but also for far-from-equilibrium dynamics of nonlinear systems, where there is a particular shortage of convenient platforms for experimentation, in addition to the practical interest in development of technically superior lasers. After introductory discussions, we report the direct generation of sub-hundred femtosecond pulses through the interaction of third order dispersion (TOD) and self-phase modulation (SPM) by using two dispersion delay lines (DDLs) inside a laser cavity. Moreover, we report dynamics that are consistent with an effective negative nonlinearity, which is explained through an interplay between self-phase modulation (SPM) and second order dispersion (GVD) for a chirped pulse.

Despite numerous studies on their nonlinear dynamics, relatively little is known about the thermodynamics and fluctuations-induced dynamics of mode-locking.

We investigate transitions from CW to single pulsing, and then to multipulsing states in the presence of nonlinearity, feedback mechanisms, laser noise (as a source of fluctuations) and the laser's response to externally injected modulations or fluctuations. Near critical points (instability attractors), dissipative soliton (DS) states are observed to interact between themselves and with their environment which is often followed by random transitions among different pulsing states. This critical behavior appears to be caused by soliton-soliton or soliton-generated dispersive wave interactions in addition to periodic breathing, due to the periodic boundary conditions of the cavity, leading to bifurcations and the onset of chaos. Irrespective of specifics parameters of states, measured noise level (*i.e.*, the strength of fluctuations) of the laser usually starts at a low value, and then slightly reduced as the DSs energy is increased. Further increases in power (nonlinearity) drive it towards a noisy critical state, where random creation or annihilation of pulses occur just before a new steady state is formed. These noise-induced transitions between steady states far from equilibrium could conceivably shed light on the thermodynamics of other far-from-equilibrium systems.

Finally, we demonstrate direct electronic control over mode-locking states using spectral amplitude and phase modulation by incorporating a spatial light modulator (SLM) at a Fourier plane inside the cavity. The modulation enables us to halt and restart mode locking, suppress instabilities, induce controlled reversible and irreversible transitions between mode-locking states, and perform advanced pulse shaping inside a cavity. We also introduce a simple method to manipulate femtosecond optical pulses by directly applying dynamic periodic phase modulation mask on the optical spectrum inside oscillator. With the application of such dynamic periodic linear spectral phase mask we can control the pulse dynamics, demonstrating the capability to tune the pulse-to-pulse separation time, pulse tweezing, blue- and red-shifting of spectral components and pulse splitting. This technique, which is introduced for the first time to our knowledge, may be used in a range of applications such as coherent quantum control, nonlinear spectroscopy, microscopy, in data storage, in the switching of optical and magnetic properties of materials, as well as studies on the fundamentals of oscillator dynamics and other self-organized phenomena in spatiotemporally extended systems.

Keywords: Mode-locking, fiber lasers, effective negative nonlinearity, soliton dynamics, non-equilibrium thermodynamics, complex systems, dissipative adaptation.

ÖZET

FIBER SALINGAÇLARDA OPTİK DARBELERİN DOĞRUSAL OLMAYAN VE DENGEDEN UZAK DİNAMİKLERİ

Tesfay Gebremedhin Teamir
Fizik, Doktora
Tez Danışmanı: Fatih Ömer İlday
Ağustos 2017

Son otuz yıldır lazerinde kip kilitlemesinin temelleri kapsamlı olarak incelenmiş ve iyi kurulmuştur. Bununla birlikte, yoğun olarak incelenen bir alan olmaya devam etmektedir. Bu devam eden ilgi, kısmen, mod kilitleme kullanarak ultra-kısa ışık atımlarının üretilmesiyle sağlanan bilimsel ve teknolojik uygulamalardan kaynaklanmaktadır. Ayrıca ilgi için daha derin bir sebep de vardır. Onlarca yıldır çaba gösterilmesine rağmen, modern mod kilitli lazerler, özellikle fiber lazerler tarafından görüntülenen zengin dinamiklerin tamamı için geçerli olan bir mod kilitleme teorisi hala ortaya konulmamıştır. Mod kilitleme, genellikle lazer kovuğu içinde mevcut gürültüden (salınımlardan) kendiliğinden başlayan, binlerce optik mod arasında mevcut doğrusal olmayan etkileşimlerin ortaya çıkardığı ortak (kollektif) bir fenomendir. Doğrusal olmayan dinamikler perspektifinden gelen birçok cevapsız soruya ek olarak, mod kilitlemenin lazerin termodinamik dengeden uzakta süregelen bir kararlı durumuna karşılık gelmesine rağmen, termodinamik perspektif açısından anlaşılması yönünde çok sınırlı ilerlemeler olmuştur.

Bu tezin temel iddiası, mod kilitleme fenomeni ve mod kilitli lazerlerin, sadece doğrusal olmayan fenomenlerin daha iyi anlaşılması için değil, aynı zamanda doğrusal olmayan sistemlerin dengeden uzaktan dinamiklerinin daha iyi anlaşılması için deney platformları olarak paha biçilmez olduğunu ortaya koymaktadır. Teknik açıdan üstün mod kilitli lazerlerin geliştirilmesine pratik yeni yöntemler önerilmesi ise ikinci bir amaçtır. Temel lazer ve mod kilitleme fiziğini tanıtıcı bir girişten sonra, bu tezin ilk orijinal kısmı, iki kırınım-ağı tabanlı gecikme hattı (dispersive delay line, DDL) kullanarak üçüncü derece dağılımın (third-order dispersion, TOD) ve kendi kendini faz modülasyonunun (self-phase modulation, SPM) etkileşimi yoluyla orta düzeyde enerjiyle doğrudan yüz altmış femtosaniye darbe üretimini bildirir. Bu sonuçlar etkin olarak negatif (kendinden dağıtıcı, self-defocusing) doğrusal olmayan etkinin üretilmesine denk gelmesidir.

Doğrusal olmayan dinamikleri üzerine çok sayıda çalışmaya rağmen, osilatörler içerisinde optik darbelerin termodinamiği hakkında nispeten az ilerleme vardır. Doğrusal olmayan etkiler, geridöngü (feedback) mekanizmaları, lazer gürültüsü (salınımların kaynağı olarak) ve harici olarak enjekte edilen modülasyonlara veya salınımlara lazerin verdiği tepki konusunda, CW'den tekli darbeli ve daha sonra çoklu darbeli duruma geçiş durumlarını araştırıyoruz. Kritik noktaların (istikrarsız çekicilerin) yakınında, sönümlü solitonların (dissipative soliton, DS) kendi aralarında ve çevreleriyle etkileşimde bulunduğu gözlemlenir ve genellikle farklı atım halleri arasında rasgele geçişler izlenir. Bu kritik davranış, lazer kovuğunun periyodik sınır koşullarından dolayı, bifurkasyonlara ve kaosun başlamasına neden olan, periyodik solunumun yanı sıra soliton-soliton veya solitonun ürettiği dağınık dalga etkileşimlerinin neden olduğu görülebilir. Durumların özellik parametrelerinden bağımsız olarak, lazerin ölçülen gürültü seviyesi (örneğin, salınınların gücü) düşük bir değerde başlar ve daha sonra DS'nin enerjisi arttıkça hafifçe azalır. Daha fazla güç artışı (doğrusal olmayanlık), onu yeni bir kararlı durum oluşmadan hemen önce ortaya çıkan gürültülü kritik bir duruma iter. Denge dışındaki kararlı durumlar arasındaki bu gürültüye bağlı geçişler, diğer termal dengeden uzak sistemlerinin termodinamiğine ışık tutabilir.

Son olarak, bir Yb katkılı fiber lazerin kovuğunun içinde bir Fourier düzlemine uzaysal ışık modülatörü (spatial light modulator, SLM) dahil ederek atım şekillendirmesi için spektral genlik ve faz modülasyonu kullanan mod kilitleme durumları üzerinden doğrudan elektronik kontrolünü gösteriyoruz. Modülasyon, mod kilidini durdurup yeniden başlatmamızı, istikrarsızlıkları bastırmanızı, mod kilitleme durumları arasında kontrollü geri döndürülebilir ve geri döndürülemez geçişler başlatmamızı ve bir boşluk içinde gelişmiş darbe şekillendirme yapmamızı sağlıyor. Aynı şekilde, osilatörün içindeki optik spektrumda doğrudan dinamik periyodik faz modülasyonu maskesi uygulayarak femtosaniyelik optik darbelerin manipüle edilmesini sağlayan daha basit bir yöntem sunuyoruz. Doğrusal ve sinüzoidal spektral maskenin sırasıyla boşluğun gecikmesi ve atım bölünmesi için kullanıldığı etkileri periyodik doğrusal veya testere dişi benzeri faz ile birleştirilebilir. Bu gibi dinamik periyodik doğrusal spektral faz maskesinin uygulanmasıyla, atım dinamiklerini kontrol edebilir, atım-atım ayırma zamanını ayarlama yeteneği, atım cımbızması, spektral bileşenlerin maviye- ve kırmızıkaydırma, atım bölme ve üretimi yeteneğini gösterebildik. Bildiğimiz kadarıyla ilk kez tanıtılan bu teknik, evreuyumlu kuantum kontrolü, doğrusal olmayan spektroskopi, mikroskopi, veri saklama, malzemelerin optik ve manyetik özelliklerinin

değiştirilmesi gibi bir dizi uygulamada kullanılabilir. Ayrıca, osilatör dinamiğinin temelleri ve zaman uzayda genişletilmiş sistemlerde diğer kendi kendini organize edilen fenomenler üzerinde yapılan çalışmalarda yararlı olabilir.

Anahtar sözcükler: Kip kilitleme, fiber lazer, etkin olarak negatif dogrusal-olmayan etki, soliton dinamikleri, dengede olmayan termodinamik, karmaşİk sistemler, sönümlemeli adaptasyon.

Acknowledgement

I have no words that would be sufficient to thank my advisor for giving me enormous freedom and opportunity to find my way in personal and professional development. It includes provision of research topics with quality laboratory environment, opportunities to participate in precious seminars, conferences, and collaborations as well. I have received continuous support and encouragement to push my personal limits in a way that no more can be expected from a human. I am grateful for the way he has been a boss, an advisor, and a friend.

I have got a valuable support from Dr. Ghaith Makey especially on adaptive algorithm and on interfacing SLM. I have had the opportunity to work with and had valuable discussions with Dr. Ghaith Makey, Dr. Parviz Elahi, Dr. Hamit Kalaycıoğlu, Dr. Onur Tokel, Dr. Sarem Ilday, Dr. Ihor Pavlov throughout my stay. I also want to thank former and current members as well as Gizem Gençoglu, who manages and takes care of all administrative issues, thus creating an extremely efficient research environment.

I would like to extend my gratitude to my family for everything they have done for me on my way up to this point. I would like to thank my fiancée Fevu for her valuable patience and support too.

Finally, I want to thank Department of Physics of Bilkent University for providing me a scholarship to pursue my PhD in a such elegant environment which is full of very nice people from accomplished professors to the kind and caring janitors and house staff in the dormitory. I want to also acknowledge financial support from Türkiye Bilimsel ve Teknolojik Arastirma Kurumu (TÜBITAK 113F319) and European Research Council Consolidator Grant (ERC 617521).

Dedicated to my family

Contents

List of Figures

List of Tables

Chapter 1

Introduction

Ultrafast lasers are passively mode-locked lasers that can generate so-called ultrafast or ultrashort optical pulses. Here, the terms ultrafast and ultrashort refer to a few picoseconds and shorter regarding the pulse duration in the more inclusive usage of the terms and the less restrictive usage implies to a few hundred femtoseconds. Pulse durations in the sub-picosecond range can only be generated by optical means only because their rise/fall times and associated bandwidths surpass the capabilities of state of the art in electronics by a large margin. In addition to the fantastic temporal resolutions afforded by ultrashort pulses that can be used for viewing, analyzing and even manipulating various natural phenomena, such as chemical reactions, also known as femtochemistry [2], the ultra-broadband frequencies generated by ultrafast lasers have countless applications, most notably in the field of optical frequency metrology [3]. Furthermore, by localizing all the energy of an optical pulse within such a short temporal window, extremely high intensities can momentarily be achieved at the peak point of pulse, which has numerous applications, ranging from ultrafast laser-material interactions [4, 5] to extreme nonlinear optics [6], to generation of coherent extreme ultraviolet and soft x-ray radiation through a process known as high-harmonic generation [7].

Lasers have been at the heart of much major scientific progress since their

invention. Pulsed lasers were first demonstrated only six years after the first realization of a continuous-wave (CW) laser in the Hughes Research Laboratories in 1960 [8, 9]. Pulse generation is made possible by ensuring a fixed phase difference between multiple cavity modes created in a laser resonator. The number of such locked modes can easily exceed ten thousand in a modern mode-locked laser, where the term mode-locking refers to the locking of the phases of the modes. Here, we are focussed on so-called passive mode-locking, where no external electronic modulation is used and mode-locking arises solely from the dynamics of the laser. There are various methods for passive mode-locking, but this is commonly accomplished by a nonlinear amplitude modulating element, which is often called saturable absorber (SA). It can be a material that actually absorbs light, such as a semiconductor saturable absorber mirror (SESAM) [10], layers of graphene, carbon nanotubes [11], even topological insulating materials [12]. Alternatively, it can be a nonlinear optical process that alters the beam propagation or the gain experienced by the pulses in a manner that depends on the (nearly) instantaneous intensity of the beam, known as an effective saturable absorber, such as Kerr lens mode-locking [13], gain switching [14], nonlinear polarization evolution (NPE) [15], a nonlinear amplifying loop mirror [16], dissipative Faraday instability (modulation instability) [17], or pump-frequency detuning with respect to the cavity resonance in micro resonators [18].

The onset of mode-locking that leads to the formation of ultrashort pulses is typically initiated from intra-cavity noise, or fluctuations in light intensity. A range of physical processes are effective in this mechanism, such as gain and loss, spectral or gain filtering, chromatic dispersion, four wave mixing processes, including self-phase and cross-phase modulation, intra-pulse Raman scattering, self-amplitude modulation, including saturable absorption and in the case of sub-100 fs pulses, self-steepening. However, during the onset typically saturable absorption and linear gain/loss are the dominant mechanisms, creating a positive feedback through which the fluctuations in the cavity are amplified: The presence of a saturable absorber ensures that a fluctuation with higher-than-average intensity experiences reduced loss, whereas all parts of the waveform amplified equally by the gain. As this process is repeated hundreds and thousands of times within

the cavity, nearly all of the energy of the waveform becomes concentrated within one or several localized peaks, which form pulses. As the pulses grow reduce in duration and grow in intensity, other effects mentioned above, such as self-phase modulation and dispersion become stronger. In a well-design cavity, the combined dynamics of these processes support stable, nonlinear waveforms, such as solitons or similaritons. Consequently, the pulses are gradually shaped into the particular nonlinear waveform supported by the cavity, slowing the changes per each roundtrip as the pulse evolves into this shape like a negative feedback mechanism. The final state of mode-locking corresponds to a steady state, which balances exactly all the effects with each other such that at the end of one roundtrip through the laser cavity, all changes experienced by the pulse are exchanged cancelled out. This steady state can differ a lot in its characteristics according to the mode-locking type or regime. For instance, in the case of a soliton laser, the changes are almost completely balancing at each step through the cavity with only minute changes within a roundtrip, whereas a modern similariton laser can experience order-of-magnitude variations in its amplitude, spectral and temporal widths within one roundtrip. Of course, a stable steady state is not the only possible outcome, and a laser cavity can exhibit a wide range of less stable or completely unstable operations as well, including generation of multiple pulses, which may or may not be stable, operation known as period-doubling, where the pulse repeats the same shape after two or more roundtrips, as well as chaotic behavior. However, for much of the discussion in this thesis, our focus will be stably mode-locked lasers unless noted otherwise.

As a result of the rich dynamics and numerous technological applications, mode-locked fiber oscillators have been developed and built as a result of a diverse set of motivations, including basic scientific understanding of their nonlinear dynamics, for applications benefiting from their practical features, such as better robustness in adverse environmental conditions compared to solid state lasers, capability to reach higher average powers or to generate beams with diffraction-limited quality, insensitivity to misalignment by guiding the beam inside a fiber in much of the cavity, lower overall system complexity, low intensity noise, etc. [10, 19, 20]. In particular, there has been tremendous interest in the generation of as short

pulses as possible, but generation of few-cycle pulses has been largely elusive in case of fiber lasers, despite a large number of reports of even nearly single-cycle pulses from solid state lasers, such as Ti:sapphire [21]. In case of fiber lasers, the realization of 20-30 fs-long pulses was possible with dispersion management inside the cavity [22–24], limited by their relatively narrow gain bandwidths. Recently, 20-fs pulses were obtained through nonlinear spectral broadening and strong spectral filtering [25]. In this case and many related work, nonlinearity of the form of SPM plays a positive role by broadening the spectrum, and the researchers used a complex de-chirping technique to shorten the pulses afterwards. Though this was quite an achievement, one is faced with the difficult technical problem of compressing the pulses to their transform limit. Recently, we showed spatial light modulator-based (SLM) intracavity pulse shaping, which may allow a higher degree of control through phase and amplitude modulation towards realization of a few-cycle pulsed oscillator [1]. Despite encouraging initial results, this possibility remains an open question, where any success would be revolutionary.

Pulse energy is another pulse parameter, which attracts intense attention in the design mode-locked fiber lasers. This is so, because higher energies are extremely desirable for most applications, but also the pulse energy is extremely influential on the mode-locking dynamics. Together with the pulse duration, the pulse energy sets the peak intensity of the pulse, hence the strength of the nonlinear effects. While nonlinearity is an essential and indispensable component of mode-locking, too much nonlinearity can destabilize the mode-locking process. Thus, nonlinearity sets a limit for the achievable pulse energy. There are various ways for increasing this limit, such as using large mode area fibers, which reduces the peak intensity for given peak power, as well as chirped and divided pulse amplification, which reduce the peak power by spreading the pulse in the time domain. Complimentary to the efforts to reduce the nonlinear effects, there are various approaches based on managing the strong nonlinear effects with appropriate, nonlinearity-resistant pulse forms, such as similaritons and dissipative soliton resonance. Balancing of self-phase modulation (SPM) with group-velocity dispersion (GVD), third-order dispersion (TOD) and spectral filtering are also commonly used to significantly push the limits of pulse energy up in fiber lasers.

These techniques together with dispersion management have helped to scale up the pulse energies of fiber lasers from the few-picojoule regime in the 90's to the microjoule-level, which is high enough for even industrial material processing [26]. Alternatively, the oscillator energy can be kept at a modest level and fiber amplification outside of the laser cavity can be used to reach multi-microjoule and higher levels. The largest pulse energies reported from a rod-type fiber amplifier is 2.2 mJ [27]. However, the above techniques have intrinsic limitations. For example using large-mode areas is associated with generation of higher-order modes or mode instabilities and the largest mode-area fibers are really totally rigid glass rods, which represent a significant step backwards in terms of the practical advantages of fiber lasers. Therefore, there continues to be a lot of motivation for further advances in dealing with strong nonlinearities, in particular, in combination with effects such as gain filtering and higher-order dispersion.

As mentioned earlier, the idea of dispersion management enabled to push the limits of generation of shorter and more energetic pulses from fiber oscillators during the soliton era [25, 26, 28]. Researchers were doing numerical and experimental efforts to extend this idea of dispersion management to nonlinear management [29]. The fact that effective negative nonlinearity can be generated from phase mismatch of cascade of quadratic and cubic nonlinear elements, where the cubic (Kerr) is dominated by the quadratic nonlinearity [29, 30], four wave mixing, inverse four wave mixing and cascade of gain and passive fibers are expected to lead oscillator dynamics in a new and exciting research direction. Chapters 3 and 4 of this dissertation are efforts in this research direction.

The oscillator dynamics can be qualitatively understood as a dynamic balance between phase and amplitude evolution. This naturally leads to the prospect of opening up new pulsing regimes and new pulse properties through the inclusion of a electronically controllable amplitude and phase shapers inside the laser cavity.

So far we tried to shortly summarize the generation and technological advances of some important optical pulse parameters. Apart from being excellent, robust, reliable, cost efficient and environmentally friendly sources for application, fiber lasers systems always are research platforms for basic scientific understanding of

self-assembled complex spatiotemporal structures far from their thermodynamic equilibrium in optics [20, 31] and related fields such as hydrodynamics, plasma [32], Bose-Einstein condensation [33], nonlinear phenomena, thermodynamics and biophysics or biochemistry as well [34–36]. So far there are more than three Nobel Prize winning entities related to far-from-equilibrium thermodynamics, but an entirely satisfactory understanding of such dynamics is far from having been achieved [2, 37].

Currently, thermodynamics of optical pulse propagation and the onset of lasing are drawing increasing interest from the scientific community and are being investigated both experimentally and theoretically. Understanding the thermodynamics of oscillator dynamics especially the phase transition from CW to pulse formation has been extensively studied [20]. Thermodynamic terms like free energy and order parameter were introduced. Even-though the effective partition function derived does not help on farther derivation and understanding of pulse parameters, it lies a basic foundation and strengthens the idea of treating optical pulses as a particle, Supramolecular systems, or other thermodynamic entities [38]. Phenomena like the noise dynamics starting from pulse formation, stable pulsing, initiation of multi pulsing, stochastic emergence of pulsing states, interaction of pulses and their environment reveals that such systems are full of intrinsic interaction and can provide a vast research environment both in nonlinear and nonequilibrium systems.

Mode-locked lasers are inherently nonequilibrium systems that have lasing states that can be classified as near and far from equilibrium thermodynamic systems. Near equilibrium of a laser system can be characterized by interaction free single or multi pulsing (usually with smaller number of pulses) [39, 40]. These states are stationary states characterized by a constant entropy production as well as a constant entropy flow. Here, effective thermodynamic flows and their conjugated forces are linearly related to each other. Hence they formulated near equilibrium systems. When perturbation is applied here, it will displace the equilibrium position of the system. When this perturbation is removed the laser will come to its unperturbed state, The probability of the laser system to occupy possible macrostates of the system follows a Boltzmann like distribution for such

systems are locally at equilibrium [40]. Such type of states were important from application point of view. Here, cyclic processes in phase space can be selectively chosen to build an oscillator for intended applications with a proper choice of physical or fiber components.

Nonlinearity, feedback mechanism and its effects together with optomechanical efficacy can perturb and drive the system from its thermodynamic equilibrium by initiating multi pulsing, intrinsic modulation, phase hopping and energy exchange between pulses, bifurcation, and chaos that can result from cavity boundary condition. The introduction of a perturbation at this points transforms into a new emergent spatiotemporal structures. Up on removal of the perturbation, states never go back to their original unperturbed states, which is a finger print of far from equilibrium systems. The fact that such systems exist in a controlled environment and its formation similarity (driven by modulation instability of uniform stable states) of large number of emergent natural coherent spatiotemporal physical (such as Karman vortex street), biological (such as morphogenesis), and chemical structures (such as Belousov-Zhabotinsky reaction) made such system to be considered as a research hub for understanding far from-equilibrium thermodynamics in other adaptive complex systems as well [1,17,41–43]. This should start by adopting established principles and theories of far-from equilibrium thermodynamics of self-organized complex chemical and biological systems into the laser system [38, 44–46].

This dissertation is organized as follows. Chapter 1 provides an introduction to ultrafast lasers, mode-locking, its brief history and recent developments along the general direction of concern to this thesis. Chapter 2 reviews the basic theoretical background and principles of ultrafast pulse propagation and generation, through passive mode-locking of laser cavities, while introducing the non-equilibrium thermodynamic perspective in a manner that is relevant to this dissertation.

The two following chapters, Chapter 3 and Chapter 4, report advances made possibly through improved understanding and exploitation of the nonlinear dynamics of mode-locking lasers. In these studies, fluctuations and noise, therefore, the thermodynamical perspective do not play a prominent role. The subsequent

three chapters, Chapter 5, Chapter 6 and Chapter 7, in contrast, are immediately concerned with the thermodynamical perspective, analyzing the impact of noise and externally induced power modulations, followed by noise-induced transitions of the laser's mode-locking state and finally, presenting a new technique to control the mode-locking state of a laser electronically.

Chapter 3 reports direct generation of chirp-free pulses from a passively mode-locked fiber oscillator through optimization of the interaction of third-order dispersion and Kerr nonlinearity (self- and cross-phase modulation). The introduction of a second DDL is shown to enable tuning of the total TOD level, while keeping the net GVD inside the cavity unchanged.

In Chapter 4, the generation of an effective negative nonlinearity through the cascaded interplay of passive and active fiber segments is shown theoretically and experimentally. Collective behavior of sequentially arranged passive (dispersive) and active (nonlinear) fibers generate an effective negative nonlinearity such that pulse compression can take place while the opposite is to be expected. This can be understood as a result of interaction between pulse chirp, dispersion, SPM and their spatial distribution across the cavity. This approach can also provide a fresh perspective for the transformation of a soliton pulse into a similariton pulse for the only laser oscillator with double attractors, namely, the soliton-similariton laser [47]. A general message of the results in these chapters is that fine-tuning of the pulse evolution inside the cavity is important not only for optimized laser performance, but also for revealing entirely new and often unexpected, initially counter-intuitive oscillator dynamics.

In Chapter 5, the linear and nonlinear cavity response to an external driving force is explored by electronically controlling the power of the pump laser. This way, we characterized both the changes in the background noise and response to modulation at specific frequencies using a transfer-function formalism that connects the pump power modulation to the output signal power of different mode locking regimes. Our results show that the cavity response to modulation can reveal information about interaction, stability, and complexity of mode locking

regimes, including, a clear delineation with the largely linear and strongly nonlinear regimes of the laser's response. Moreover, the presence of a modulation can be used to nudge unstable mode-locking states to their nearest relatively stable state points within the energy landscape. Analysis of such dynamics using concepts of stochastic resonance or dissipative adaptation are shown to be exciting possibilities for future studies.

In Chapter 6, we report rich, nonlinear dynamics that are characteristically far from thermodynamic equilibrium, using dissipative soliton systems or bound soliton states, also known as soliton molecules. The nature of the interactions of multiple pulses within these states are explored. We also show, through numerical simulations and experiments, that their mutual interactions can alter the stability and cause either creation or annihilation of certain pulses (solitons). Specifically, we find that phase transitions to new mode-locking states take place after a previously stable mode-locking state exhibits intrinsically driven giant fluctuations at critical parameter values (typically controlled by the pump power, which effectively alters the effective nonlinearity). Consequently, random creation or annihilation of dissipative solitons are observed near these critical points. Every mode-locking regime is observed to exhibit a qualitatively similar dependence (on nonlinearity, as controlled by the pump power) whereby the fluctuations are characterized on the integrated relative intensity noise (RIN) of the output power of the mode-locked laser. This quantity usually starts at a moderate value, then it reduces, corresponding to the most stable point of the mode-locking state with increasing nonlinearity and power, before undergoing a giant fluctuation, immediately after which the laser jumps abruptly to an entirely different mode-locking state.

In Chapter 7, we demonstrate, for the first time, the use of intracavity adaptive pulse spectral phase and amplitude shaping mechanisms for direct control of the mode-locking states of a laser. We report a range of practically motivated demonstrations, such as generation of shorter pulses, cleaning up the shape of pulse (to remove its "pedestal"), removal of undesired spectral structures. In addition, and much more importantly for the purposes of this thesis, we demonstrate well-controlled reversible and irreversible transitions between mode-locking

states, including, "tweezing", thereby, control of pulse separation for multiple, bound pulses, suppression of instabilities, initiation and halting of mode-locking, access to nominally inaccessible mode-locking states. This new capability of control renders mode-locked lasers as a potentially very well controlled experimental platform for highly quantitative studies of phenomena far from equilibrium, including testing of emerging theories.

Finally, a summary of our results and perspectives on future work building on the findings of this thesis are provided in Chapter 8.

Chapter 2

Theoretical basis of fiber oscillator dynamics

2.1 Basic theories and principles of ultrafast optics

Much of the current theoretical understanding of optical pulse propagation is based on modeling pulse propagation with the generalized nonlinear Schrödinger equation (NLSE), which includes, in addition to the usual terms of dispersion, Kerr nonlinearity, loss, gain, and (in some Raman effects of the propagation medium. In some formulations, saturable absorption or nonlinear loss is included instead of Raman effects, in which case the equation is often called complex Ginzburg-Landau equation. This section reviews basic theoretical background of pulse propagation, generation, and intracavity pulse interaction that are related to our experimental results based on approaches of ref. [48] and compares it with theory of other physical systems in related fields.

2.1.1 Pulse propagation

When a pulse propagates through a medium it experiences physical effects as a result of material response. Chromatic dispersion and non-linearity are the most common effects.

2.1.1.1 Chromatic dispersion

Chromatic dispersion is resulted from frequency dependent refractive index of a material or phase velocity of light passing through a medium. Mathematically it is defined from Taylor expansion of wave number as

$$k(\omega) = \beta_0 + \frac{1}{2}\frac{\partial k}{\partial \omega}(\omega - \omega_0) + \frac{1}{2}\frac{\partial^2 k}{\partial \omega^2}(\omega - \omega_0)^2 + \frac{1}{6}\frac{\partial^3 k}{\partial \omega^3}(\omega - \omega_0)^3 + ..., \quad (2.1)$$

where the zero order term is a constant phase or common phase shift, the first order dispersion $\frac{\partial k}{\partial \omega} = \frac{1}{v_g}$ is related to the phase velocity and adds delay, $\frac{\partial^2 k}{\partial \omega^2} = \beta_2$, and $\frac{\partial^3 k}{\partial \omega^3} = \beta_3$ are the second and third order group velocity dispersion, respectively. The first two terms does not affect shape of the pulse while the second and third order are the most common effects considered in analysing pulse propagation in fiber.

2.1.1.2 Nonlinearity response

The most common nonlinear instantaneous response in optical fiber is Kerr nonlinearity which is due to optical intensity dependent change in refractive index.

$$\Delta n = n_2 I \quad (2.2)$$

Self-phase modulation (SPM) is one of these Kerr effects which is phase shift of propagating pulses as a result of its own optical intensity in time domain. The maxima phase shift experienced by the center of a pulse can be given as

$$\phi_{max} = \frac{L_{eff}}{L_{NL}} = \gamma p_0 L_{eff} \quad (2.3)$$

L_{eff} is effective fiber length and p_0 peak power.

Cross phase modulation and self-focusing effects are other common effects together with a delayed nonlinear response called Raman effect. These effects are important when one is dealing supercontinuum generation and their details can be found ref. [48].

2.1.1.3 Maxwell equations and wave theory

Optical pulse propagation or electromagnetic waves in general is governed by the well-known Maxwell equations.

$$\nabla.\mathbf{D} = \rho \tag{2.4}$$

$$\nabla.\mathbf{B} = 0 \tag{2.5}$$

$$\nabla X\mathbf{E} = -\frac{\partial \mathbf{B}}{\partial t} \tag{2.6}$$

$$\nabla X\mathbf{H} = \mathbf{j} + \frac{\partial \mathbf{D}}{\partial t} \tag{2.7}$$

Where $\mathbf{D}$, $\mathbf{B}$, ρ, $\mathbf{j}$, $\mathbf{E}$ and $\mathbf{H}$ are electric flux, magnetic flux, free charge density, current density, electric and magnetic fields respectively. Mathematical simplification by using vector identity calculus and assuming no free charge carriers in fiber wave guides, one can drive the wave equation (eqn. 2.9), with D and E related as

$$\mathbf{D} = \varepsilon_0\mathbf{E} + \mathbf{P} \tag{2.8}$$

$$\nabla^2.\mathbf{E} - \frac{1}{c^2}\frac{\partial^2 \mathbf{E}}{\partial t^2} = \frac{1}{\varepsilon_0 c^2}\frac{\partial^2 \mathbf{P}}{\partial t^2} \tag{2.9}$$

2.1.1.4 Nonlinear Schrödinger equation (NLSE)

NLSE was driven from wave equation by considering the following two main assumptions. Local and instantaneous material response and a small nonlinear component of polarization that can be assumed as perturbation term for its effect is weak in fibers. With the above assumptions, the wave equation can be written as

$$\nabla^2.\mathbf{E} - \frac{1}{c^2}\frac{\partial^2 \mathbf{E}}{\partial t^2} = \mu_0 \frac{\partial^2(\mathbf{P}_L + \mathbf{P}_{NL})}{\partial t^2} \tag{2.10}$$

Where the polarization components are related to the electric field as

$$\mathbf{P}_L(r,t) = \varepsilon_0 \int_{-\infty}^{\infty} \chi^{(1)}(t-t^{'})\mathbf{E}(r,t^{'})dt^{'} \tag{2.11}$$

$$\mathbf{P}_{NL}(r,t) = \varepsilon_0 \int_{-\infty}^{\infty} dt_1 \int_{-\infty}^{\infty} dt_2 \int_{-\infty}^{\infty} dt_3 [\chi^{(3)}(t-t_1, t-t_2, t-t_3) \mathbf{E}(r,t_1)\mathbf{E}(r,t_2)\mathbf{E}(r,t_3)] \tag{2.12}$$

Assuming the electric field has slowly varying envelop such that

$$\mathbf{E}(r,t) = \frac{1}{2}\widehat{x}[E\text{exp}(-i\omega_0 + c.c.)] \tag{2.13}$$

Wave equation for the slowly varying envelop can be reduced to Helmholtz equation in frequency domain as

$$\nabla^2 E(\omega) + \varepsilon(\omega)k_0^2 E(\omega) = 0 \tag{2.14}$$

Where $k_0 = \omega/c$, $\varepsilon(\omega) = 1 + \chi_{xx}^{(1)} + \frac{3}{4}\chi_{xxx}^{(3)}|E(r,t)|^2$ and $\frac{3}{4}\chi_{xxx}^{(3)}|E(r,t)|^2 = \varepsilon_{NL}$ are wave number, dielectric constant and its nonlinear component, respectively. By using separation of variables method, The above Helmholtz equation can be solved

$$E(r, \omega - \omega_0) = F(x,y)A(z, \omega - \omega_0)\text{exp}(\text{iz}\beta) \tag{2.15}$$

$$\frac{\partial^2 F}{\partial x^2} + \frac{\partial^2 F}{\partial y^2} + [\varepsilon(\omega)k_0^2 - \beta^2(\omega)]F = 0 \tag{2.16}$$

$$2i\beta_0 \frac{\partial A(\omega)}{\partial} + (\beta^2(\omega) - \beta_0^2)A(\omega) = 0 \tag{2.17}$$

The first equation gives modal distribution in fibers and Fourier transformation of the second equation with some approximations leads to the NLSE in time domain (Note: The details of the derivation is found in Ref. [48]).

$$\frac{\partial A}{\partial z} + \beta_1 \frac{\partial A}{\partial t} + i\beta_2 \frac{\partial^2 A}{\partial t^2} - \frac{\alpha}{2} A = i\gamma |A|^2 A \tag{2.18}$$

β_1, β_2, α and γ are group velocity, group velocity dispersion, loss coefficient, and the nonlinear parameter respectively. Pulse formation is initiated from noise in the presence of SA in a laser cavity. Its propagation is dictated by the interplay of physical processes (such as dispersion and nonlinearity) that play engineered major roles. Now a days researchers design different forms of cavities with varying complexity level and use different forms of NLSE to govern the dynamics depending on the application or optical phenomena they want to focus on (as an example we use the one with details described in ref. [47] to guide our experiments).

2.1.1.5 NLSE for Soliton pulse dynamics

Soliton has been studied in fiber optics very intensively since 1973 [49]. Such type of solution is a fixed point or solitary solutions representing nonlinear integrable evolution of a system [50]. It maintains its shape as a result of balanced effects of negative GVD and nonlinearity during its propagation in fiber. Such types of pulses are governed by NLSE with negligible loss. Using coordinate transformation $T = t - \beta_1 z$, $U = \sqrt{\gamma L_D}$, $\xi = \frac{z}{L_D}$, $\tau = \frac{T}{T_0}$, and $N^2 = \frac{L_D}{L_{NL}}$, Eqn. 2.16 can be written in a normalized form as.

$$i\frac{\partial u}{\partial \xi} - \frac{1}{2}\beta_2 \frac{\partial^2 u}{\partial \tau^2} + N|u|^2 u = 0 \tag{2.19}$$

Where N= $\frac{L_D}{L_{NL}}$ is called the soliton order number.

Using inverse scattering method such equation has a solution which is integral multiple of the form

$$U = N sech(\eta\tau) \exp(\mathrm{i}\frac{\eta^2 \xi}{2}) \tag{2.20}$$

Soliton area theorem (soliton energy is constant which is product of peak power and pulse width is limited by nonlinearity and GVD) limits the pulse energy in this regime. Inclusion of dispersion management provided the stretched pulse in which the pulse breathes during its propagation on a dispersion map. In doing so the pulse experiences less nonlinearity hence pushed the energy limit of solitons to sub ten nanojoule level. This energy limit is further pushed by discovery of similariton and all normal dispersion regimes.

2.1.1.6 NLSE for similariton pulse dynamics

Similariton solution arise in fiber optics when the interaction between gain, dispersion and nonlinearity converge any input pulse in to asymptotic solution that evolves self similarly (similariton atractor) with the pulse duration and amplitude increase exponentially. Pulse propagation in the presence of gain can be described by Eqn. 2.19 with the loss coefficient replaced by gain parameter [51, 52].

$$i\frac{\partial A}{\partial z} - \beta_2\frac{\partial^2 A}{\partial t^2} + i\frac{gA}{2} - \gamma|A|^2A = 0 \tag{2.21}$$

Similariton pulses are asymptotic solution of the above equation and it accumulates a parabolic phase during propagation [53, 54].

$$A(z,T) = \varphi(z,T)\mathrm{exp}(\mathrm{i}\Phi(\mathrm{z},\mathrm{T})) \tag{2.22}$$

$$\varphi(z,T) = \varphi_0\mathrm{exp}(\frac{\mathrm{g}}{3}\mathrm{z})\sqrt{1-\frac{T^2}{T_p^2}(z)} \tag{2.23}$$

$$\Phi(z,T) = c + \frac{3\gamma\varphi_0}{2g}\mathrm{exp}(\frac{2}{3}\mathrm{gz}) - \frac{g}{6\beta_2}T^2 \tag{2.24}$$

$$\varphi_0 = 0.5(\frac{gE_{in}}{\sqrt{\frac{\gamma}{\beta_2^2}}})^{\frac{1}{3}} \tag{2.25}$$

$$T_p = \frac{6\sqrt{\frac{\gamma\beta_2}{2}}}{g}\varphi_0 exp(\frac{gz}{3}) \tag{2.26}$$

Where Φ, E_{in}, φ_0, and T_p are phase, energy, pulse width and amplitude respectively [54]. For such solutions to exist in a fiber cavities there has to be a mechanism which returns self similarly evolution of the parabolic pulse back to its starting point. It can be a filter, gain narrowing, spectral compression or presence of another nonlinear attractor [47, 52].

2.1.1.7 NLSE for dissipative soliton pulse dynamics

The Hause master equation or NLSE has similar mathematical form, hence can be taken as one form of generalized complex Ginsburg-Landau equation (CGLE). Ginsburg received a Nobel prize for this equation in 2003 and it has been used to describe dissipative stable structures in space and time in various fields of nonlinear systems in science such as oscillatory chemical reaction, hydrodynamics, mode locked lasers, super conductivity, in collective behaviour of micro-organisms and plant ecology, self-assembly of molecular motors and systems that can be described by far-from equilibrium in general [55–58]. Dissipative solitons structures persist for longer period of time even-though their parts are experiencing loss/gain. Such dissipative systems can be described by solutions of Complex quintic Ginsburg-Landau (CQGLE) equation that describe a vast number of pulse dynamics that range from ANDi to dispersion managed and soliton laser systems with proper parameter management [59, 60].

$$iU_z + \frac{DU_{tt}}{2} + \mid U \mid^2 U + \nu \mid U \mid^4 U = i\delta U + i\xi \mid U \mid^2 U + i\beta U_{tt} + i\mu \mid U \mid^4 U \tag{2.27}$$

Where U, ν, δ, ξ, β, and μ are field envelop, coefficients for quintic Kerr, linear loss/gain, nonlinear gain, spectral filtering or gain dispersion and nonlinear gain

saturation respectively. Equation parameters of CQGLE determine the CW or a range of stable and unstable Pulsing solutions [61, 62]. The fact that large set of variables can give different solutions to this equation gives a laser oscillator science vast degree of freedom in exploring new forms of pulsing regimes as well as in representing different but similarly behaving nonlinear dynamical systems which are far-from-thermodynamic equilibrium in and outside optics.

2.1.2 Mechanism of passive mode locking

2.1.2.1 Classical Electromagnetic theory of pulse formation

According to electromagnetic modeling a pulse is formed when a number (usually in the order of 10^5) of longitudinal modes in a cavity have the same phase or maintain their phase difference through the effects of saturable absorber. Gain amplification band width induces additional selection rule on the selection of frequencies of longitudinal modes that can be part of the pulse spectrum as shown in Fig 2.1 (a). The wider the spectral width, the shorter the generated pulse is. Such a pulse is described by a product of slowly varying envelop and fast oscillatory component called carrier wave. Frequency difference between consecutive frequency modes gives repetition rate of the cavity. While Carrier envelop offset frequency is defined as the phase difference between the phase of the carrier wave and the envelope position which is determined by dispersion and nonlinearity.

Nonlinear polarization rotation or evolution is the one we used as SA in our experiments. It is an artificial amplitude modulator mathematically represented by a transmittance curve of the form [63]

$$T = \sin^2(\theta)\sin^2(\phi) + \cos^2(\theta)\cos^2(\phi) + \frac{1}{2}\sin(2\theta)\sin(2\phi)\cos(\phi_l + \phi_{nl}) \qquad (2.28)$$

θ, φ, $\phi_l = 2\pi L\frac{\delta n}{\lambda}$ and $\phi_{nl} = \frac{2}{3}\gamma LPcos(2\theta_1)$, $\delta n, L, P$ are the angle between polarizer and the vertical polarization axis of the fiber, analyser and the vertical polarization axis of the fiber, linear, nonlinear phase shifts, birefringent, cavity

length, and optical power in the cavity, respectively. Its operational principle can be simply demonstrated by polarizer, nonlinear medium and analyzer as in Fig 2.1 (c).

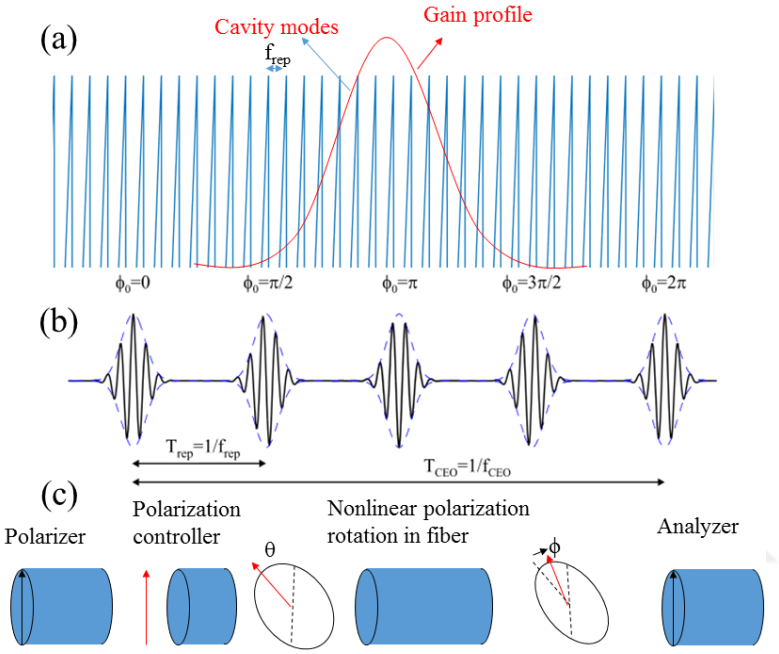

Figure 2.1: Pulse formation: (a) Longitudinal cavity modes generated inside a cavity. (b) Schematics of pulse profile. (c) Schematics of the working principles of nonlinear polarization evolution (NPE).

2.1.2.2 Mode locking as a stochastic phase transition process

In the previous section we have seen electromagnetic formalization of how propagation of different pulses is theoretically governed and how pulse is formed in a cavity. According to statistical physics modelling, Passive mode locking is generated or spontaneously emerge from quasi CW through unique and non-repetitive (as indicated in Fig. 2.2 where both the pulse evolution happened on a cavity with the same parameters) stochastic process in nanosecond time scale [64]. It is described as a first order phase transition using an effective thermodynamic modelling of Such laser system where the CW and pulsing states being disordered and ordered phases respectively [65]. In this model effective partition function is derived from effective Hamiltonian which leads to free energy and order parameter

given by

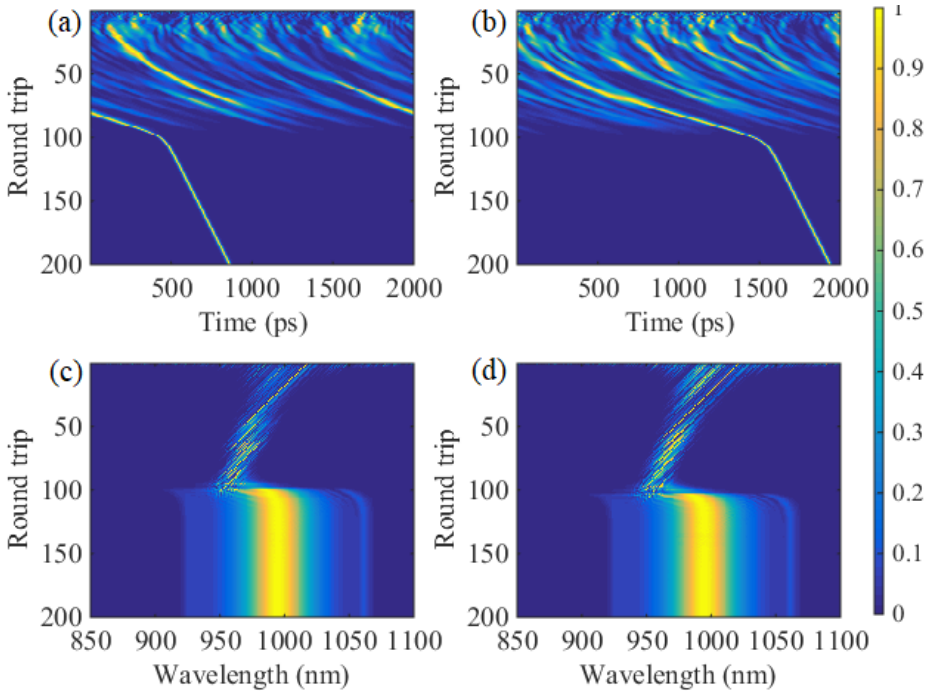

Figure 2.2: Pulse dynamics per round trip: Simulation result showing stochastic pulse build up dynamics inside oscillator

$$f(\gamma, y) = (\frac{\gamma y^2}{2} + log(1-y)) \tag{2.29}$$

$$y = M^2 \text{ and } \gamma = \frac{\gamma_s p^2}{T} \tag{2.30}$$

Where M is order parameter, γ_s saturable absorption parameter, p is pump power and T is a value related to noise of the system. Depending on the value of γ the free energy has zero, local and global minimum values representing disordered (CW), meta stable and stable states. Fig. 2.3 shows behaviour of effective free energy as a function of order parameter for different pump powers. It has one minimum at $y = 0$ for $\gamma < 4$ and double minimum at $\gamma \cong 5$ where phase transition takes place and it has a single minimum at $y \neq 0$ for $\gamma > 5$. This order parameter is contineous function but its derivative shows discontinuity at the critical point where the phase transition takes place. This is a behaviour of systems undergoing first order phase transition.

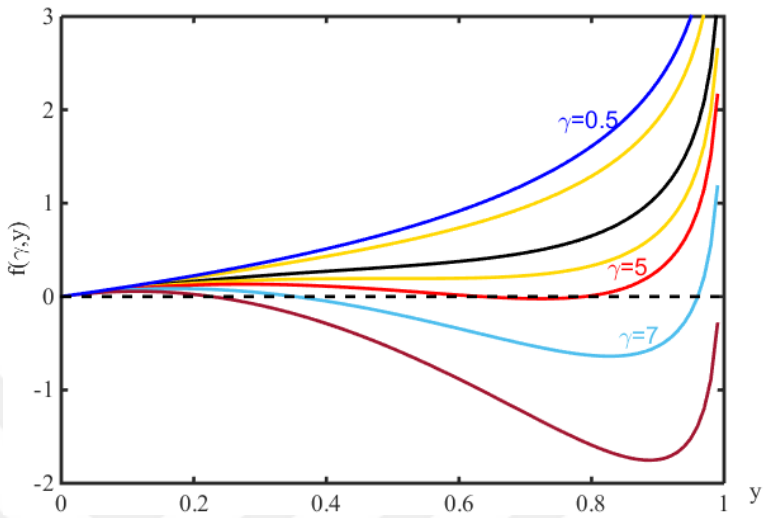

Figure 2.3: Free energy: Effective free energy diagram for different values of pump power.

2.1.3 Soliton pulse interaction

Nonlinearity and other intracavity interactions can drive a stable pulse in to periodic bifurcation and chaos. The interaction become more complicated When there are higher order soliton solutions or when there are more than one pulses per cavity round trip. The most common types of such interaction are soliton-soliton interaction, soliton-dispersive wave interaction, soliton-acoustic wave and interaction through modulation instability. By tuning some parameters which affect the nonlinearity additional phase transition between multipulsing mode locking states can take place. Such types of transition are important in studding complexity of far from equilibrium laser systems.

2.1.3.1 Soliton-soliton interaction

Mutual interaction between solitons depend on the relative amplitude and relative phase difference. Lets consider two closely separated solitons u_1, u_2 that have a total field $u = u_1 + u_2$. Inserting this field to NLSE, we will have

$$i\frac{\partial u_1}{\partial \xi} + \frac{1}{2}\frac{\partial^2 u_1}{\partial \tau^2} + \mid u_1 \mid^2 = -2 \mid u_1 \mid^2 u_2 + u_1^2 u_2^* \tag{2.31}$$

The above equation is solved in Ref. [48] with the perturbation theory by considering the right side of the equation as a small perturbation. The solution provides a coupled phase and separation differential equations as.

$$\frac{\partial^2 q}{\partial \xi^2} = -4e^{-2q}\cos(2\psi), \frac{\partial^2 \psi}{\partial \xi^2} = -4e^{-2q}\sin(2\psi) \tag{2.32}$$

The pulse separation as a function of ξ can be solved from the above equations as

$$q(\xi) = q_0 + \frac{1}{2} in[\cosh^2(2\xi e^{-2q_0}\sin(\psi_0)) + \cos^2(e^{-2q_0}\sin(\psi_0)] \tag{2.33}$$

Where q_0 and ψ_0 are the initial pulse separation and relative phase. As seen in Fig. 2.4 the separation can be stable, increase (effective repulsive force) or decrease (effective attractive force) depending on the initial relative phase and temporal separation of the interacting soliton pulses. The nonlinear phase shift due to self and cross phase modulation also have additional effects.

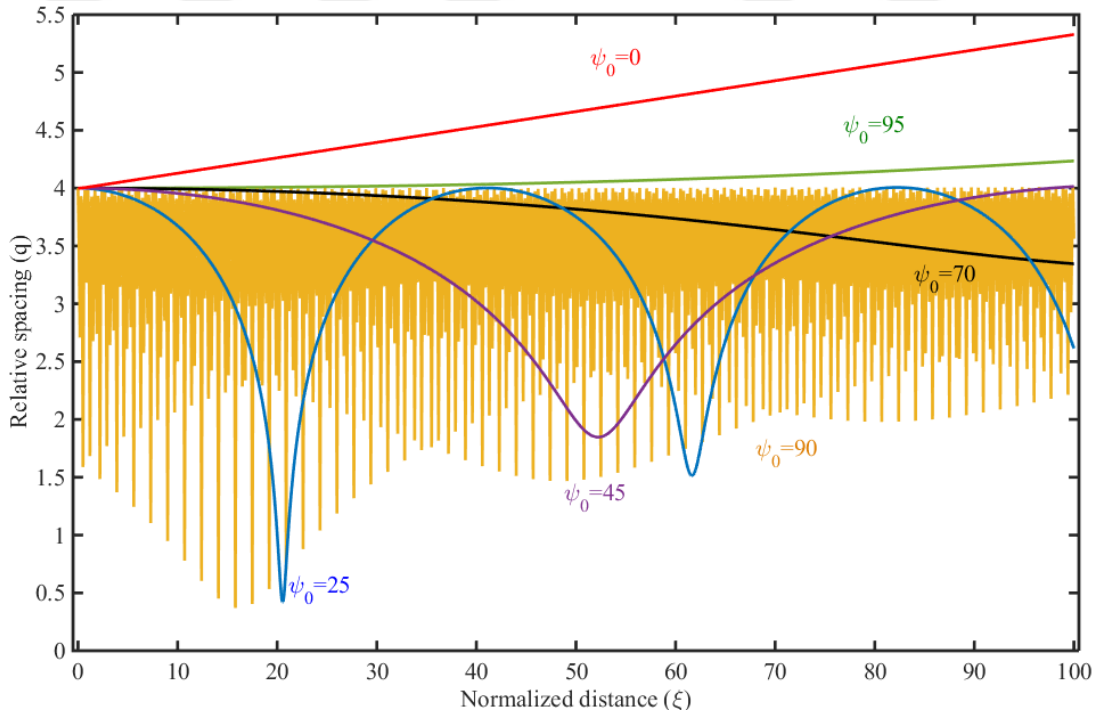

Figure 2.4: Soliton - soliton interaction: Interaction that cause oscillatory($\psi_0 = 25$, $\psi_0 = 45$, and $\psi_0 = 90$), effective attractive ($\psi_0 = 70$), and repulsive forces ($\psi_0 = 0$ and $\psi_0 = 95$) that depends on initial relative phase difference when the initial separation $q_0 = 5$.

2.1.3.2 Soliton-dispersive wave interaction

Solitons shed extra energy to dispersive waves when its phase is matched [66]. This phase matching can happen in the presence of higher order dispersion [67,68], nonlinearity loss and gain inhomogeneity. For example considering a periodic gain, A frequency shift between the centre of soliton spectrum and side band can be written as [69, 70].

$$\delta\upsilon_n = \frac{1}{2\pi t_p}\sqrt{(1+\frac{8nL_s}{La})} \tag{2.34}$$

Where t_p, $L_s = \frac{\pi}{2}L_D$, L_D, and L_a are pulse width, soliton period, dispersive length and amplification period receptively. The interaction of this side band (Kelly side band) plays significant role in the stability of the pulses circulating the cavity.

The phase matching between soliton and dispersive waves can also happen in the presence of TOD. This is theoretically shown in ref. [67, 68]. The central carrier frequency difference and the peak power of the dispersive wave is given by respectively as.

$$(\upsilon_d - \upsilon_s)t_p = \frac{1}{4\pi\delta_3}[1 - 4\delta_3(2N-1)^2)] \tag{2.35}$$

$$p_d = \frac{5\pi N}{4\delta_3}[1 - \frac{2\pi}{5}((2N-1)\delta_3)^2]\exp(-\frac{\pi}{2(\mathrm{2N}-1)}\delta_3) \tag{2.36}$$

where N, t_p are soliton order number and initial pulse duration and $\delta_3 = \frac{\beta_3}{6|\beta_2|}t_p$

2.1.3.3 Soliton-acoustic wave interaction

When a pulse pass through a fiber (dielectric), it generates transversely propagating acoustic waves through a well-known phenomenon called electrostriction [66]. These generated acoustic waves interact with solitons coming after the first one. This type of interaction also plays significant role both in the harmonics of repetition rate and the stability of pulses in the cavity [69, 71].

The above interaction rules together with other complex interactions generally can be summarized in terms of oscillating lose and constant gain as shown on Fig. 2.5. Interaction shifts the position of stability point of the pulsing state and then a pulse or pulses will be detached from a bunch, created or annihilated before the state come back to its stability point. Such process set individual rules that dictate the complexity of self-assembly in such systems.

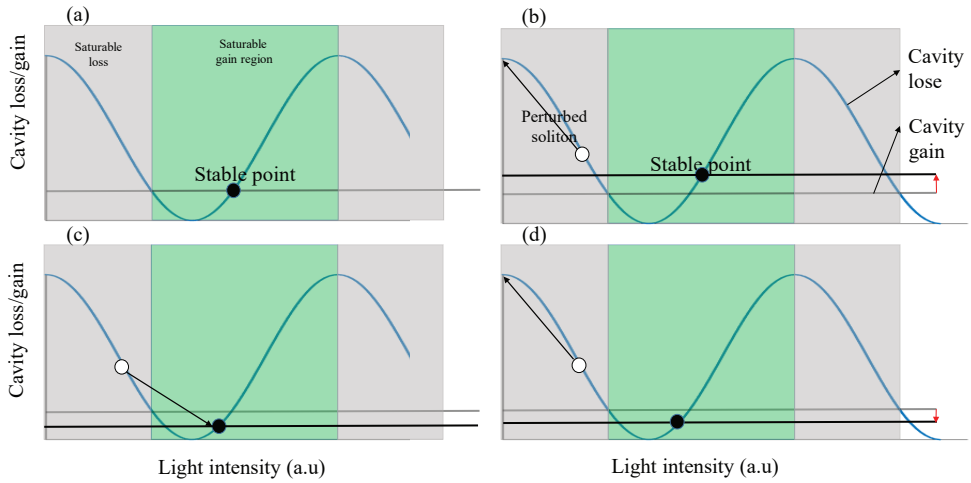

Figure 2.5: Summery of cavity stability operating in multi soliton regime: (a) stable pulsing in the presence of modulated lose and constant gain. Pumping increase cavity gain and the state stabilizes either by erasing (b) or creating (c) solitons with in the state. (d) the same stability behaviour can be observed with decreasing the pump power.

2.1.4 Dissipative adaptation and entropy production for laser systems

Humankind had been formulating social and cultural patterns throughout our experience with simple rules following nature. Music, Dance, the Mexican wave, ancient middle east architecture, Egyptian design heritages, African cultural cloth designs ...etc following a simple individual rules. So far, there are few theories which try to unlock the mystery how nature has done natural patterns that our eye loves to see and our ear starves to hear. The Darwinian theory states that structures on living things come as a result of natural selection and fitness

towards environmental experience [72]. Whereas according to dissipative adaptation, which is emerging inclusive theory states that patterns or structures develop as a result of driven stochastic process and it favours structures formed by dissipating more of the driving energy [73]. Mode locked laser is one of the promising candidate that can be used to test such theory among other multi-disciplinary fields. Here we are going to try to adopt a theory of near and far from equilibrium states (dissipative adaptation) to a laser system following approaches of ref. [40, 73, 74].

Mode locked laser systems are inherently nonequilibrium thermodynamic systems. Pulses exhibit particle like property that can be described by both near and far from equilibrium systems. Power is already described as inverse temperature like thermodynamic variable [65]. In order to describe the near equilibrium property we need to make the following two assumptions. Pump power and the coupling out power can be modelled as hot and cold reservoirs at a temperature T_h and T_c, respectively as shown on Fig. 2.6(a). The power in the oscillator (system) is assumed to be linearly distributed along its length. These two assumptions helped as to adopted the near equilibrium thermodynamics of a system in contact with two heat reservoirs developed in Ref. [40]. An oscillator will evolve to its steady state, which is characterized by constant entropy flow and constant entropy production. The entropy produced per unit length will have the form

$$\sigma(x) = J_{qx}.\frac{\partial}{\partial x}\frac{1}{T(x)} = J_{qx}.\frac{1}{T(x)^2}\frac{\partial T(x)}{\partial x} \tag{2.37}$$

The total entropy production will be

$$\frac{d_pS}{dt} = \int_0^L \sigma(x)\mathrm{dx} = \int_0^L J_q.\frac{1}{T(x)^2}\frac{\partial T(x)}{\partial x}\mathrm{dx} \tag{2.38}$$

Stationary power implies that the power flow is uniform. This implies that the temperature (inverse power) a linear function of x. Hence, at steady state J_{qx}=constant (detail justification can be found on [40]). Then the entropy produced will be

$$\frac{d_pS}{dt} = \frac{J_q}{T}\ |_0^L = \frac{J_q}{T_c} - \frac{J_q}{_h} > 0 \tag{2.39}$$

The total entropy is also constant for a steady state. J_q should be positive Since the positivity of entropy production is required. The entropy flowing to the outside is $\frac{J_q}{T_h} - \frac{J_q}{c} < 0$. This implies the nonequilibrium steady state is maintained through net entropy flow to the external environment.

When the relationship between thermodynamic flows and conjugate forces are not longer linear, then the system becomes far-from equilibrium system. Now, lets consider the laser system (oscillator and hot reservoir (pump power) on Fig.2.6(a) for simplicity) in contact with large heat bath (it includes the cold reservoir on Fig. 2.6(a)) at temperature (noise) T. Thus, total Hamiltonian of the whole system will be

$$H_{Tot} = H_{sys}(x, \xi(t)) + H_{bath}(y) + h_{int}(x, y) \tag{2.40}$$

$H_{sys}(x, \xi(t)), H_{bath}(y)$ and $h_{int}(x, y), \xi(t), x$, and y are the Hamiltonian of the laser system, bath and interaction force Hamiltonian, time dependent driving field, generalized coordinates of the system and the bath, respectively. The heat bath interacts in the form of perturbation through thermal and mechanical fluctuation of the environment and through controlled injected modulation or noise. The laser interacts with the bath in the form of dissipation of energy, gain and through output coupling. At thermal equilibrium the system will occupy microstates with a Boltzmann probability distribution given by.

$$\frac{p(i)}{p(k)} = \exp(-\frac{E_i - E_k}{k_B T}) \tag{2.41}$$

Where k_B, E_i, and E_k is a Boltzmann constant and the free energy of i and k microstates. If such system is left open for interaction or driven externally, it will not be in equilibrium state and things become completely different. The probability will depend not only the energies, but also on the evolutionary path and their time reversed trajectories.

Lets have a phase space that contains mode lock states that are coexisting at a given specific condition and in the neighbourhood of this state that can

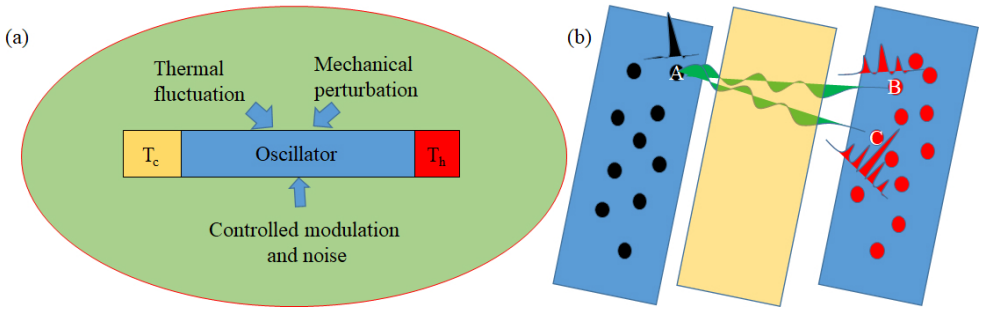

Figure 2.6: Laser oscillator as thermodynamic nonequilibrium system (a) interaction of a laser system with two heat bath at different temperatures (b) Path dependent irreversibility and entropy production in driven evolution of soliton states. Each Point represents a number of soliton macrostates which have the same power output at a fixed pump power.

be considered as accessible macrostates of the system. Here, we are considering the coordinates of pulse in a mode locking state formulates the microstates of the system. Hence, the macrostates are collection of such microstates with the common observable. Perturbation through the driving force can let the system to switch its occurrence between macrostates (different mode locking states) and on doing so, it will follow certain path. The probability of such a evolutionary path $P(x(t), \xi(t))$ which starts at macrostate $x(0)$ at time t=0 depends on the the probability of time reversal video of the path followed and the energy of driving force $\xi(t)$ dissipated by the system as.

$$\frac{P(x^*(\tau - t), x^*(\tau - t); \xi(t))}{P(x(t), x(0), \xi(t))} = \exp(-\beta \Delta \mathrm{Q}) = \exp(-\Delta \mathrm{S}) \tag{2.42}$$

Where ΔQ and ΔS are the heat dissipated to and entropy change (increase) of heat bath, respectively. This equation tells us the relationship between irreversibility and entropy production which is the basic principle in far from equilibrium phenomena. that is, when a forward trajectory is more likely than its time reversal, entropy of the surrounding (universe) increases due to dissipation of heat to the surrounding.

The probability of the system to go from property A (can be output power or noise level of states) of the system common to certain macrostates to another

macrostate property B can be given by

$$\frac{P(B^* \rightarrow A^*); \xi(\tau - t))}{P(A \rightarrow B; \xi(t))} =< \exp(-\Delta \mathrm{S_{tot}}) > A \rightarrow B \tag{2.43}$$

and this can be expanded to a system shown in Fig 2.6b (b) where pulsing macrostates are represented by dotes in the phase space.

$$ln[\frac{P(A \rightarrow B); \xi(t))}{P(A \rightarrow C; \xi(t))}] - ln[\frac{P(B^* \rightarrow A^*); \xi(t))}{P(C^* \rightarrow A^*; \xi(t))}] = ln[\frac{< \exp(-\Delta \mathrm{S_{tot}}) > A \rightarrow B}{< \exp(-\Delta \mathrm{S_{tot}}) > A \rightarrow C}] \tag{2.44}$$

Such a system creates conducive experimental platform to shed light on understanding the behaviour of far-from equilibrium systems in general. Never the less statistical understanding of laser dynamics is yet to be developed hence, setting a proper modelling is a challenge needed to be overcome in this direction.

2.1.5 Characteristics of intensity noise

The presence of noise limits devise performance on the other hand its presence plays crucial role like the picosecond fluctuation that initiates or builds up optical pulses from continuous wave in cavities [64], and a performance improvement through stochastic resonance in the presence of nonlinearity. Thus understanding noise dynamics is always important. In this subsection a review of theoretical studies that are important for qualitative explanation of our experimental results will be revised. Classical mathematical definition for noise spectral density is squared modulus of the Fourier transform of autocorrelation of optical power.

$$s(\omega) = \frac{1}{2}\pi \int_{-\infty}^{\infty} G(\tau) \exp(\mathrm{i}\omega\tau) d\tau \tag{2.45}$$

$$G(\tau) =< p(t)p(t - \tau) > \tag{2.46}$$

Relative intensity noise (RIN) gives a figure of merit for quantifying noise in optical sources.

$$\frac{RIN}{\Delta f} = \frac{\langle \delta p_0^2 \rangle}{p_{0,rms}}[Hz^{-1}] = \frac{2\langle |\Delta s(\omega)|^2 \rangle}{\langle s \rangle^2} \tag{2.47}$$

where δp_0, $p_{0,avg}$, $\langle s \rangle$, and $\Delta s(\omega)$ are spectral density root mean square fluctuation, rms optical power, average optical power, and spectral density of noise in Δf respectively [75]. Recently quantum mechanical modelling of noise revel characteristics of RIN spectrum in response to loss/gain properties, output or vacuum coupling, pump noise, spontaneous emission of laser systems and dipole fluctuation [76]. Accordingly the low frequency (below relaxation oscillation) spectrum is dominated by noise from pump sources and mechanical instabilities from environment, noise from dipole fluctuations dominate higher frequencies and the highest frequencies are dominated by vacuum or cavity loss fluctuations. The last one determines cut-off frequency in modulation transfer function (details are given in chapter 5).

2.1.6 Pulse shaping with spatial light modulator (SLM)

Pulse shaping in time domain of optical short pulses is difficult if not impossible because it requires ultrafast real time modulators with femtosecond resolution. But pulse shaping of the spectral phase and amplitude in frequency domain has been a common practice since 1980s and currently arbitrary pulse shapers such as spatial light modulator (SLM) can do the specified job. In case of linear filtering, input electric field to a pulse shaper is modified by its response function and a different wave form is found as an output. Mathematically it is given by

$$E_{out}(t) = H(t) \bigotimes E_{in}(t) \tag{2.48}$$

$$E_{out}(\omega) = H(\omega) E_{in}(\omega) \tag{2.49}$$

Where $H(t)$ and $H(\omega)$ are the response function in time and frequency domain respectively.

Figure 2.7 shows a standardized zero dispersion 4-f configuration for pulse shaping. A blazed grating first introduces angular dispersion of spectral components then a lens preforms a Fourier transform of the beam and focus each spectral components on to the SLM surface (placed a focal length away from the lens) where pulse shaping takes place. Then the next lens does the inverse Fourier transformation, and then a grating compensates the dispersion introduced by the first grating. Hence the configuration is called zero dispersion 4-f pulse shaping configuration [77].

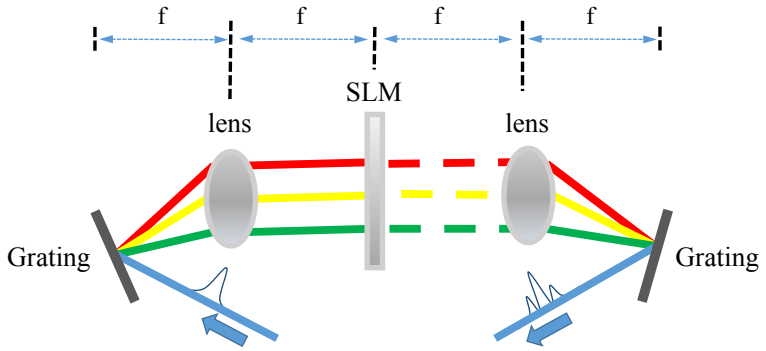

Figure 2.7: Zero dispersion 4-f configuration: It consists of a pair of grating, two lenses, and spatial light modulator placed a focul length away from each other.

Considering optical field of the form

$$E_{in}(x,t) = E(x)A(t)\exp(i(\omega_0 t + \varphi(t))) \tag{2.50}$$

And taking the response function of the first grating and the Fourier transformation by the lens, the electric field incident on the SLM surface will be modified by the mask function m(x)

$$E(x,\Omega) = \sqrt{\frac{2\pi}{\beta\lambda_0 f}} E'_{in}\left(\frac{2\pi x}{\beta\lambda_0 f} + \frac{\gamma}{\Omega\beta}\right)A(\Omega)\exp(i\Omega)m(x) \tag{2.51}$$

With $\beta = \frac{\cos\theta_i}{\cos\theta_d}$, $\gamma = \frac{2\pi}{p\omega_0\cos\theta_d}$, $\Omega = \omega - \omega_0$ where θ_i, θ_d and p are the incident, refraction angles and spacing between grating lines respectively. This will be

modified by the response functions of the other lens and grating and finally the output will be

$$E_{out}(x,t) = \sqrt{\frac{2\pi}{\beta\lambda f}}\exp(i\omega_0 t)\int E_{in}(-(x+\frac{t\beta}{\gamma}),t+\tau)M(\frac{2\pi\tau}{\gamma\lambda f})d\tau \tag{2.52}$$

Coupling of the spatial and spectral components on the mask results in the spatial and time coupling of the output wave form. The final temporal shape of the wave form is manipulated by the shape of the phase and amplitude mask on the SLM. Note that: the details of this derivation can be found in Ref. [77–79].

Lets try to use the above concept to a specific case used in our experiment. It is known that any periodic function can be expanded in Fourier series in terms of sum of cos and sin functions. For example a linear periodic function or saw tooth function (a case for chapter 7) can be written as a sum of a constant and sum of sine function (Fourier series) as.

$$s(\omega) = \frac{1}{2} - \sum_{n=1}^{\infty}\frac{1}{n\pi}\sin(\frac{n\pi(\omega-\omega_r)}{L}) \tag{2.53}$$

Where T=2L is period and ω_r is the reference frequency in which the phase mask starts. When such a phase mask is applied to a pulse in frequency domain

$$E_{out}(\omega) = E_{in}e^{is(\omega)} \tag{2.54}$$

Using eqn. 2.49

$$E_{out}(\omega) = CE_{in}(\omega)e^{-i\sum_{n=1}^{r}\frac{1}{n\pi}\sin(\frac{n\pi(\omega-\omega_r)}{L})} \tag{2.55}$$

C is a complex constant and by using Jacobi-Anger relation of trigonometric and Bessel function of the first type

$$e^{i\mathrm{Asin}(\nu)} = \sum_{-\infty}^{\infty}J(A)e^{in\nu} \tag{2.56}$$

$$E_{out}(\omega) = C(-1)^n E_{in}(\omega)\prod_{n=1}^{\infty}\sum_{k=-\infty}^{\infty}J_k(\frac{1}{n\pi})e^{ikn\pi(\omega-\omega_r)} \tag{2.57}$$

Using product of sum as sum of products, the above equation will be

$$E_{out}(\omega) = C' E_{in}(\omega) \sum_{n_1,\ldots n_r=-\infty}^{\infty} [\prod_{k=1}^{r} J_{n_k}(\frac{1}{n\pi})] e^{i\frac{\pi}{L}(\omega-\omega_r)\sum_{k=1}^{r} n_k k} \tag{2.58}$$

Fourier transform of the above equation (eqn. 2.58) gives

$$E(t) = C' e^{i\omega_0 t} \sum_{n_1 \ldots n_r=-\infty}^{\infty} (\prod_{k=1}^{r} J(\frac{1}{n\pi}))(e^{-i\Delta\omega\frac{\pi}{L}\sum_k kn}) E_{in}(t + \frac{\pi}{L}\sum n_k k) \tag{2.59}$$

This equation gives temporal split structures or waveform. This shows that a periodic linear spectral phase applied on a spectral domain can create pulse splitting the same as effects of sine or cosine spectral phases shown in ref [80, 81]. A dynamic phase mask introduces varying temporal phase proportional to $\Delta\omega$. If this is varying linearly with time then it will create additional delay between the fragmented pulses.

Chapter 3

Generation of 1.2 nJ 61 fs pulses directly from Yb-doped fiber oscillators

There is an impressively large number of publications reporting on the development of or relying on the use of compact ultrashort pulse laser sources. Most applications require close to 1 nJ of pulses energy. In many cases that require higher energies, external amplification is used. When the laser is to used directly, external-cavity pulse de-chirping or more complex forms of pulse shaping is almost a regular procedure in certain application fields [82]. External pulse compression close to the transform limit of the pulse is, then, required. Possibility to approach the transform limit is mainly determined by higher-order dispersion, nonlinear phase accumulation, gain filtering, the saturable absorber, and their placement within the cavity as well as their mutual interactions. Second- and third-order dispersion need to be compensated for the generation of transform-limited pulses outside oscillators. Different techniques ranging from the use of diffraction grating [83, 84], prism [84], prism and grating pairs [85], chirped mirrors [86], optical fiber grating compressors [87], photonic crystal fibers [88] are used. Approaches that compensate TOD with SPM [23] have also been used. Also, spatial light modulators [89, 90] have been used to compensate dispersion

outside cavity. However, there is a general shortage of using such techniques inside a laser cavity for directly generating linear chirp free pulses in case of fiber lasers, even though generation of transform-limited pulses is routine for solid state oscillators. The reason for the difference is that the typical average dispersion and nonlinearity of a fiber laser is about 3-4 orders of magnitude larger than that of a solid state laser producing the same pulse duration and pulse energy. However, there is substantial demand for a fiber oscillator producing nJ-level and transform-limited pulses for use in optical communications, coherent control of atomic systems, nonlinear spectroscopy, molecular reaction dynamics, and microscopy. It can also help eliminate the amplification stage that often precedes supercontinuum generation, at least for lasers systems at 1 μ.

Here, we propose and demonstrate a laser cavity with two sections of DDL and from this cavity, we report the generation of 1.2-nJ, 61-fs pulses directly. Besides, from the point of view mode-locking physics, using more than one diffraction grating compressor (DDL) gives a new degree of freedom allows, which one can use to study the interaction of higher-order dispersion with nonlinearity. For example, one can fix the GVD, while tuning TOD or more importantly, one can adjust the dispersion map and consequently nonlinearity map in a cavity to a much greater extend. We managed to optimize the level of second- and third-order dispersion (GVD and TOD) and its interaction with SPM to a significant degree just by incorporation of the second DDL. To the best of our knowledge, these are the shortest pulses directly generated from Yb-based fiber laser oscillator, improving previous reports of generation of 74-fs pulses from a micro resonator [91].

3.1 Numerical model of the oscillator

Our numerical simulations are based on solving the extended nonlinear Schrödinger equation with a split-step algorithm method used by [47]. The hypothetical oscillator set up is indicated in Fig. 3.1(a). Fig. 3.1(b) shows the spectral and temporal evolution of the pulse with parameters of each component indicated in Table 3.1. A 53-fs pulse with 47-nm spectral bandwidth evolves to

3.25 ps in DDL1 and then the negative chirp or accumulated temporal linear phase is compensated in the next 410 cm of SMF with negligible spectral compression before it enters the gain fiber with a slightly negative chirp that can be compensated by the next 16 cm (ignoring the accumulated nonlinear phase shift) to avoid gain narrowing or filtering effect. The spectral width goes down to 14 nm in the gain fiber and then increases to 47 nm at the end of 10 cm passive fiber after the gain fiber through self-similar evolution. In these dynamics, NPE has a negligible effect on the pulse evolution. Finally, the pulse is de-chirped by DDL2 to reach its original width to maintain the periodic boundary conditions, resulting in an output pulse duration of 53 fs.

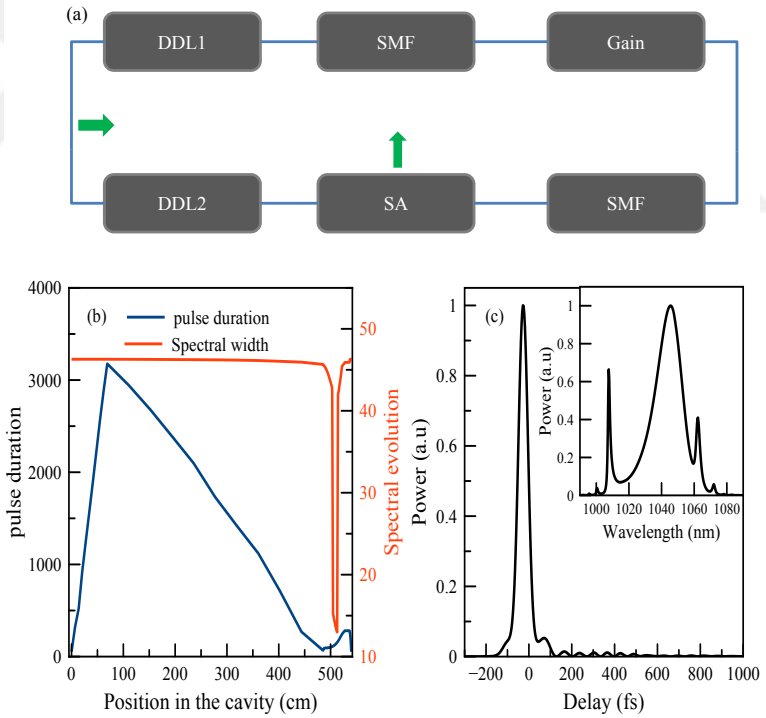

Figure 3.1: Simulation result: (a) Schematic of the simulation setup. M (mirror), SMF (single mode fiber), SA (saturable absorber), DDL1 and DDL2 (diffraction grating with 600 lines/mm and 300 lines/mm respectively). (b) Evolution of pulse duration and spectral width in the cavity. (c) Autocorrelation signal and optical spectrum of a pulse at the output between the DDLs.

Table 3.1: Parameters of segments used for oscillator simulation results in Fig. 3.2 (b). Segment number (S.N), Length (L) [cm], GVD [fs^2/mm], TOD [fs^2/mm], Kerr coefficient with n_2 [10^{-16}-1 cm^2/W], Effective mode area (EMA) [μm^2], GBW gain band width and FBW filter band width[nm].

S.N	L	GVD	TOD	n_2	EMA	GBW	FBW
1	6.9	-1422	2500	0	3-	-	-
2	417	23	28	2.73	30	-	-
3	32	23	28	2.73	30	$\triangle\lambda$:40 nm	-
4	10	23	28	2.73	30	-	-
5	10	-	-	-	-	-	
1	0.56	-710	1250	-	30	-	-

3.2 Experimental setup and results

We designed our oscillator following the simulations-guided design. The experimental setup is schematically shown in Fig. 3.2. It has a 32 cm Yb-gain fiber, 395 cm of standard single-mode fiber (SMF), two diffraction gratings pairs (DDL) built using gratings with 300 and 600 grooves/mm, a 50/50 beam splitter, a polarizing beam splitter, two quarter-wave and one half-wave plate for polarization control, a 95/5 output fiber coupler, an optical fiber isolator followed by WDM. The oscillator has a repetition rate of 32 MHz and is pumped with two 980 nm pump diodes that can produce a total pump power up to 800 mw. It is mode-locked by nonlinear polarization evolution, which is implemented with the two quarter wave plates, the half wave plate, and the polarizing beam splitter.

The cavity dispersion is varied from net negative (up to ~ -5000 fs^2) to net positive (up to $\sim$ 3000 fs^2). The stable and self-starting oscillator exhibits a range of pulsation dynamics from dispersion-managed solitons (stretched pulses) to effectively solitons and can be fully mode-locked or can generate noise-like pulses (NLP). Our goal was to arrange for the pulse evolution within the cavity to be such that the output from the beam splitter between the two DDLs is the shortest possible. As the first step, output is taken before the second DDL (DDL-2) just after PBS and compressed outside the cavity. The net GVD of the oscillator is adjusted to get a pulse that can be compressed fully. As the next step, DDL-2 is adjusted to impart dispersion the same as the external compressor

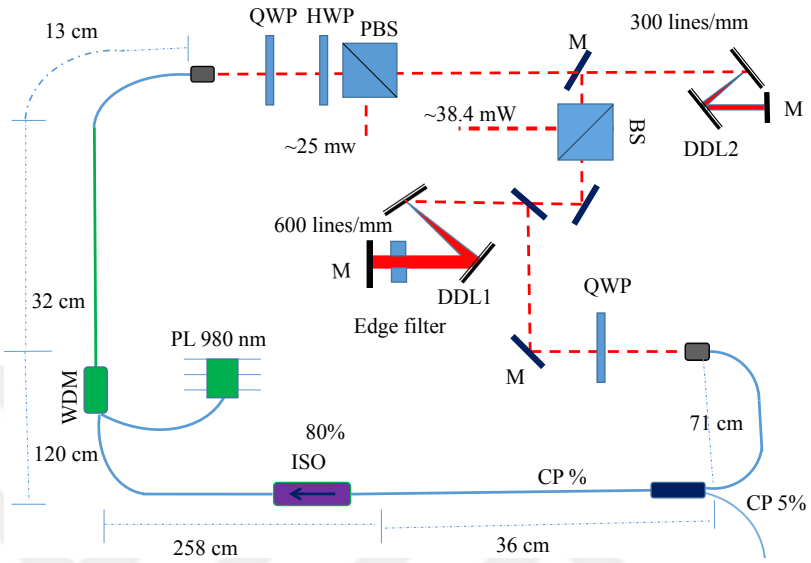

Figure 3.2: Schematic of the experimental setup: DDL-1 and DDL-2 (diffraction grating with 600 lines/mm and 300 lines/mm, respectively), M (mirror), PBS (polarizing beam splitter), QWP (quarter waveplate), HWP (half waveplate), CP (output coupler), ISO (isolator), BS (beam splitter), and PL (diod pump).

used to compress the pulses in the first step. Then, DDL-1 is adjusted so that the net value of the cavity dispersion remains the same. With such a procedure, we get 1.2 nJ, 62 fs and spectral width of 47 nm as shown in Fig. 3 (a and b). Nonlinear phase accumulation together with spatial chirp introduced with the DDL's and the TOD level of the cavity limited further compressibility of the pulse. The RF measurement shows 74-dB signal-to-noise ratio as shown on the inset of Fig. 3.3 (b). Different combinations of grating separation that can give the same net GVD have different values of the net TOD. This helps us tune the TOD level so that its interaction with SPM will be optimized as well as to achieve the shortest pulse duration as indicated in Fig. 3.3(c).

3.3 Conclusion

We were able to generate 1.2-nJ, 62-fs, linear-chirp-free pulse from a custom-designed fiber oscillator without requiring external compression. With the help of two diffraction grating we were able to tune the TOD level in the oscillator and

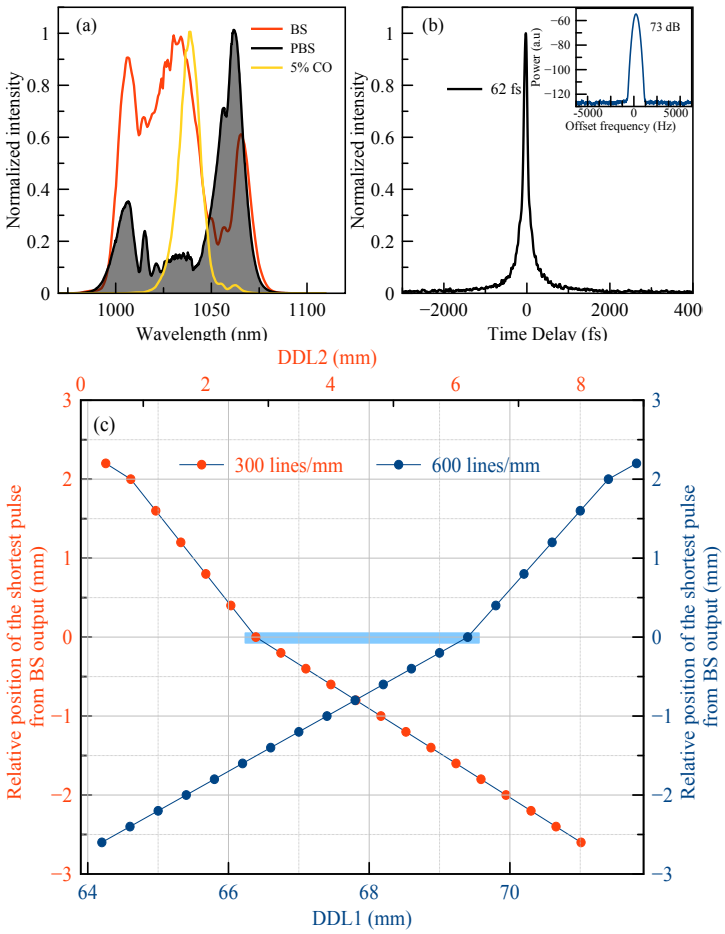

Figure 3.3: Experimental results: (a) Optical spectrum measured from theindicated ports. (b) Autocorrelation signal of the pulse measured from an output between the two DDLs, where optical spectrum indicated by the black line. (c) Relative DDL separations corresponding to the shortest pulse.

manipulate the dynamics such that position of the shortest pulse in the cavity is projected into the free space, in addition to demonstrating manipulation of the TOD-SPM interaction to some extend. The cavity was designed numerically according to a clear algorithm, the details of which will be reported elsewhere, and the methodology for finding the matching condition experimentally has been outlined. These results constitute a step forward in the design of advanced, custom oscillators that can exhibit almost any desired dynamics. Further efforts can incorporate other dynamics including extreme nonlinear broadening for ultrashort pulses, intra-cavity Cherenkov radiation generation for broadband spectral tunability and even intra-cavity higher harmonic wave generation, among others.

Chapter 4

Nonlinearity management in a fiber oscillator with two gain segments

4.1 Introduction

The earliest mention of compensating nonlinear effects in pulse propagation using negative Kerr nonlinearity dates back to 1996 [92]. The term of Nonlinearity Management (NLM) appears to have been coined simultaneously by Ilday, *et al.* [28] and Gabito, *et al.* [93], who proposed NLM for mode-locked oscillators and for optical transmission lines, respectively. NLM has then been considered in the context of layered media to prevent beam collapse [94, 95]. Fundamental interest into NLM has continued in parallel, in the context of preventing wave collapse [96].

Direct use of NLM in mode-locked lasers has been delayed owing to the difficulty of finding materials with negative (self-defocusing) nonlinear Kerr response and reasonably small loss. It has been demonstrated very recently using phase-mismatched cascaded quadratic processes [60], modifying the nonlinear

refractive index with external pressure for a cubic nonlinear medium [95], and through four-wave mixing [97], inverse wave mixing and self-parametric amplification [98]. Meanwhile, indirect forms of NLM have been successfully applied to mode-locked oscillators, including exploitation of nonlinearity-resistant pulse evolution mechanisms of self-similar (similariton) propagation [52, 99, 100], dissipative solitons solutions [101–103], using dissipative mechanism such as deliberate or non-intentional filtering like gain or edge filtering, control of nonlinear effects through spectral sculpturing [89]. However, there continues to be a strong desire for a versatile implementation of NLM, which requires materials with negative Kerr nonlinearity.

In this report, we designed and developed an oscillator with two gain segments for the purpose of managing nonlinearity accumulation and distribution inside fiber oscillators both in experiments and through numerical simulations, with our approaching being mainly based on the interaction of SPM with GVD in case of a chirped pulse. We found managing of nonlinearity strength, distribution, and the observation of effects of pulse chirp on its interaction with group velocity dispersion (GVD) to be relatively easier in this oscillator configuration than the usual fiber cavities that use a single active fiber. Intra-cavity spectral compression of the pulse after it passes through a second active fiber and $\sim 30\%$ reduction in the chirp (as judged by the corresponding decrease of required dispersion for dechirping in an external compressor) are observed following this interaction. This property is associated with the generation of an effective negative nonlinearity. The pulse continuously modifies itself when nonlinearity level and distribution is varied to keep the boundary condition as is the case with intra-cavity dispersion variation. In order to provide a deeper insight into the nature of pulse evolution interaction, we resort to simulations on a passive propagation system, which basically can be explained by the interaction of GVD and SPM without requiring complex gain dynamics. To the best of our knowledge, these results are completely original. The likely application of our design to passive propagation in amplifiers also suggests that a master oscillator and a pre-amplifier system can be constructed as a single, high-power, high-energy, compact laser source with reduced complexity than traditional designs.

4.2 Theory and numerical simulation

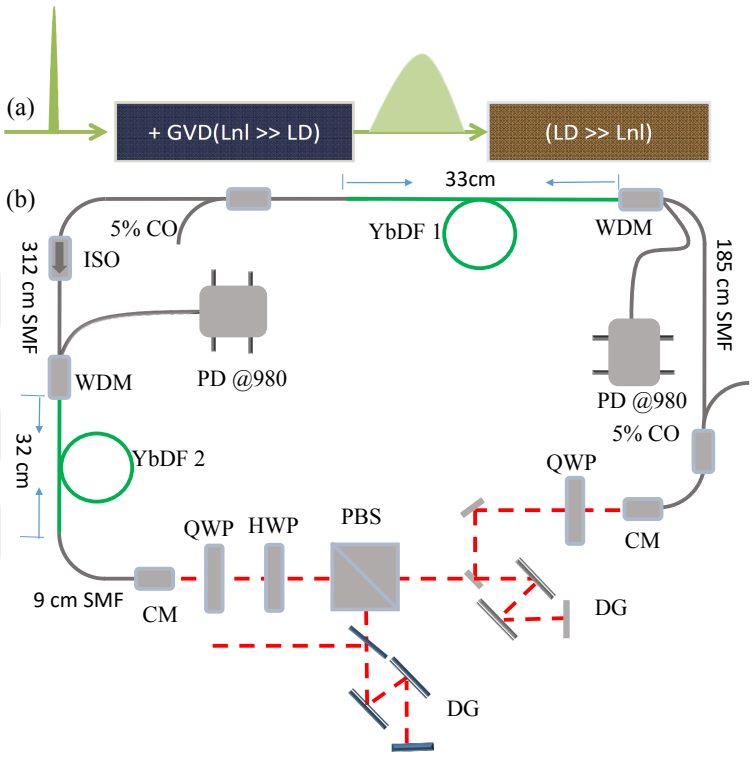

Figure 4.1: (a) Block diagram showing a pulse traversing a stretcher ($L_{nl} >> L_D$) and then through a nonlinear medium ($L_D >> L_{nl}$). (b) Schematic diagram of the experimental setup: PL, pump diode; CO, output coupler; WDM, wavelength-division multiplexer; YbDF, ytterbium-doped fiber; QWP, quarterwave plate; HWP, halfwave plate; ISO, isolator; M, mirror; DG, diffraction grating; PBS, polarizing beam splitter.

In addition to the well-known effects such as negatively chirped pulse propagation in a medium with normal dispersion, gain filtering [99, 100], self-parametric amplification [98], and phase mismatched second harmonic generation [60], SPM can cause spectral compression for a negatively chirped pulse in a medium with normal GVD. This theoretical model explains most of our experimental and simulation results based on the interaction of GVD and SPM on a chirped pulse similar to the results of [104, 105].

Consider a pulse passing through a stretching medium ($L_{nl} >> L_D$) before it passes a nonlinear segment ($L_D >> L_{nl}$), as shown in Fig. 4.1(a), in order

to qualitatively depict the effects of initial chirp on pulse propagation through nonlinear medium. In the first segment, pulse propagation is governed by the nonlinear Schrödinger equation of the form

$$i\frac{\partial U_1}{\partial Z} = \frac{\beta_2}{2}\frac{\partial^2 U_1}{\partial T^2}, \tag{4.1}$$

for which a chirped pulse solution is given by [48]

$$U_1(Z,T) = \frac{T_0}{(T_0^2 - i\beta_2 Z)^{\frac{1}{2}}} exp(\frac{-T^2}{2(T_0^2 - i\beta_2 Z)}), \tag{4.2}$$

where T_0 and β_2 are the input pulse widths and the GVD of the propagating segment. At the end of the first segment, the pulse and its intensity will be

$$U_1(T) = \sqrt{\frac{1}{1-i\eta}} exp(\frac{-T^2}{2T_0^2(1-i\eta)}), \tag{4.3}$$

$$|U_1(T)|^2 = I_0 exp(\frac{-T^2}{T_0^2(1+\eta^2)}) \cong I_0(1 - \frac{T^2}{T_0^2(1+\eta^2)}), \tag{4.4}$$

where $\eta = \frac{\beta_2 L_1}{T_0^2}$ and $I_0 = \sqrt{\frac{1}{1+\eta^2}}$ are stretching factors related to GVD and maximum intensity of the pulse at the end of the first segment, respectively. On the second segment, the pulse will experience a phase shift proportional to its intensity (SPM).

$$U_2(T) = U_1(T) exp(i\frac{L_{\text{eff}}}{L_{nl}}|U_1(T)|^2), \tag{4.5}$$

$$U_2(T) = \sqrt{\frac{1}{1-i\eta}} exp(\frac{-T^2}{2T_0^2(1+\eta^2)}(1 + i(2B+\eta)), \tag{4.6}$$

where L_{eff}, L_{D}, and $B = I_0\frac{L_{\text{eff}}}{L_{nl}}$ are the nonlinearity coefficient, effective propagation length, the dispersion length and the B-integral, respectively, defined in the same way as in [48]. In equation (4.4), the higher-order terms are neglected for simplicity because they do not contribute to the linear chirp. Contribution from a constant phase is also neglected in equation (4.6) by the same reasoning. The Fourier transform of equation (4.6) is given by

$$U_2(\omega) = \sqrt{2T_0^2\frac{1+i\eta}{1+i(2B+\eta)}} exp(\frac{-2\omega^2 T_0^2(1+\eta^2)}{(1+i(2B+\eta)}). \tag{4.7}$$

Table 4.1: Parameters of segments used for simulation results in Fig. 4.2(b)-4.2(e). Segment number (S.N), Length (L) [cm], GVD [fs^2/mm], TOD [fs^2/mm], Kerr coefficient with n_2 [10^{-16}-1 cm^2/W], Effective mode area (EMA) [μm^2], GBW gain band width and UG Unsaturated gain [dB].

S.N	L	GVD	TOD	n_2	EMA	GBW	UG
1	130	5 - 80	0	-	30	-	-
2	20	4	0	2.73	20	$\triangle\lambda$:40 nm	4

The imaginary part of the exponential function of equation (4.7) gives the total spectral phase,

$$\Phi_{total} = \frac{(2B+\eta)(1+\eta^2)T_0^2}{(1+(2B+\eta)^2)}. \tag{4.8}$$

Here, Φ_{total} is the total spectral phase accumulated at the end of the second segment. As shown in Fig. 4.2(a), it can be less than the stretching phase (Φ_{total} at $B = 0$) for a larger value of the normal GVD in the presence of nonlinearity. Effects of an increase in nonlinearity or B-integral in the second segment are more pronounced for stronger stretching of the pulse in the first segment for a medium with normal GVD. The stretching phase indicated by the black line ($B = 0$) decreases with increasing nonlinearity or B-integral up to a certain level. Its effect is the same as that of a compressor, which has opposite GVD to the stretcher, which is not physically present there. For a medium with negative GVD, the compensation of phase from the stretcher by phase coming from nonlinearity on the second segment is evident for a smaller value of stretching phase. Generally, the linear stretching effect of SPM is strong for highly chirped pulses for normal dispersion medium while the effect is strong for a slightly chirped pulse in an anomalous dispersion medium.

Figure 4.2(b)-4.2(e) shows the results of a numerical simulation based on solving generalized nonlinear Schrödinger equation with details mention in [47]. The parameters for these simulations are indicated in Table 4.1 and the simulations are intended for clarifying the qualitative description provided above. In Fig. 4.2(b), a 100 fs-long Gaussian-shaped pulse with 15 nm of spectral width is stretched in 130 cm-long SMF with normal GVD (5 fs^2/mm) and then it passes through a nonlinear segment, ending up with a spectral width of 44 nm. When the stretching element gets stronger and stronger (GVD of 10 fs^2/mm in Fig. 4.2(c), and 40

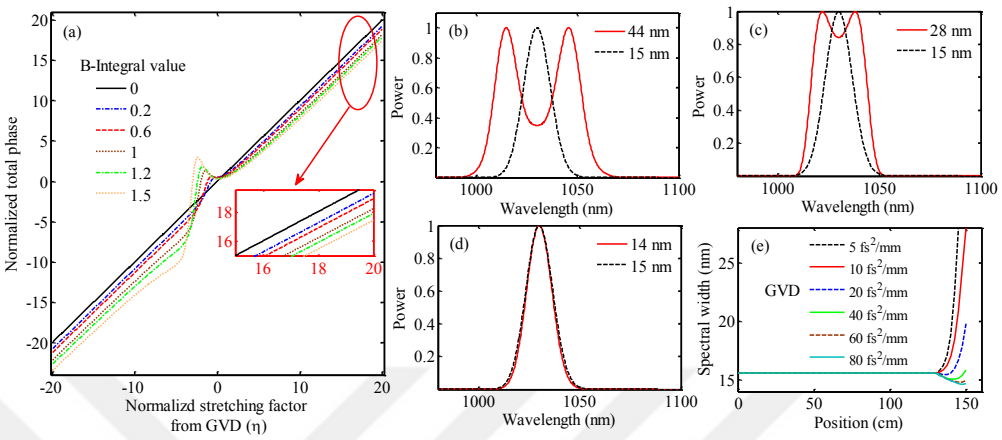

Figure 4.2: (a) Graph showing the interaction of phase contribution from GVD and SPM which results in a linear pulse chirp for corresponding values of the indicated B-integral. The optical spectra of the pulse at the end of the 130 cm-long stretching fiber (black dashed) and at the end of the 20 cm-long second nonlinear segment (red solid) for (b) 5 fs^2/mm), (c) 10 fs^2/mm, and (d) 40 fs^2/mm. (e) The evolution of the total spectral width in the two segments for the all simulation parameters provided in Table 4.1.

fs^2/mm in Fig. 4.2(d) spectrum width after the nonlinear element shrinks from 44 nm to 14 nm, as shown in Fig. 4.2(e). When the GVD of the first segment is large enough, the spectral width of pulse behaves as if it passes through a medium with negative GVD while the GVD of the second segment is still positive (4 fs^2/mm). Hence, one is justified to introduce an effective negative nonlinearity to explain the pulse compression in a such medium. We note that the nature of the nonlinearity is not such that it can directly compensate for positive nonlinearity, which is why it is referred to as an effective negative nonlinearity.

The above simulation ignores many of the effects that act on a pulse in real fiber systems. Next, we use two segments (passive fiber followed by gain fiber) with parameters similar to commercially available fibers, as indicated in Table 4.2. Fig. 4.3(a)-4.3(c) shows pulse propagation information for a 100-fs parabolic pulse when the first segment has normal GVD. Similar to the above result, as the chirp acquired by the pulse in the first segment increases (by scanning the GVD of passive fiber from 10 fs^2/mm to 120 fs^2/mm), spectral compression is induced or initiated in the gain or the nonlinear segment. Fig. 4.3(d)-4.3(f) also shows pulse propagation statistics for 100 fs parabolic pulse when the first

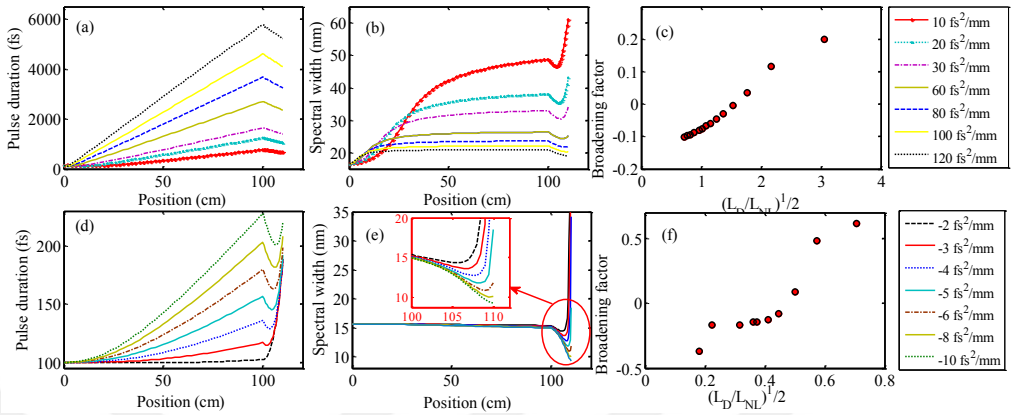

Figure 4.3: (a)-(c) The effect of chirp on spectral evolution when the pulse is stretched by normal GVD on the first segment. (d - f) The effect of chirp on spectral evolution when the pulse is stretched by anomalous GVD on the first segment. The corresponding simulation parameters are indicated in Table 4.2.

segment has anomalous GVD. Smaller negative GVD on the first segment shows stronger spectral broadening on the second nonlinear segment with normal GVD. This result is in agreement with a qualitative analytical result in Fig. 4.2(a). By varying the GVD of passive fiber from -2 fs^2/mm to -10 fs^2/mm spectral broadening is induced or initiated in the gain or nonlinear segment. When the GVD is -2 fs^2, one would expect that the spectral expansion is due to SPM since all the negative chirp acquired by the pulse in the first segment can be compensated within the second segment, which has normal GVD. Starting from -3 fs^2 the pulse remains negatively chirped in the second segment. Pulses with smaller net negative chirp experience increased spectral expansion.

This spectral compression in the first case (Fig. 4.3(a)-4.3(b)) or broadening in the second case (Fig. 4.3(d)-4.3(f)) cannot be explained unless one defines effective negative nonlinearity or it will contradict with well-known effects of nonlinearity on a chirped pulse which are expected to give contrary effects [48]. Two different parameters with different length and GVD but with the same dispersion (product of length and GVD) have the same impact. Nonlinearity can be also managed with the level of pumping on each segment.

It is well known that the distribution and not only the amplitude of nonlinear phase accumulation significantly alters the pulse evolution in a mode-locked

Table 4.2: Parameters of segments used for simulation results on Fig. 4.3. Segment number (S.N.); length (L) [cm]; GVD [fs^2/mm]; TOD [fs^3/mm]; Kerr coefficient with n_2 [10^{-16} cm^2/W]; effective mode area (EMA) [μm^2]; GBW, gain bandwidth; NLP, accumulated nonlinear phase; UG, Unsaturated gain (dB).

S.N	L	GVD	TOD	n_2	EMA	GBW	UG
1	100	10 - 120	28	2.73	40	-	-
2	10	23	28	2.73	5	$\triangle\lambda$:40 nm	20
1	100	-2 - -10	28	2.73	40	-	-
2	10	23	28	2.73	5	$\triangle\lambda$:40 nm	20

oscillator [99,102,106,107]. Manipulation of pulse dynamics by accumulated nonlinearity phase and its distribution in fiber can cause pulse dynamics that can also be described with the generation of controllable effective negative nonlinearity. When a pulse goes from a medium where it acquires relatively larger nonlinear phase (a medium with larger nonlinear refractive index) to a medium where it acquires smaller nonlinear phase (medium with smaller nonlinear refractive index) the pulse experiences an effective negative nonlinearity. Thus, it undergoes spectral compression for a positively chirped pulse on a normal dispersion segment. With the same approach, one can generate spectral expansion on anomalous dispersion segment. Generally speaking, one can manipulate pulse dynamics just by managing nonlinear distribution on individual segments of cascaded or connected fiber components.

Figs. 4(a)-4(c) shows simulation results for a pulse propagating through 7 connected passive and active fiber segments with parameters given in Table 4.3. The nonlinear phases accumulated in each segment are 0.71π, 0.18π, 1.11π, 0.03π, 4.42π, 0.42π, and 3.56π, respectively. The pulse undergoes spectral compression in regions where the accumulated nonlinear phase (SPM) is relatively smaller than that of immediate neighbors. This clearly indicates that the pulse propagation is not only sensitive to the level of accumulated nonlinear phase but also to the way it is distributed in each of the propagating media. This observation can be explained with the above argument where the phase by positive GVD is counterbalanced by the phase from SPM for chirped pulse. Gain filtering and other recently mentioned nonlinear effects such as self-parametric amplification [98] and phase mismatched second harmonic generation [60] can result similar

Table 4.3: Parameters of segments used for simulation results on Fig. 4.4. Segment number (S.N), Length (L) [cm], GVD [fs^2/mm], TOD [fs^3/mm], Kerr coefficient with n_2 [10^{-16} cm^2/W], Effective mode area (EMA) [μm^2], GBW gain band width, NLP accumulated nonlinear phase and UG Unsaturated gain (dB).

S.N	L	GVD	TOD	n_2	EMA	GBW	NLP	UG
1	150	23	28	2.73	5	-	0.71π	-
2	50	23	28	2.73	5	$\triangle\lambda$:40 nm	0.18π	20
3	200	23	28	2.73	9	-	1.11π	-
4	3	23	28	3.73	5	$\triangle\lambda$:40 nm	0.03π	30
5	200	23	28	2.73	20	-	4.42π	-
6	23	23	28	1	100,	$\triangle\lambda$:40 nm	0.42π	20
7	90	23	28	2.73	35	-	3.56π	

effects. It is obvious that understanding the whole dynamics is difficult because of complexity of interaction of all physical processes. But no matter the individual interactions there, the resulting dynamics can be equivalently explained with interaction of generated effective negative nonlinearity.

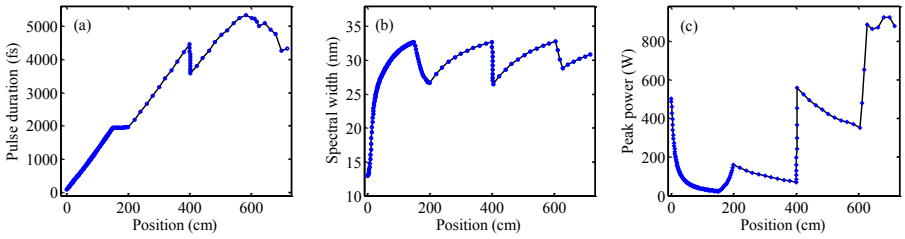

Figure 4.4: (a)-(c) The effect of nonlinear distribution on pulse evolution.

Our third set of simulation results expand the above idea to oscillator dynamics. Namely, we show that two qualitatively distinct oscillator dynamics can be supported by the same dispersion managed oscillator with double gain segments. These results are used to guide our experiments, which will be presented in the next section. Fig. 4.5(a) shows a dynamics which generally can be considered as stretched pulse dynamics [102] except in the gain segments. Simulation parameters are indicated in Table 4.4. The pulse undergoes negligible spectral compression in the passive fiber just after the DDL until all of its negative chirp is compensated. Next, it acquires a little positive chirp, followed by rapid spectral expansion in the gain fiber with normal dispersion and the SMF fiber, also with normal dispersion, after it. Saturable absorber reduces the pulse duration and

the spectral width. Finally, the spectral width remains the same while the chirp increases in opposite sign on the DDL to return to its original form at the end of one roundtrip, thereby satisfying the periodic boundary condition.

The second set of dynamics are shown in Fig. 4.5(b). This evolution can be supported by the same physical oscillator (with parameters indicated in Table 4.5) as the one explained above. Their only difference is the gain segments, the nonlinearity of which may controlled with pump level in experimentally. In this case, the pulse acquires a positive chirp with evolution that can be considered as a passive similariton evolution in the passive fiber part of the oscillator [102]. This chirp will be partially or fully compensated in the DDL (compressor) of the cavity. We also observe that one can switch from one evolution regime to the other by only varying the nonlinearity and its distribution on the gain segments of the oscillator the same way one can achieve by varying GVD of the system and its distribution [106, 108, 109].

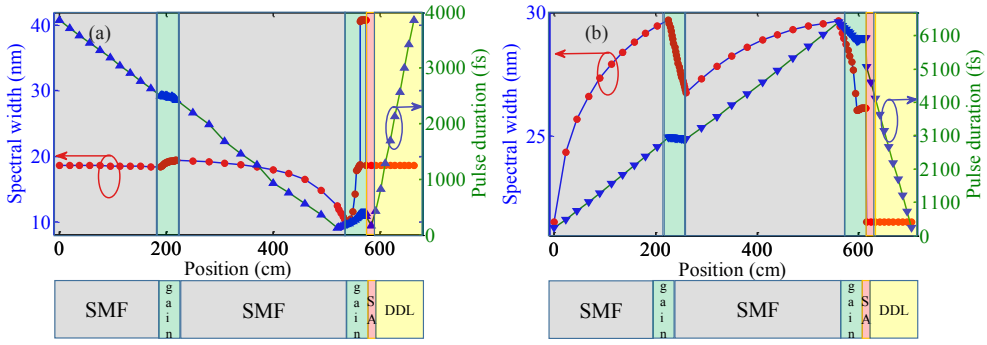

Figure 4.5: Simulation results of pulse evolution inside a cavity with approximately the same parameters as the oscillator in our experiments described in the next section: (a) Spectral and temporal evolution of a pulse that can be considered as a stretched dissipative soliton. (b) Spectral and temporal pulse evolution that can be considered as passive similariton pulse dynamics with parameters indicated in Table 4.4 and Table 4.5, respectively.

The above explanation is a general approach to the whole dynamics. An explicit investigation is important based on the concepts mentioned for linear systems above specifically on the active part of the cavities. Spectral compression takes place in the gain fibers while the opposite is expected on gain section 2 of Fig. 4.5(b). The pulse evolves in the first gain segment as if the chirp from

Table 4.4: Parameters of segments used in simulation for the first oscillators (Fig. 4.5(a)). Segment number (S.N.); length (L) [cm]; GVD [fs^2/mm]; TOD [fs^3/mm]; Kerr coefficient with n_2 [10^{-16} cm2/W]; effective mode area (EMA) [μm^2]; GBW, gain bandwidth; unsaturated gain (dB); EG, effective gain saturation energy [nJ]; SA, saturable absorber.

S.N	L	GVD	TOD	n_2	EMA	GBW	UG	EG	SA
1	190	23	28	2.73	30	-	-	-	-
2	30	23	28	2.73	30	$\triangle\lambda$:40 nm	20	4000	-
3	300	23	28	2.73	30	-	-	-	-
4	37.0	23	28	2.73	15	$\triangle\lambda$:40 nm	10	4	-
5	9	23	28	2.73	30	-	-	-	-
6	10	-	-	-	30	-	-	-	NPE
7	8.9	-1420	250.6	-	30	-	-	-	-

Table 4.5: Parameters of the segments used in the simulations for the first oscillator (Fig. 4.5(b). Segment number (S.N.); length (L) [cm]; GVD [fs^2/mm]; TOD [fs^3/mm]; Kerr coefficient with n_2 [10^{-16} cm^2/W]; effective mode area (EMA); [μm^2]; GBW, gain bandwidth; unsaturated gain (dB); EG, effective gain saturation energy [nJ]; SA, saturable absorber.

S.N	L	GVD	TOD	n_2	EMA	GBW	UG	EG	SA
1	190	23	28	2.73	30	-	-	-	-
2	32	23	28	2.73	15	$\triangle\lambda$:40 nm	20	4000	-
3	300	23	28	2.73	30	-	-	-	-
4	37.0	23	28	2.73	15	$\triangle\lambda$:40 nm	10	4	-
5	8	23	28	2.73	30	-	-	-	-
6	10	-	-	-	30	-	-	-	NPE
7	8.9	-1420	250.6	-	30	-	-	-	-

GVD of this fiber is compensated by the chirp from SPM. The chirp even starts to decrease on the second gain fiber since the effects of SPM are more prominent for largely chirped pulse in normal regime. Moreover, slight spectral expansion occurred while the chirp was negative in the first gain fiber of Fig. 4.4(a). Temporal evolution shows that the pulse propagated in the gain medium with chirp by GVD from it is almost completely compensated by the chirp from SPM. Meanwhile, the pulse enters to the second gain with very small positive chirp, hence spectral expansion takes place as expected. These results are in total agreement with results of interaction of physical processes explained in the theoretical and numerical simulations results above. Thus it can be explained with the generation of an effective negative nonlinearity. Effective negative nonlinearity creates spectral broadening in the first gain segment of Fig. 4.5(a) while chirp is negative and it creates spectral compression in the two gain segments of Fig. 4.5(b), while the chirp is positive.

4.3 Experimental results

Schematic diagram of the experimental setup of the oscillator is provided in Fig. 4.1(b). It is a dispersion-managed fiber oscillator with two gain segments. Mode-locking is initiated and stabilized by nonlinear polarization evolution (NPE). It has a repetition rate of ∼26 MHz with approximately 675 cm of total length of fiber. The two gain segments are comprised of Yb-doped gain fibers with a length of 33 cm and 32 cm each. The gain bandwidth of the Yb-1200/125/6 μm core diameter, singlemode fiber is approximately 45 nm for the typical pump powers used in these experiments and the gain is centered at a wavelength of 1025 nm. They are forward pumped by 980 nm laser diodes. Diffraction gratings are used for dispersion management inside the cavity. Three mode-locked regimes with a net total dispersion of ∼-4000 fs^2, 600 fs^2, and 3800 fs^2 are examined to characterize the cavity pulse evolution. Each support two distinct, stable and self-starting pulse evolutions. Based on the pulse evolution characteristics, they can be considered as passive similariton and stretched pulse evolutions [106, 107].

In our experiments, the pump levels of the two segments of the gain fiber were varied such that the total pump power remained almost constant whereas nonlinearity varied both in level and distribution across the oscillator. This experiment has three major outcomes: (**i)** The oscillator exhibits stable self-starting mode-locking in all regimes with reasonable signal-to-noise ratio (sideband suppression of $\sim 65dB$, measured by an RF spectrum analyzer over 1 kHz scanning range with a resolution bandwidth of 10 Hz). Thus, it can be used as a stable, low-noise source of femtosecond pulses, but this is not our intention in this experiment. (**ii)** Output pulse was compressed to almost the same pulse width with different external DDLs as the pump powers on the two gain segments were varied, keeping the total pump power almost constant while nonlinearity was alterted both in magnitude and distribution inside the cavity. (**iii)** Spectral width after gain segment 2 was observed to be smaller than the spectral width of its input in all the three regimes even if input band width is below the band width of the gain fiber as shown in Figs. 6(a)-6(c). This observation forces one to raise a question on whether gain narrowing is the only process responsible for narrowing the spectrum after the second gain fiber (gain section 2). In fact, recent results show that spectral narrowing in normal regime can take place due to a nonlinear process called self-action such as inverse four mixing and self-parametric amplification [98]. report on the realization of de-focusing structures by using phase mismatched second harmonic generation inside a solid state laser further supports our idea of defining effective negative nonlinearity which is also qualitatively explained in the theory and numerical simulation parts as well. Note that: The spectral intensity is taken from spectrum analyser and divided by the power of corresponding ports then, the spectral intensity from PBS and 5 % coupler before gain 1 are added and the full width at half maxima of this spectrum is compared with the full width at half maxima of spectrum from the 5 % coupler after gain segment 1 for the comparison, according to all of our measurements.

Subject to normal dispersion, the spectral evolution is relatively less sensitive to the dispersion map as shown in Fig. 4.6(c). Spectral width evolution experiences relatively smaller spectral compression and broadening in this regime [101]. The pulse width of ∼5.8 ps from the PBS port was compressed to ∼110 fs, which

is very close to its transform limited duration. The pulse acquires a chirp larger than the net GVD of the cavity. It can be pumped to the full capacity of the two diodes without multi pulsing. The spectrum starts to become steeper on the edges as a result of SPM when the cavity is more pumped in the gain section 2 [101, 105]. It is less sensitive to pumping of gain segment 1. We have done our experiment of nonlinearity management in this passive similariton evolution regime not only for its tolerance to larger nonlinearity, but also because the spectral phase of such a pulse can optimally compensate the stretching phase coming from the positive GVD [102, 105].

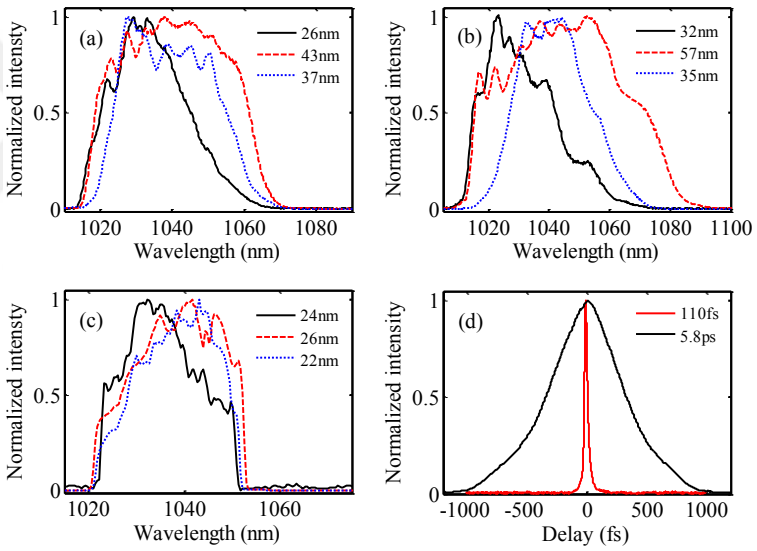

Figure 4.6: (a)-(c) Optical spectra for different regimes taken from the 5% output coupler before gain section 1 (blue dotted), 5% output coupler after gain section 1 (red dashed), and the PBS output (black solid) when the net dispersion of the oscillator is $\sim$ -4000 fs^2, $\sim$+600 fs^2 and $\sim$+3800 fs^2, respectively. (d) Pulse duration before and after compression at the optimized interaction point in the normal regime.

The pump for gain segment 2 was decreased from 328 mW to 5 mW, as shown in Fig. 4.7 (increased from 98 mW to 400 mW, as shown in Fig. 4.8), while pump for gain segment 1 was increased from 378 mW to 746 mW, as shown in Fig. 4.7 (decreasing from 950 mW to 660 mW, as shown in Fig. 4.8) via small intervals. We ensured that the total pump power remained almost the same, while allowing the nonlinearity to change both in amplitude and in terms of its distribution, as shown in Fig. 4.7(a) and 4.7(d) (Fig. 4.8(a) and 8(d)). The experiment was

conducted first with conditions indicated in Fig. 4.7 until mode-locking was gone and then the mode locking was obtained by increasing pump 2 and decreasing pump 1 until the minimal conditions for mode-locking was reached. For these experiments, the nonlinearity is estimated as the sum of $\frac{2\pi}{\lambda_0 A_{\text{eff}}} n_2 \int_0^L P_{\text{p}} dz$ for the passive SMF part and $\frac{2\pi}{\lambda_0 A_{\text{eff}}} n_2 \int_0^L P_{\text{avg}} dz$ for the active fiber sections, where P_{p} and $P_{\text{avg}} = \frac{1}{2}(P_{\text{pi}} + P_{\text{pf}})$ are the peak power and average peak power respectively. Spectral width after gain segment 2 was observed to change from 16.5 nm to 21 nm (14 nm to 21 nm). Pulse duration from the PBS output, passing through a fixed DDL also varied from ∼140 fs to ∼215 fs (from ∼132 fs to ∼305 fs) mainly as a result of the effects of accumulated nonlinear phase shift from SPM, its distribution, its interaction with normal GVD for a chirped pulse and the resulting effects of polarization evolution due to repositioning of the pulse to maintain the boundary conditions [106, 110–112]. From Fig. 4.7(e) (Fig. 4.8(e)), one can conclude that the spectral width is larger for shorter pulse duration but this can be recompressed to ∼140 fs (∼130 fs) with ∼ 20%(∼ 30%) smaller external DDL. This shows that uncompensated SPM in the process results in spectral broadening. Spectral width is smaller for most pulses with larger nonlinear phase as shown in Fig. 4.7(c) or it remains almost the same for some conditions as in the case of Fig. 4.8(c). This is apparently in contradiction with spectral broadening by SPM. This shows part of the accumulated nonlinear phase is compensated in the interaction process with phase due to normal GVD. The fact that the pulse often has broader bandwidth when pumping in gain segment 2 is larger as seen in Fig. 4.7(f) and 4.8(f) is also an indication that the interaction is sensitive to the nonlinear phase distribution and the spectral width narrowing is not related to gain filtering as well. SPM accumulated in gain segment 2 ends up broadening the optical spectra.

Most of the nonlinear phase is expected to be accumulated in the passive fiber between the two gain fibers. Nonlinearity is high when pumping of gain segment 1 is relatively larger. This is an indication of that the spectral broadening in gain segment 2 is not solely related to the level of accumulated nonlinear phase (SPM). As indicated in Fig. 4.7(f) (Fig. 4.8(f)), these can be equivalently explained with the following: **(i)** When pump of gain section 1 increases, the nonlinear phase

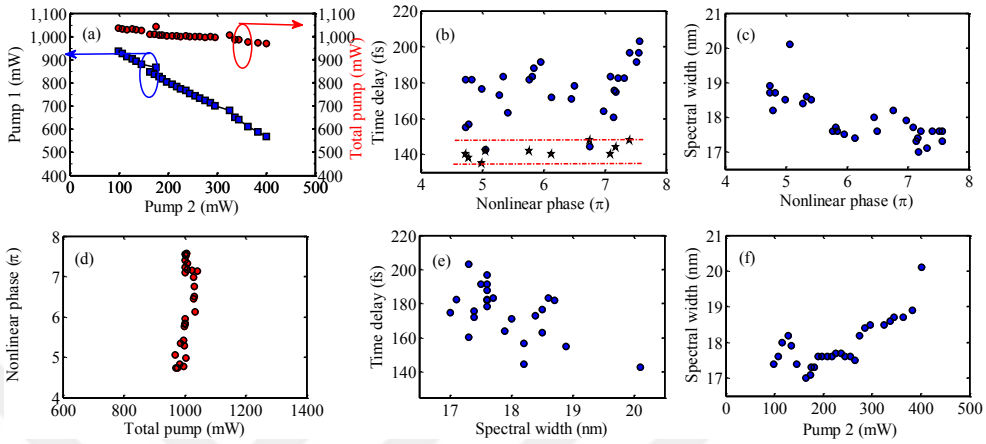

Figure 4.7: The experimental result showing a relationship between (a) variation of the two pump powers and the total pump; (b) nonlinear phase shift with pulse duration (each pulse duration can be compressed to the region between the red lines); (c) nonlinear phase shift with spectral width; (d) nonlinearity with total pump power; (e) pulse duration with spectral width and (f) spectral width with pump power of gain section 2, when pump 1 is increasing and pump 2 is decreasing.

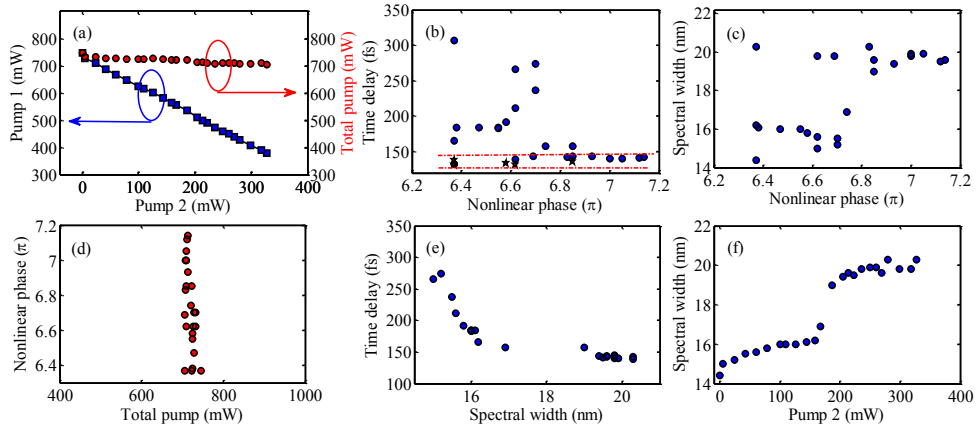

Figure 4.8: The experimental result showing a relationship between (a) variation of the two pump powers and the total pump; (b) nonlinear phase shift with pulse duration (each pulse duration can be compressed to the region between the red lines); (c) nonlinear phase shift with spectral width; (d) nonlinearity with total pump power; (e) pulse duration with spectral width and (f) spectral width with pump power of gain section 2, when pump 1 is decreasing and pump 2 is increasing.

interacts with the dispersive phase shift due to longer fiber (interaction) length. Hence, it is possible for the effects of the nonlinear phase accumulation to be offset by the effects of GVD. While pumping gain 2 harder, it is more difficult to compensate the nonlinearity due to relatively shorter fiber length or more accurately, shorter interaction length. This can be seen from the relatively larger spectral width changes in Fig. 4.8(f) relative to Fig. 4.7(f) even though the total pump power is larger in the first case. Note that nonlinear phase and stretching phase due to GVD interact in an optimized way. Excess of nonlinearity causes spectral broadening. (**ii)** It can also be explained in terms of nonlinearity distribution on the two active fibers and passive fiber in between them. The collective effect of pulse propagation as it experiences high and low nonlinearity interfaces generates an effective negative nonlinear index. Hence spectral compression takes place for a positively chirped pulse on a medium of positive GVD similar to our simulation results. As we increase pumping on gain section 2 we are increasing the nonlinearity or the difference in nonlinearity in comparison to the adjacent segments decreases, thus effective negative nonlinearity decreases and spectral compression decreases or relative spectral broadening takes place as result.

4.4 Conclusion

We showed in simulation and experiment that pulse propagation can be managed through manipulation of nonlinearity level, distribution and its interaction with GVD on chirped pulses. Experimentally, we managed to reduce up to $\sim 30\%$ of the dispersion required for external compression of the pulses just by varying nonlinearity level and distribution inside the novel cavity. The dynamics is explained qualitatively by defining an effective negative nonlinearity. Collective behavior of sequentially arranged passive (dispersive) and active (nonlinear) fibers generated an effective negative nonlinearity such that pulse compression can take place while the opposite is expected and vice versa. This was explained as a result of interaction between pulse chirp, dispersion, SPM and its distribution. The experimental observations are consistent with these explanations. Although the complexity of oscillator dynamics make it very difficult to exactly follow the

interaction process, the experimental results support the merit of regarding the observed effects as an effective negative nonlinearity. Such a perspective is useful not only because it qualitatively explains the observed dynamics, but also because it provides new perspectives, such as the evolution of the pulse towards the similariton attractor from the soliton attractor and vice versa at the interfaces of the soliton-similariton laser [47]. These results are reminiscent of the well known generation of effective negative (and positive) Kerr nonlinearities from cascaded phase-mismatched quadratic nonlinear processes.

Chapter 5

Linear and nonlinear response of mode-locking to injected intensity modulation and noise

5.1 Introduction

Spontaneous emergence of structure and pattern formation is ubiquitous in dissipative and nonequilibrium systems and numerous such systems have been identified and analyzed [113–116]. However, despite significant advances over the recent decades, an overarching theory that can predict the outcome of such system, short of actually running the systems either experimentally or numerically, remains a distant goal. Mode-locking of lasers [117] falls within this broad category (also lacking a general theory that would allow one to calculate a priori a specific combination of optical segments that would give rise to the mode-locked operation of desired properties). At the same time, mode-locking also stands out in the sense that it is not a natural phenomenon, but has broad scientific, industrial and medical applications. In addition, unlike most natural systems, we have very well-developed capabilities at our disposal for controlling the dynamics and its characterization. Studying of mode-locking dynamics is interesting from

a fundamental point of view and a new understanding typically leads to broad technical impact. This is particularly true for fiber lasers, where the guided propagation of pulses leads not only to exceptionally strong nonlinear effects, but also underlies the desirable practical features, such as robustness and compact size of these lasers [118, 119].

Despite its evident importance when one regards a mode-locked laser as a dissipative system far from equilibrium, the evolution of fluctuations (i.e., noise) in mode-locked lasers [120, 121] has received much less attention than the stationary characteristics of mode-locking, such as pulse duration, energy, and power. In the existing studies, the focus was often on its consequences for a specific application such as frequency combs [120]. Here, we report the influence of externally injected intensity noise or modulation on the dynamics of mode-locking, including transitions between meta stable mode locking states. We analyse and distinguish two cases: (i) the near-equilibrium case, where the response of the laser to injected noise is essentially linear and (ii) the far-from-equilibrium case, where the laser responds nonlinearly, with noise initiating multi-pulsing, energy competition between pulses forming bound states, bound states with hopping phase difference or dynamic variation of pulse separation.

Our method of injection of noise is through the pump laser due to its experimental convenience. However, a strong filtering effect of the relatively long gain relaxation lifetime, this approach limits our study to the low-frequency range (below 200 kHz). From an applications point of view, noise transfer from a pump laser to a mode-locked laser has well-appreciated negative consequences. Intensity noise below resonant relaxation oscillation frequency of lasers is dominated by pump noise, arising from a various physical effects [122–125]. Various theoretical and experimental approaches have been followed to predict the influence of pump noise on laser noise, and a noise or modulation transfer function (MTF) is commonly used to characterize this phenomenon [126–128]. J. McFerran, *et al.* modeled linear or one-to-one coupling of pump intensity noise to signal intensity noise [129], whereas K. Wu, *et al.* reported linear and nonlinear coupling of pump modulation to signal for an Er-doped fiber laser, which was mode-locked with carbon nanotubes but the origin of the nonlinear response, intra-cavity noise

dependence and its extension to all different mode-locking regimes were not explored.

Much more importantly, while useful and highly intuitive, an MTF-based approach intrinsically assumes (nearly) linear response. Therefore, it is applicable only to stochastic dynamics near the steady state of the laser, which we refer to as near-equilibrium dynamics following the terminology of statistical physics [40, 130]. Using this approach, we first have analyzed the linear dynamical response of all-normal-dispersion, near-zero-dispersion (stretched pulse), and dispersion-managed soliton mode-locking regimes to pump modulation, where the modulations are weak enough and the laser is in a stable enough state that it does not deviate from this linear regime and the MTF approach suffices. Next, we have investigated the case where the externally induced modulation is strong enough to drive the laser system further away from its steady state, or some cases, into a different state. In this regime, the pulse propagation dynamics change qualitatively and the response is no longer linear. This constitutes far-from-equilibrium dynamics [40, 130] and a description based purely on the MTF becomes inadequate.

5.2 Modulation transfer: simulation and experimental results

We have constructed a generic and easily reconfigurable Yb-doped fiber laser oscillator for this study. Schematic of the laser oscillator and the measurement setup are shown in Fig. 5.1. The oscillator operates at a repetition rate of 44 MHz and comprises 350 cm-long passive fiber and 23-cm long gain fiber. It is pumped by a temperature and wavelength stabilized single-mode diode operating at 976 nm through a wavelength division multiplexer (WDM). A standard dispersive delay line (DDL) incorporating a pair of gratings with 600 l/mm is included to control the total dispersion of the cavity and to switch between mode-locking regimes. In the case of all-normal dispersion operation, the DDL is replaced by a

bandpass filter centered at 1030 nm and with a bandwidth of 10 nm (not shown in the figure for clarity). A signal generator (33220A, Agilent, Inc.) is employed to modulate the current of the pump power over the frequency range of 3 Hz - 250 kHz. In this frequency range, the modulation is directly transferred to the optical power from the diode, thus into pump power for the laser oscillator. Optical output from the cavity is converted to an electrical signal with an amplified silicon photodetector (PDA-10A-EC, Thorlabs, Inc.), and analyzed with an audio (baseband) analyzer (UPV, Rodhe and Schwarz, Inc.). In addition, an optical spectrum analyzer (MS9740A, Anritsu Corporation) and a long-range autocorrelation (FR-103HS, Femtochrome Research, Inc.) are used as standard characterization techniques.

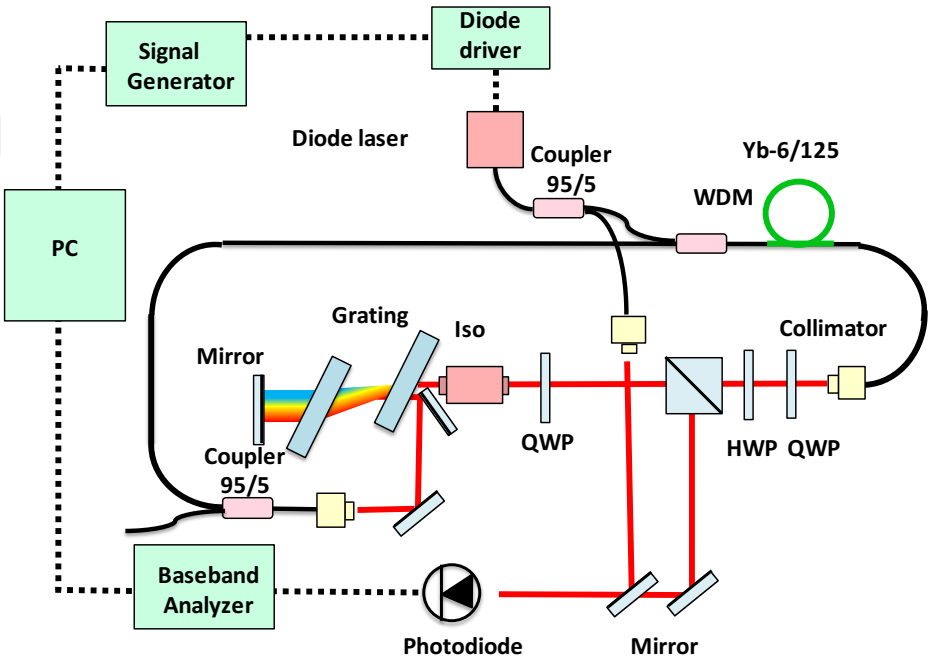

Figure 5.1: Experimental setup: Schematic diagram of experimental set up. WDM, wavelength division multiplexer; QWP (HWP) quarter (half) wave plate; ISO, isolator.

A simple theoretical model is used to predict the transfer random fluctuations or coherent modulations of the pump to the laser power. In this model, we consider gain, linear loss and nonlinear loss occurring at the saturable absorber. Pulse shaping physical effects such as Kerr nonlinearity or dispersion are not considered

explicitly although the saturable absorber indirectly does since the particular implementation that we use, nonlinear polarization rotation, depends on nonlinear phase accumulated in the fiber. In the near-equilibrium limit, where the MTF description is adequate, there is the negligible effect of one frequency component on another. As a result, both random fluctuations over a broad frequency range and narrow, coherent modulations at specific frequencies are well described by this approach. In this model, we consider the dynamical response of a cavity to be linear (the modulation frequency of the signal is the same as the pump), even though the nonlinear response of the cavity to any given modulation is taken into account. To this end, the oscillator is modeled as comprising an amplifier, linear loss and nonlinear loss (saturable absorber), whereby a portion of the output is fed back to the system after passing through the nonlinear segment described by a nonlinear transmission function describing the saturable absorber. Then, the modulation on pump and population density for a given angular frequency, ω, at a position, z, along the gain medium, and during the m^{th} round trip, can be written as,

$$
\begin{aligned}
i_{\mathrm{p},(m)}(z,t) &= I_{\mathrm{p}}(z)(1+q_{\mathrm{p},(m)}(z,\omega)\mathrm{e}^{i\omega t})+c.c., && (5.1)\\
i_{\mathrm{s},(m)}(z,t) &= I_{\mathrm{s}}(z)(1+q_{\mathrm{s},(m)}(z,\omega)\mathrm{e}^{i\omega t})+c.c., && (5.2)\\
n_{1,(m)}(z,t) &= N_1(z)(1+q_{1,(m)}(z,\omega)\mathrm{e}^{i\omega t})+c.c., && (5.3)\\
n_{2,(m)}(z,t) &= N_2(z)(1+q_{2,(m)}(z,\omega)\mathrm{e}^{i\omega t})+c.c.. && (5.4)
\end{aligned}
$$

Here, $i_{\mathrm{p},(m)}(z,t)$ and $i_{\mathrm{s},(m)}(z,t)$ are the time-dependent and $I_{\mathrm{p}}(z,t)$ and $I_{\mathrm{s}}(z,t)$ are the average (or modulation-free) values of pump and signal intensities, respectively. Likewise, $n_1(z,t)$ and $n_2(z,t)$ are the time-dependent and $N_1(z,t)$ and $N_2(z,t)$ are the average (or modulation-free) values of the fractional population densities of the upper and lower states. $q_{\mathrm{p},(\mathrm{m})}(z,\omega)$ and $q_{\mathrm{s},(\mathrm{m})}(z,\omega)$ present the amplitude of the intensity modulation for pump and signal respectively. $q_{1,(\mathrm{m})}(z,\omega)$ and $q_{2,(\mathrm{m})}(z,\omega)$ denote the amplitude of the fractional population density for pump and signal respectively and *c.c.* denotes complex conjugate. Eqn. (5.1) to (5.4), along with the coupled equations for the laser rate equations and population densities [48] yield the signal amplitude modulation at the end of the gain

segment as follows:

$$q^{'}_{\mathrm{s},(m)}(L,\omega) = \frac{\delta i^{'}_{\mathrm{s},(m)}}{i^{'}_{\mathrm{s},(m)}} = \xi_{\mathrm{s},(m)}(\omega) q_{\mathrm{s},(m)}(0,\omega) + \xi_{\mathrm{p},(m)}(\omega) q_{\mathrm{p}}(0,\omega). \tag{5.5}$$

Here, the individual MTF of the amplifier for pump and signal are defined as follows, respectively.

$$\xi_{\mathrm{p},(m)}(\omega) = \frac{q_{\mathrm{s},(m)}(L,\omega)}{q_{\mathrm{p}}(0,\omega)}, \tag{5.6}$$

$$\xi_{\mathrm{s},(m)}(\omega) = \frac{q_{\mathrm{s},(m)}(L,\omega)}{q_{\mathrm{s},(m)}(0,\omega)}. \tag{5.7}$$

Where L is length of gain fiber. Let p_m be the intra-cavity laser signal power at a point right before the saturable absorber for the m^{th} roundtrip. The nonlinear transmittance of the saturable absorber is introduced, $T(p_m)$. The output power, $p^{''}_m$, after the saturable absorber is given by,

$$p^{''}_m = T(p_m) p_m. \tag{5.8}$$

Next, we make a power series expansion of T in terms of p_i and keep the linear and quadratic terms to obtain the amplitude of modulation after passing through the saturable absorber as follows,

$$Q_{\mathrm{s},(m)} = [\xi_{\mathrm{s},(m)}(\omega) q_{\mathrm{s},(m)} + \xi_{\mathrm{p},(\mathrm{m})}(\omega) q_{\mathrm{p}}] - \beta [\xi_{\mathrm{s},(m)}(\omega) q_{\mathrm{s},(m)} + \xi_{\mathrm{p},(m)}(\omega) q_{\mathrm{p}}]^2, \tag{5.9}$$

Where β is a constant related to the power series. The output signal, which is re-launched into the amplifier for the next round trip, is subject to the following boundary condition in order for stable pulsation that repeats itself after each roundtrip,

$$Q_{\mathrm{s},(\mathrm{m})}(L,\omega) = q_{\mathrm{s},(\mathrm{m}+1)}(0,\omega). \tag{5.10}$$

By considering $\xi_{\mathrm{s},(\mathrm{m})} = |\xi_{\mathrm{s},(\mathrm{m})}| e^{i\phi_{\mathrm{s},(\mathrm{m})}}$ and $\xi_{\mathrm{p},(\mathrm{m})} = |\xi_{\mathrm{p},(\mathrm{m})}| e^{i\phi_{\mathrm{p},(\mathrm{m})}}$ the amplitude of intensity modulation can be expressed as the following recurrence relation,

$$q_{\mathrm{s},(\mathrm{m}+1)} = a q^2_{\mathrm{s},(\mathrm{m})} + b q_{\mathrm{s},(\mathrm{m})} + c. \tag{5.11}$$

Here, $a = -\beta|\xi_{\mathrm{s},(m)}|^2 e^{2i\phi_{\mathrm{s},(m)}}$, $b = \xi_{\mathrm{s},(m)} = |\xi_{\mathrm{s},(m)}|e^{i\phi_{\mathrm{s},(m)}}(1 - 2\beta q_{\mathrm{p}}|\xi_{\mathrm{p},(m)}|\mathrm{e}^{i\phi_{\mathrm{p},(m)}})$, and $c = q_{\mathrm{p}}|\xi_{\mathrm{p},(m)}|\mathrm{e}^{i\phi_{\mathrm{p}}}(1 - \beta q_{\mathrm{p}}|\xi_{\mathrm{p},(m)}|\mathrm{e}^{i\phi_{\mathrm{p},(m)}})$. Therefore, the steady-state MTF of the laser oscillator has to be evaluated as the limit of infinitely many roundtrips,

$$\xi_{\mathrm{s}}(\omega) = \lim_{m\to\infty} |\frac{q_{\mathrm{s},(m)}(L,\omega)}{q_{\mathrm{p}}}|. \tag{5.12}$$

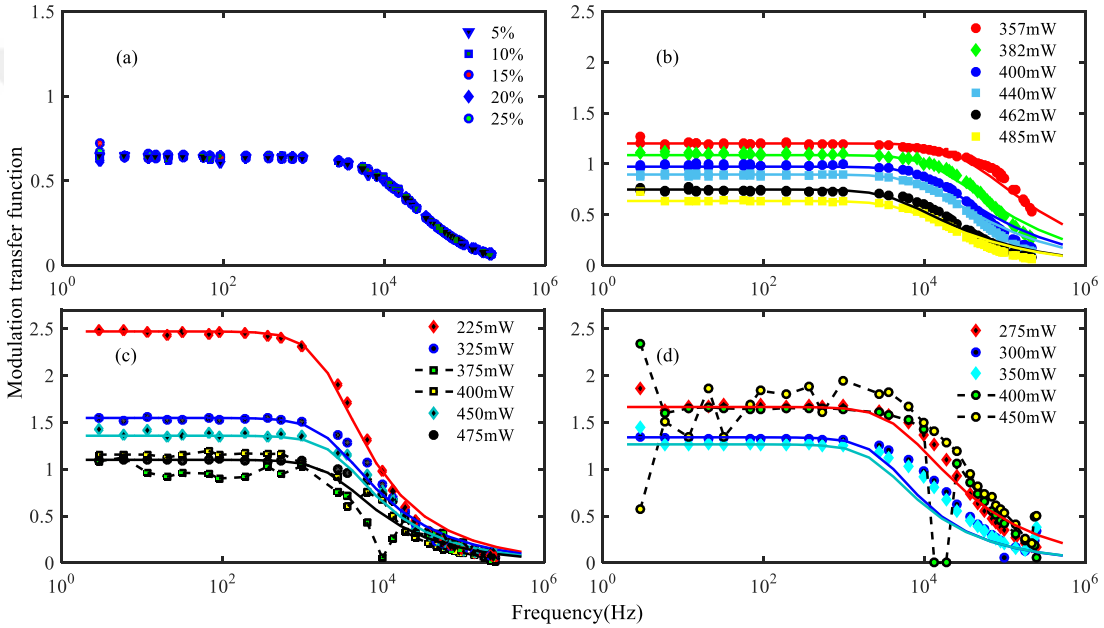

Figure 5.2: Experimental results of MTF: (colored online) (a) Experimental measurement of modulation transfer function (MTF) versus modulation depth. Experimental measurements (doted) and simulation results (solid-line) of MTF versus modulation frequency at indicated pump power for (b) all-normal dispersion, (c) nearly zero dispersion, and (d) soliton-like regimes with 10% Modulation depth.

In general, the expression derived above has to be evaluated numerically. The following parameters are used, in the laser rate equations and population densities, to obtain MTF for amplifier: core diameter, 6 μm; cladding diameter, 125 μm; L=30cm; $N_{\mathrm{tot}} = 10 \times 10^{25}\mathrm{m}^{-3}$; σ_{ap}=$2.7 \times 10^{-24}\mathrm{cm}^2$; σ_{ep}=$2.7 \times 10^{-24}\mathrm{cm}^2$; σ_{as}=$6 \times 10^{-26}\mathrm{cm}^2$; σ_{es}=$7.5 \times 10^{-25}\mathrm{cm}^2$; and τ =800μs. Parameter β is used to fit experiment with the simulation result.

Although we have kept only the first nonlinear term in the power series expansion, the MTF indeed turns out to be independent of the modulation depth,

which is an intrinsic condition for such an MTF-based approach to be internally consistent. This situation is confirmed by experiments, as long as the laser is in a stable mode-locking state corresponding to the generation of a single, isolated pulse. Fig. 5.2(a) shows that the modulation depth is virtually constant when the laser is mode-locked in the all-normal-dispersion regime. While this graph corresponds to the specific pump power of ∼460 mW, the results are similarly independent of modulation depth at different pump powers. The value of the MTF, however, reduces with increasing the pump power, which is illustrated in Fig. 5.2(b). This is expected as stronger pump results in increased saturation of the gain medium, consistent with the results in [122]. In this regime measured and calculated MTF decreases with increasing pump power as illustrated in Fig. 5.2(b), which shows good agreement between theory and experiment. It remains relatively large and almost constant at frequencies up to ∼ 10 kHz and then decreases. The 3-dB cutoff frequency decreases from ∼180 kHz at a pump power of 357 mW to ∼30 kHz at a pump power of 485 mW.

The situation is quite different in other mode-locking regimes, where the nonlinear effects are stronger at comparable levels of pump power or pulse energy. When the laser is operating in nearly zero net GVD, the MTF develops a more complex profile, as shown in Fig. 5.2(c). First, the measured MTF is substantially higher than that of the all-normal-dispersion oscillator at low frequencies (up to ∼1 kHz) at the same pump power. The 3-dB cut off frequency increases from around 5 kHz to ∼ 10 kHz as the pump power increases from 225 mW to 475 mW. In contrast, at higher frequencies, the MTF is smaller than for the all-normal-dispersion laser and has reduced dependence on the pump power. However, the most striking difference is that the MTF becomes nonlinear at pump powers beyond 375 mW. Furthermore, the amplitude of the MTF for 375 mW pump power is even smaller than MTF value at 450 mW over nearly the entire frequency range. We attribute these observations to: (i) Strongly nonlinear response of the cavity to the modulation, (ii) nonlinear coupling between the intrinsic noise of the system and the coherent modulation during the MTF experiment.

In the dispersion-managed soliton regime, where the cavity experiences high net negative GVD, such that the laser operation is essentially soliton-like, the

dependence of the relative intensity noise (RIN) and MTF on pump power is not as regular as the other regimes as shown in Fig. 5.2(d). This more complex behavior is due to several factors, including the increased level of background RIN as a result of soliton-soliton and soliton-dispersive wave interactions and the resulting transitions between the soliton states that are supported since the laser becomes multiple pulsing at high pump powers. In our experiment, MTF decreases when the pump power is increased from 275 mW to 350 mW, then increases at 400 mW before the frequency dependence is partially disrupted at 450 mW. This is attributed to fragile nature of bound soliton which is resulted from clamping of peak power, self-assembly of solitons determined by relative pulse parameters of generated multi solitons, strong coupling between solitons and dispersive wave or interaction of solitons with itself and its environment in general [103, 117, 131, 132] .

In the linear response mode, a 3-dB cutoff frequency is larger and decreases with increasing pump power in all-normal-dispersion regime than near zero and soliton regimes at a given pump power. For example it is $\sim$ 190 kHz, $\sim$ 13 kHz and $\sim$18 kHz at $\sim$350 mW, respectively. This is mostly due to the blue shifting of relaxation oscillation frequency as a result of dissipative nature of all-normal-dispersion regime induced by spectrum filtering [133]. The slight difference between the other two regimes is also a manifestation of difference in pulse stability and the difference in the physical processes experienced by a pulse in these regimes to keep periodic boundary conditions determined by a balance between phase and amplitude in general. Interaction of injected modulation and the background noise level of the oscillator are also important in determining MTF characteristics.

5.3 Relative intensity noise (RIN) measurement

The transition from a stable coherent state to a disordered state which is far from equilibrium is presented in [64, 134]. Stochastic intensity fluctuations of longitudinal modes occur before a pulse is generated in the laser cavity. Optimized

competition of nonlinearity and dispersion increases relative coherence between these modes. Thus, a stable pulse emerges. Increasing pump power creates dispersive waves, initiates optoacoustic effects [135], bifurcation, chaos, competing for multi-pulses and establish a semi-disorder state which is far from equilibrium that exhibits interesting life like far from equilibrium nonlinear dynamics. Studying noise spectrum helps us to explore and understand the mechanism of transition and its effect on MTF. Input pump power is scanned to characterize and change states in the system. Standardized RIN measurement method in Ref. [122] is used to calculate experimental results.

Figure 5.3(a) presents measured integrated noise in ANDi cavity with net dispersion of ~ 0.8 ps^2. It was at CW operation regime below pump power of $\sim$345 mW. Mode-locking started at $\sim$ 350 mW and then remains stable self-starting single pulsing till available maximum pump power while the integrated RIN decreases before it levels off at high pump power ($>$ 450 mW). The mode-locking remains stable when the pump power is decreased on intervals of 5 mW up to 340 mW. The RIN increases as the nonlinearity required for pulse stabilization gets smaller and smaller between 350 and 340 mW. A hysteresis observed on the RIN between pump power of 340 mW and 350 mW, where the mode-locking is not self-starting. The RIN in this state is higher than the RIN for stable pulsing (for a pump power $>$ 420 mW) by more than tenfold.

Unlike ANDi cavity, in nearly-zero dispersion with a net dispersion of $\sim$ 300 fs^2, the laser experiences relatively complicated noise dynamics as shown in Fig. 5.3(b). Fig. 5.3 (c and d) shows autocorrelation signal and optical spectrum of CW, an onset of mode locking, stable mode locking, initiation of multi-pulsing and none self-starting pulsing regimes respectively. Close to the threshold of pulse formation the noise level is higher which is in the order of 10^{-2} (1%). As pump power is increased, the fluctuation is intensified by almost four fold than when it was very close to the mode locking threshold. For stable pulsing, the level of integrated RIN dropped by more than 100 times. The RIN level remains almost at the same level for a larger range of pump power until initiation of multi-pulsing occurred. An onset of multi-pulsing occurs when the cavity is pumped such that its spectral width exceeds the gain band width [136, 137]. Here the

pulse tolerates a certain pump power by shading energy to its tails before it breaks up into two or more pulses. This point is characterized by oscillatory dynamics [64], hence increased level of RIN is measured. In our case to the level of 10^{-3} (0.1%). By increasing pump power, the integrated RIN level can reach up to 1% due to interaction of the generated multi-pulses which depends on their relative phase, temporal separation, and energy competition that appears due to optoacoustic effect or due to the formation of CW peak on the spectrum [64,136]. This interaction can be described as a net effect of effective repulsive or attractive force between pulses. Due to this interaction switching of polarization from one state to another occurs to over drive the NPE [131, 137, 138]. The RIN is also calculated for the reverse direction by decreasing pump power. At lower pump power before mode-locking was interrupted, the balance between nonlinearity and dispersion struggle to support mode-locking dynamics and level of intensity noise increases [123,131,139]. In this regime, we have seen hysteresis on the integrated RIN of the cavity on the onset of multi-pulsing and in the regime where single-pulsing mode-locking is not self-starting.

In soliton regime, with a net cavity dispersion of ~ -90000 fs^2, the oscillator exhibits more complicated pulse dynamics that range from single pulsing to multi pulsing, bound states with a different number of solitons, harmonic mode locking, rational harmonic mode locking, period doubling, etc. All of these states are achievable either by setting the wave plates to different angles or by changing the pump power. Figures 4(a) and 4(b) show the behavior of measured integrated RIN as the pump power is scanned forward up to maximum pump power and backward close to the threshold of mode locking in one cycle for two different arrangements of wave plates.

Wave plates are arranged in such a way that the laser remains mode locked up to maximum pump power with characteristics of RIN dynamics as shown in Fig. 5.4(a). A number of coexisting bound soliton states are observed together with their random transition from single to multi-coupled soliton regimes with the same or different repetition rate as the pump power is scanned. Integrated RIN value for different states varies significantly even after a stable self-starting mode-locking is achieved. Fig. 5.4(c and d) shows autocorrelation signal and

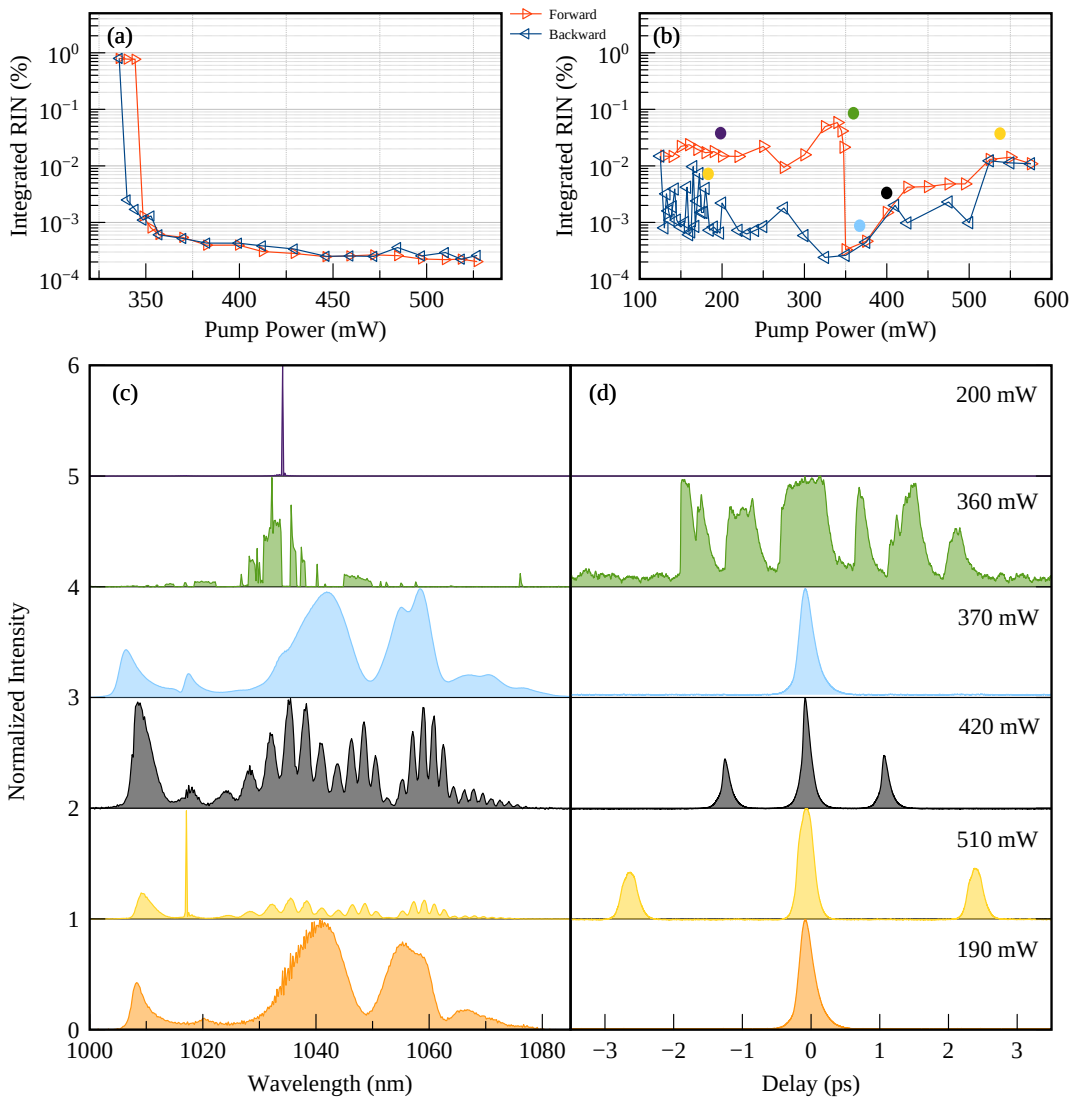

Figure 5.3: Experimental results for Measured integrated RIN: for all normal regime (a) and nearly-zero dispersion (b) when the pump power is scanned forward (red triangles) and backwards (blue triangles). Fig. 5.3 (c and d) shows autocorrelation signal and optical spectrum of CW, onset of mode locking, stable mode locking, initiation of multi-pulsing and none self-starting pulsing regimes respectively.

corresponding optical spectrum of certain states at the indicated pump powers. A single pulsing occurs at a pump power of slightly less than 200 mW. Further pumping created a pulse whose optical spectrum has a CW peak. Here, Integrated RIN increased by more than 20X. By increasing pump power single state soliton is changed into a two soliton state at a pump power of ∼330 mW. As the soliton energy increases with increasing pump power a repulsive force increases the pulse separation and the integrated RIN increased as well. A further increment of the pump power created three stable soliton state at a pump power of ∼365 mW. Integrated RIN decreases by a factor of 8X. The pulses then attract each other before forming a more compact cluster at ∼375 mW. The relative position of central wavelength of the soliton and the central wavelength of side-band also changes as the pump is scanned usually decreases with increasing pump power and jumps to a larger separation just at the point where the laser undergoes soliton state change.

So far we have seen that pulse interaction increases the background noise. It can increase by about 10X on soliton state transition points or at critical points. Soliton interaction can lead to much higher integrated RIN value such as the case observed when the pump power increases from 495 mW to 510 mw in Fig. 5.4(a). Autocorrelation signal of the pulse changes from 15 peaks to 17 peaks, then to 19 peaks and to 21 peaks at 510 mW the corresponding optical spectrum shows asymmetrically distributed peaks with amplitude peak values constantly switching from right to left. This is an indication of a change in separation, energy computation, possible hopping of relative phase difference of the solitons pulses in a bound state and a combination of all processes within the soliton cluster [140]. The autocorrelation peaks remain at 21 when we further increase pump power (the soliton gets enough energy to stabilize itself) the value of Integrated RIN comes back to the level that we found for the other stable soliton states which can be considered as near equilibrium thermodynamic states.

In general integrated RIN of these bound soliton states behaves similarly with in a state. It always starts with moderate value at the formation point or just after a transition takes place. It becomes the highest when it is about to jump (critical point) into a new bound soliton state and the most stable point of this state is

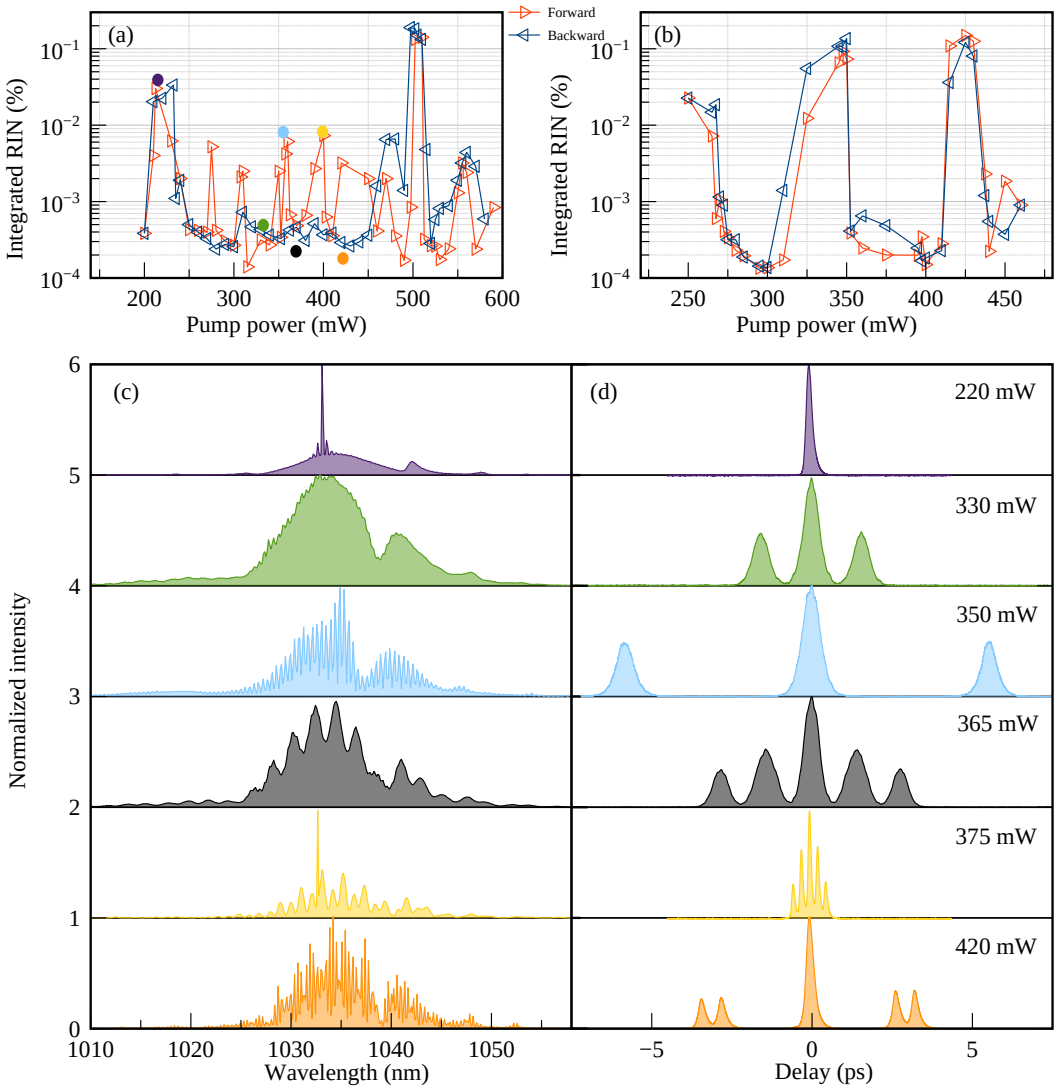

Figure 5.4: Experimental result in soliton regime: (a) and (b) measured integrated RIN for highly-negative dispersion regime in one cycle for two different set of wave plates when the pump power is scanned forward (red triangles) and backward (blue triangles). (c) and (d) shows autocorrelation signal and corresponding optical spectrum of certain states in (a) at the indicated pump powers.

between these two points. Unlike the results of ref [141, 142], In our experiment we observed a coexistence of different forms of soliton bunches with a range of repetition rate undergoing short and long range interactions [135] at a given pump power and random transition which does not follow soliton energy theorem as the pump power is scanned. At these critical points occurrence of soliton period bifurcation or energy computation between solitons themselves or soliton with generated dispersive waves followed by the occurrence of acoustic waves which create modulation on the optical power that rises the RIN level by $\sim$ 10X on average [122, 131, 143, 144]. This noise results in random soliton state transitions by creating or annihilating a soliton at the critical points when pump power was increased almost adiabatically but it did not exhibit too much transition when the pump power is scanned from a higher to lower pump power values (the number of auto-correlation peaks their temporal difference and the shape of their spectrum remains almost the same for longer range). Thus integrated RIN exhibits a hysteresis on the transition points which are characterized by RIN value more than one order of magnitude on average than of integrated RIN for stable soliton states. The appearance of CW peak on pulse spectrum also increases the RIN by a factor of more than 10 at any point in the cavity dynamics.

The behavior of integrated RIN may vary depending on the specific parameters in this regime. With a different set of wave plates the laser state changes from mode-locked to CW due to the periodic boundary condition set by the interaction of physical processes in the cavity. Corresponding integrated RIN is shown in Fig. 5.4(b). In general, we observe that the integrated RIN shows increment on CW regime or when the interaction of pulses in random transition points between soliton states takes place as the pump power is scanned and goes back to normal level when it is mode-locked from CW operation and when the interaction is stabilized for reasons mention earlier. The RIN is almost independent of the phase difference or temporal separation as long as they remain fixed (stable state), which is evident in the symmetry of modulation on the pulse spectrum [140]. Additional information of simulation result is provided in the appendix.

Similar results can be obtained by rotating wave plates of the oscillator. Fig. 5.5 shows the behaviour of mode locking states characterized by Cross correlation

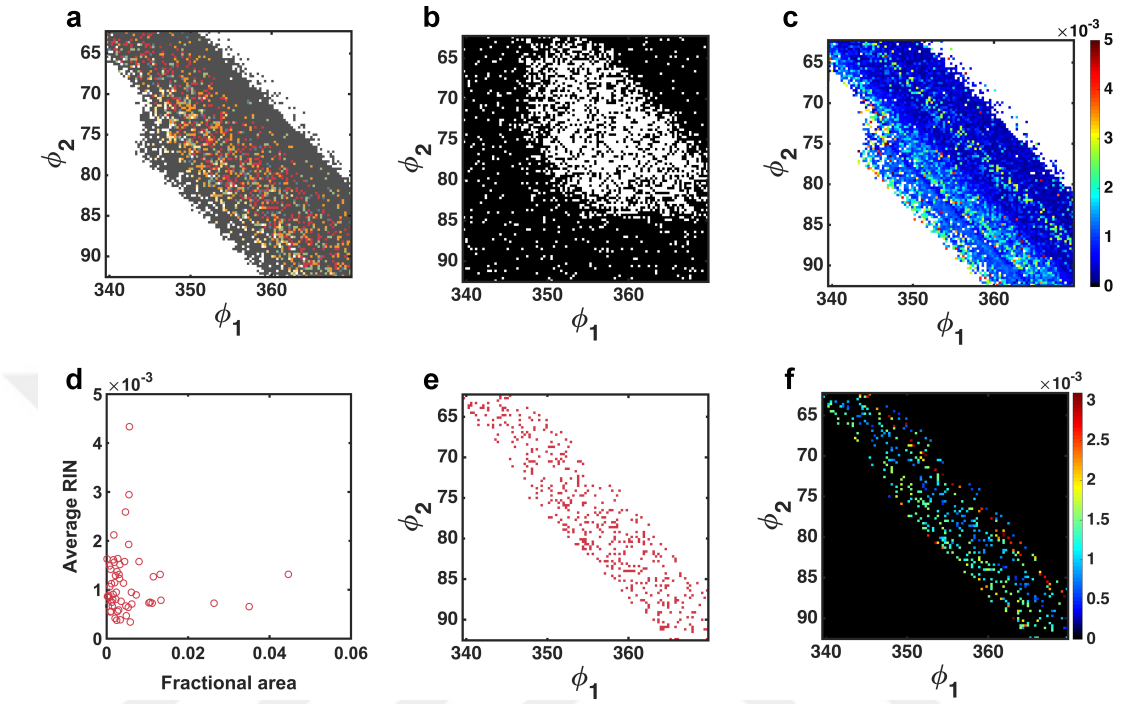

Figure 5.5: Density of states around mode locking: (a) Different mode locking states mapped on a phase space formed by scanning waveplate angles around a mode locking point. Coloured points indicate mode locking states that are grouped under the same state on the phase space. (b) Reversibility of each the central mode locking point before and after transiting is performed for every point on the phase space. (c) Integrated RIN map on the phase space (d) Average integrated RIN of states on the phase space. (e) Distribution of mode locking states on the first state of the phase space. (f) Corresponding integrated RIN map of the state indicated on (e).

of optical spectrum and autocorrelation signal projected on a phase space formulated by scanning 30^0 on half and quarter wave plate with a resolution of 0.30 around a certain mode locking state. A threshold value on the cross-correlation of optical spectrum and autocorrelation signal is used to sort states on the phase space as shown by colored region in Fig. 5.5(a). The white portion is region occupied by CW. Reversibility of initial point (indicated at the center of the phase space) of the laser system after each random transition to scan points (macro states on the phase space) is called reversibility which is indicated in Fig. 5.5(b). Mode locking states close to the central point show a higher degree of reversibility while the system showed lower value on the CW regime. In general, reversibility is highly affected by the coexistence of mode locking states and the self-starting

and self-healing nature of the system at particular parameters. The intensity distribution of Integrated RIN of each point is mapped as shown in Fig. 5.5(c). The value is high on the CW regime but it shows a pattern of distribution of the mode locked region. Its average value per fractional are of each state on the phase space is shown in Fig 5(d). Larger states on the phase space have smaller average value than smaller sized states. This is due to increase of integrated ring around transition points. For example, Fig 5(e) and 5(f) show the distribution of mode locking states with in the first state on the phase space and its corresponding Integrated RIN distribution values respectively. One can easily see that points on the boundary (transition points) of the state are characterized by higher value than the central points which is the same conclusion with the fact we had on the pump power dependence noise dynamics earlier.

At the critical points, nonlinear response of the cavity to pump modulation is enhanced. Fig. 5.6 shows the RIN spectrum of pump and signal powers resulted from the diode and corresponding cavity response to injected electrical modulation in different regimes. In ANDi regime the response was a linear as can be seen in Fig 5(a) for the available pump power range. In a linear response, a modulation on the pump is transferred to the signal in the same frequency. There is a prominent nonlinear behavior of the RIN spectrum on the signal at a pump power of 375 mW as shown in Fig. 5.5(b) compared to the RIN spectrum below 370 mW and above 410 mW pump powers in near zero net GVD regime. Pump RIN spectrum is taken from 5% output port before WDM shows no higher harmonic peaks which clearly indicates that the nonlinear response is coming from the intracavity dynamics. At this pump power, we observe initiation of multi-pulsing. So the nonlinear response is mostly due to the interaction of modulation induced intensity noise and the higher noise level of the unmodulated system (background noise). Polarization scrambling on the gain fiber initiated by nonlinearity in the presence of modulation and background intensity noise or polarization noise that resulted from anti-correlation of noise by the two linearly polarized intensities in the cavity [123,131,139] over drive NPE. Since the response of artificial saturable absorber (NPE) is determined by polarization evolution inside the cavity modification on the time response is reshaping the sinusoidal waveform which generates

higher harmonics of the modulation frequency [128, 139]. Coupling phase and energy competition of the generated two or more pulses also determines the resonance relaxation frequency of the system which intern affects RIN level [123, 138]. We have seen the similar nonlinear response (Fig. 5.5(c)) of the cavity in soliton regime where the background noise can be increased due to the interaction of solitons in addition to the above-mentioned dynamics [144].

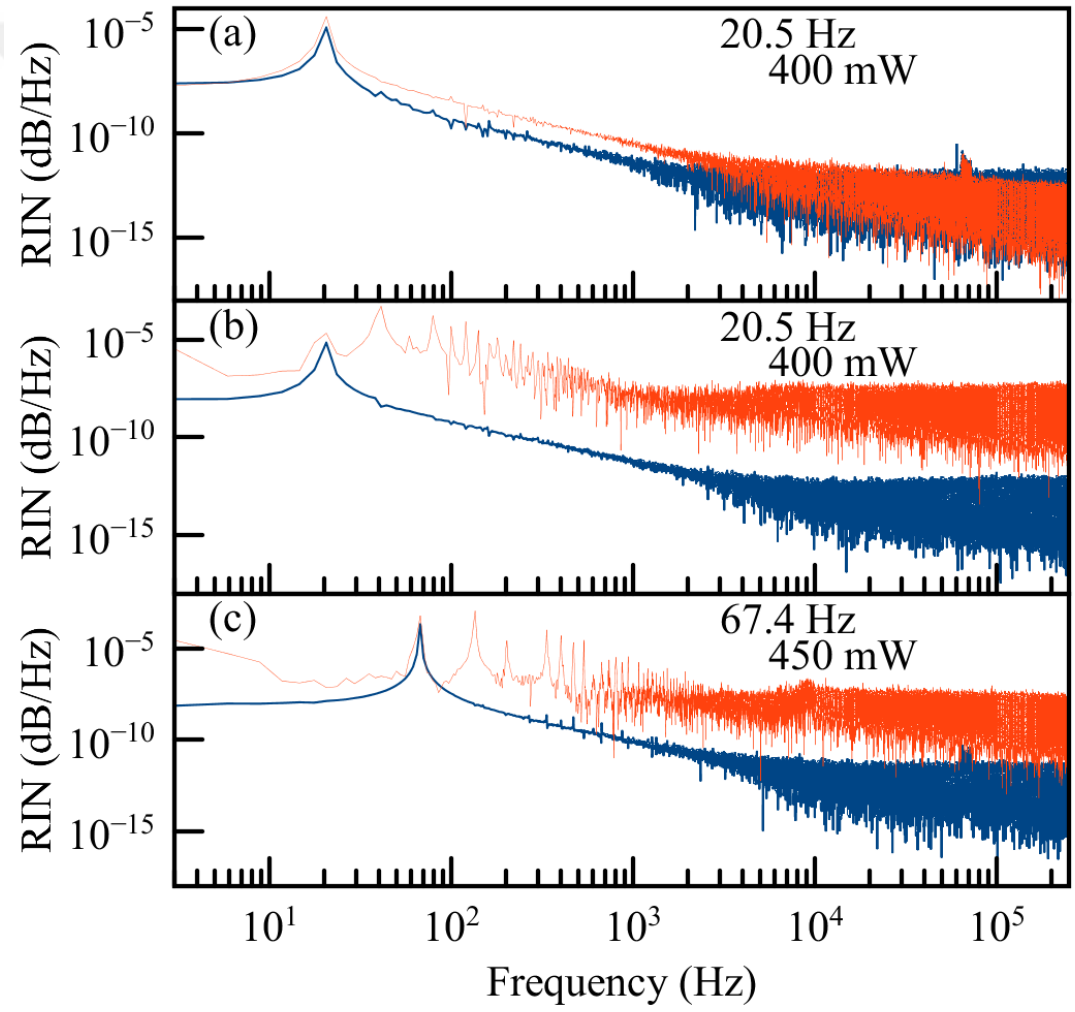

Figure 5.6: Measured relative intensity noise spectrum of modulated pump and signal intensities for ANDi (a), nearly-zero-dispersion (b), and highly negative dispersion or DM soliton (c) regimes. The corresponding pump powers and modulation frequencies are indicated on the legends.

According to the model in [128], the total coupling ratio of the pump RIN to the signal RIN can be described as sum of linear and nonlinear coupling functions

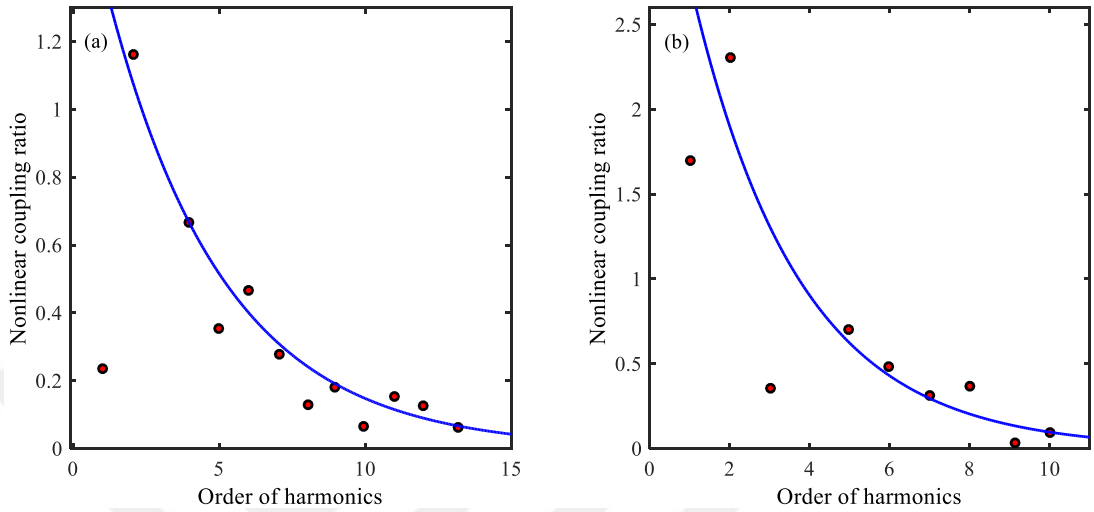

Figure 5.7: Nonlinear MTF as a function of order of harmonics, (a) at modulation frequency of 20.4 Hz and pump power of 375 mW in the near-zero-dispersion regime with $\eta = 1.8$, and $\alpha = 0.24$. (b) At modulation frequency of 67. 4 Hz and pump power of 400 mW in the DM-soliton regime with $\eta = 4$ and $\alpha = 0.37$.

which depend on the modulation frequency and its harmonics.

$$RIN_l(k, f_{mod}) = MTF_{lin} RIN_p(f_{mod}) + MTF_{nonlin}(k) RIN_p(f_{mod}), \quad (5.13)$$

$$MTF_{nonlin}(k) = \eta exp(-\alpha k), \quad (5.14)$$

Where $\mathrm{MTF_{lin}}$, $\mathrm{MTF_{nonlin}}$, $\mathrm{f_{mod}}$, and k are linear coupling coefficients or MTF, nonlinear coupling coefficient or nonlinear MTF, modulation frequency and its order of harmonics, respectively, whereas η and α are constants. The nonlinear MTF fits very well with the experimental data, when using an exponential function depending on the order of the harmonics of the modulation frequency (Fig. 5.6).

Figure 5.8 shows noise spectrum of certain mode locking states showing increased intrinsic instability due to appearance of a CW on spectrum, strong soliton pulsation or period doubling (Fig. A.1(a) red) [145], and other intracavity pulse interaction (due to acoustic waves) that can cause intrinsic modulation (Fig. 5.8(a) black). Such intrinsic background modulation/noise can cause a nonlinear response of the cavity to external modulation independent of the driving or modulating frequency as shown in Fig. 5.8(c-d). The modulation signal is applied

to a diode current with a 1 % modulation depth at three different frequencies. The superposition of the intrinsic modulation with the ejected signal modifies the sinusoidal shape. Hence, harmonics of the modulation frequency appear on the noise spectrum. Similar to previous results the nonlinear MTF also show power law distribution

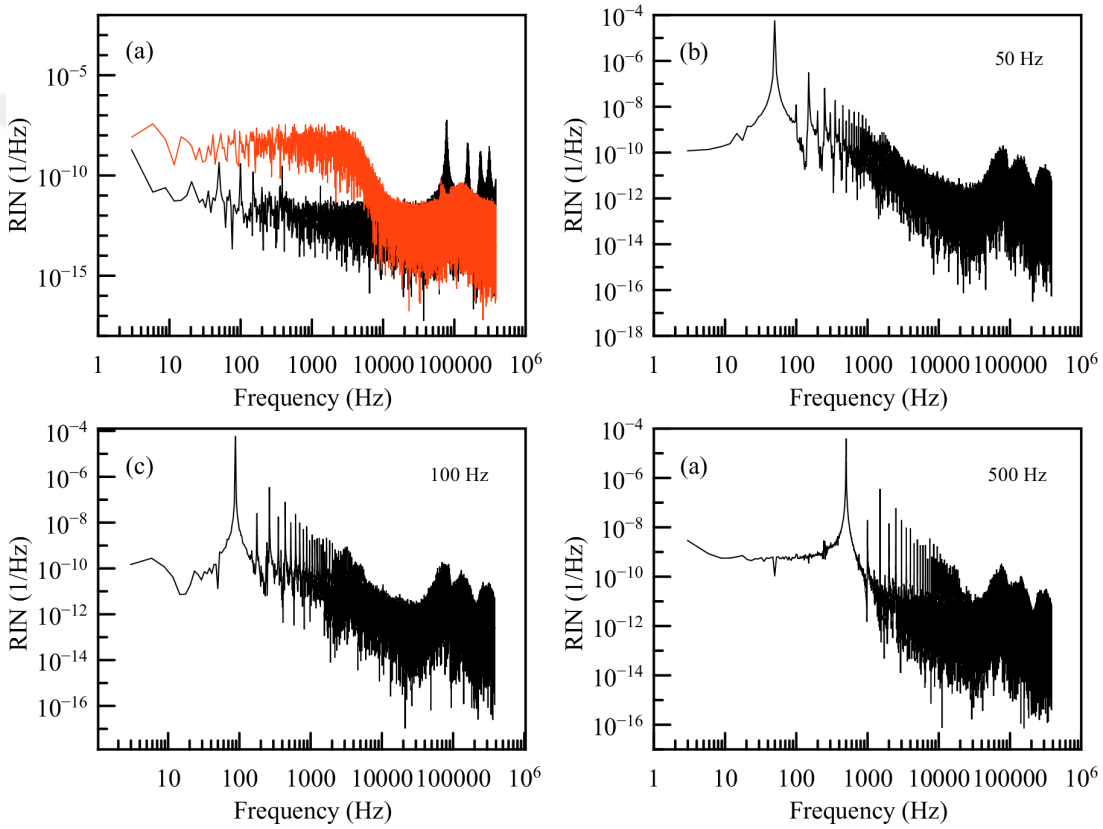

Figure 5.8: Nonlinear response: (a) RIN spectrum showing intrinsic interaction induced modulation (black) and increased noise as a result of the appearance of CW and/or period doubling (red). (b), (c) and (d) RIN spectrum showing the nonlinear response of the cavity when an external modulation is applied at a frequency of 50 Hz, 100 Hz and 500 Hz respectively to the soliton state whose noise spectrum is shown by black on (a).

5.4 Conclusion

We characterized the modulation transfer function and integrated RIN of passively modelocked fiber oscillators in different mode-locked regimes. Based on our measurements, we have explored the different operational regimes where MTF behaves linearly and nonlinearly, which can be considered as near and far-from-equilibrium dynamics of a mode-locked laser depending on the reversibility to its original pulsing state up on the removal of the modulation. Initiation of multi-pulsing, energy competition between soliton pulses, the interaction of pulses with dispersive and acoustic waves raised the integrated RIN then the nonlinear response of the cavity to amplitude modulation is intensified. The nonlinear response of this system is correlated strongly with the pulse energy (which affects the effective nonlinearity experienced by the pulses) rather than the pump power, especially in soliton regime. Our findings have implications for further understanding, control, and suppression of intensity noise of fiber oscillators in different pulsing regimes and giving important insight into the behavior of mode-locking dynamics in response to pump power or cavity loss modulations. Observation of clearly delineated regimes of essentially linear (near-equilibrium) and nonlinear (far-from-equilibrium) cavity responses shows that the mode-locked fiber lasers is a rich and accessible and experimentally convenient platform for studying phenomena that are common to a broad class of interacting physical systems [146].

Chapter 6

Noise-induced creation and annihilation of solitons in dispersion managed fiber oscillators

6.1 Introduction

Optical solitons and their interaction with other solitons or with dispersive wave shed by solitons under perturbation constitute a versatile experimental and theoretical platform for studying the nature of complex dynamics occurring in laser cavities [131, 135, 147] in addition to common physical principles in terms with a range of other nonlinear, non-equilibrium, coupled systems outside of optics.

Apart from the fact that dissipative solitons are generated by completely different mechanisms in different systems such as microresonator (based on tuning of pump frequency over cavity resonance frequency), microresonators (based on Kerr effects) and fiber oscillators (based on the presence of saturable absorber), their propagation can be governed by the complex Ginzburg-Landau equation or

one of its variants. Stable pulse propagation mainly relies on balancing the interaction of negative group velocity dispersion (GVD), nonlinearity, gain, and loss. Short and long range soliton interaction mediated by physical processes in micro and microresonators has been recently reported and becoming a growing field of research interest in nonlinear phenomena [135, 148–151]. These interactions together with nonlinear phenomena, such as bifurcations, periodic breathers, and chaotic dynamics [152] that result from the boundary condition imposed by a nonlinear cavity. Hence, studying the complex dynamics that arise from fiber oscillators is interesting both for further fundamental understanding of the nature of pulse-to-pulse interactions, its effects on propagation dynamics and its association with other nonlinear phenomena occurring in nature especially these which can be explained by far from equilibrium thermodynamic systems.

We examined the effect of interaction of dissipative solitons with generated dispersive waves and between solitons themselves in a cluster or bound state on the fluctuations of the laser's output (integrated relative intensity noise) and its effect on the creation and annihilation of solitons that cause irreversible soliton state transitions. These have been observed for first time in passively mode locked fiber oscillators to the best of our knowledge. Such emergent transitions are induced by intrinsic noise characterized by phenomena such as variation of a relative phase between solitons, variation of the temporal separation between solitons and energy exchange between solitons and with generated dispersive waves. These interactions are crucial to the formation and stability of dispersion-managed multi-soliton states as theoretically predicted in [153, 154]. Unlike the results of [155], the number of generated DM solitons can be smaller or larger than the original state at larger pump power. This is the behavior of systems far from equilibrium and is not necessarily subject to the formation and annihilation mechanism predicted by the results of ref. [155, 156]. This further supports self-organization phenomena in dissipative fiber oscillators which recently was reported by [149].

6.2 Experimental and simulation results

The experimental system is schematically described in Fig. 5.1. It is a fiber laser, which is mode-locked by NPE. The key physical parameters are as follows: A total length of 350 cm for passive fiber, 27 cm of a Yb-doped gain fiber and a net dispersion of ∼-80000 fs^2 for a repetition rate of 44.2 MHz.

Then, by varying the pump power, the oscillator can be induced to exhibit a range of dynamics that vary from a single stable DM soliton state to a multi soliton bound states with fixed and varying phase as well as temporal separation. We observe soliton bunches that repeatedly exchange energy and solitons with varying or vibrating temporal separations which often is followed by thetransformation from one to another random solitonic state are observed. This critical behavior or instability attractor is caused by long and short soliton-soliton, soliton-generated dispersive wave or optomechanical interaction. The RIN of these states is found to be higher than stable soliton states and is often times characterized by an acoustic peak on the RIN spectrum.

Dispersive waves are generated by the perturbation that a soliton experiences due to loss and gain as it propagates in the oscillator, as well as dispersion and nonlinearity if the pulse shape has deviated from the soliton condition. Its intensity can be controlled by scanning the pump power inside the cavity. We explore and examine the effects of pump power on the interaction of dispersive wave and single and double pulsing regimes whose autocorrelation trace, optical spectrum and RIN information are shown in Fig 6.1. Mode-locking is initiated at 160 mW with relatively high integrated RIN level (0.032 at 173 mW). At 176 mW, the integrated RIN is reduced to 0.0025. As the pump power increases integrated RIN decreases to 0.0002 at 210 mW and it increases afterwards until the pulse breaks up into two solitons at 228 mW as seen in Fig. 6.1(c). In our case, spectral sidebands are related to the instability of the mode-locking and the soliton states. As to be expected, bound soliton states are more stable when the intensity of the spectral side bands are relatively smaller. The relative intensity of spectral sidebands increases and their relative position from the central frequency of the

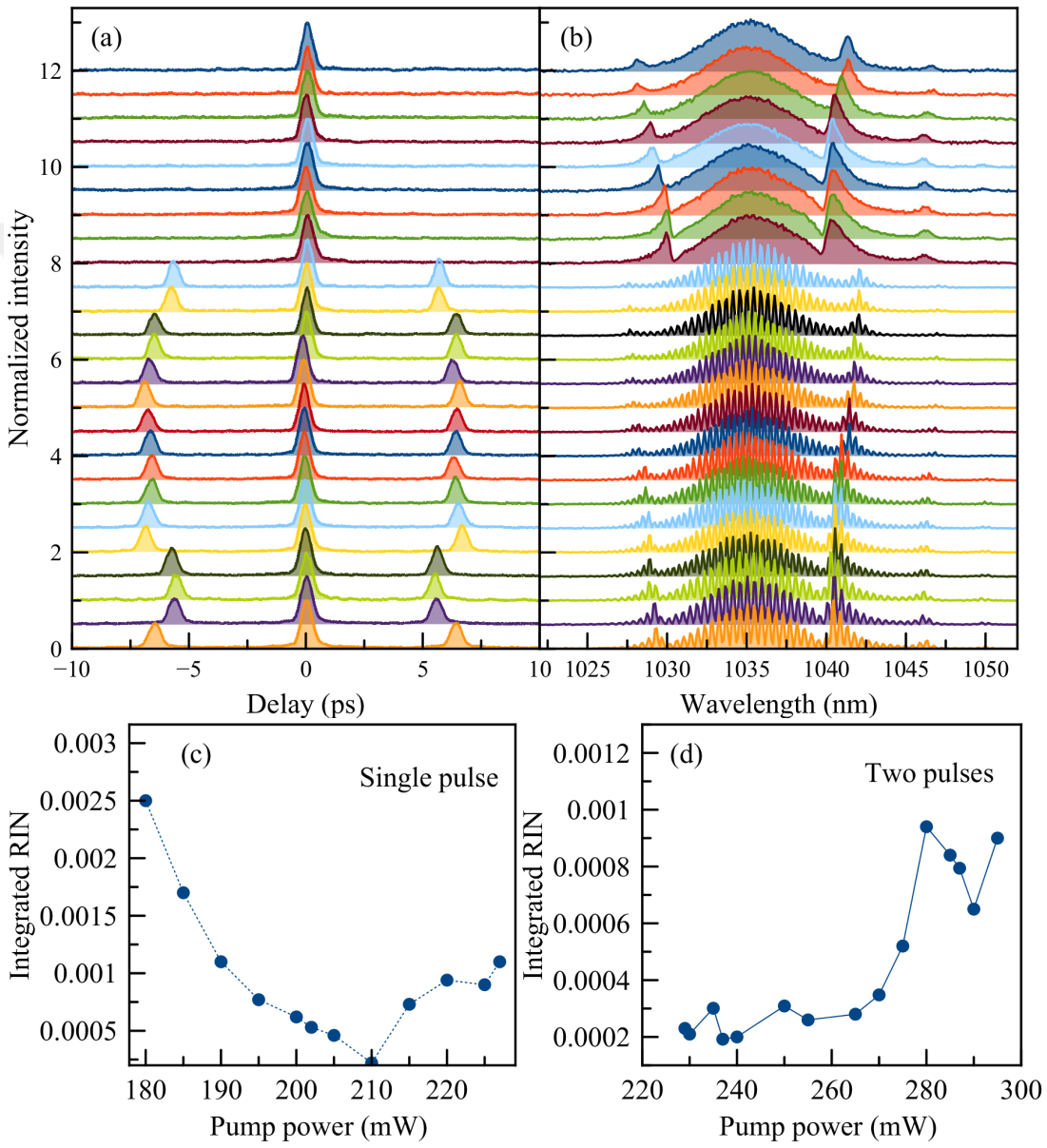

Figure 6.1: Experimental result showing pulse and dispersive wave interaction: (a) autocorrelation function (b) corresponding spectrum (c) and (d) integrated RIN dependence on pump power indicating the effect of dispersive wave Interaction on a pulse dynamics.

soliton decreases. Effective attractive and repulsive forces are associated with this phenomena. As we have seen in chapter 5, the integrated RIN is higher around the mode-locking threshold or any transition into a different mode-locking state. The relatively larger value of the RIN at lower pump powers is related with the promixity to the threshold pump power of mode locking.

Figure 6.2 indicates the effect of pulse interaction with dispersive wave. The pump power is the same but the pulses have slightly different duration (255 fs and 212 fs) with an estimated energy difference of 5 pJ, with the shortest pulse being higher in energy. When the relative intensity of Kelly side bands is stronger (fig. 6.2 (b)), which is a manifestation of strong coupling between soliton and dispersive wave, the soliton becomes unstable as also theoretically predicted in [142, 150]. Hence, the integrated RIN increases by fivefold. Asymmetry of the sidebands is an indication of relative cavity losses on the longer and shorter wavelength part of the pulse, given that the third-order dispersion is the same for both cases. This change in the asymmetry, together with the energy difference between these coexisting soliton states is a manifestation of different nonlinear polarization evolution in the cavity for the two cases.

Next, we characterize the dynamics as the pump power is varied. Fig. 6.3 shows pulse characteristics of five soliton states that exist within a certain range of pump power. Energy per pulse is calculated as the total available energy divided by the number of pulses; in other words, this quantity refers to the average pulse energy. The fraction of a dispersive wave is also estimated as the energy distributed over the cw-like spikes from the pulse spectrum, divided by the total pulse energy distributed over the optical spectrum. Every state begins with a relatively moderate noise level. When the available pulse energy increases due to slightly increasing pump power, each soliton get enough energy and this bound mode-locking state becomes stable (the minimum values of the integrated RIN are shown in Fig 6.3(b)). Additional increases in pump power further increase the total energy of the bound-pulse cluster and the fraction of energy going to dispersive wave also increases, as one can see in Fig. 6.3(c). Hence, the interaction of solitons with themselves and with the generated dispersive waves in the cluster increases and the noise level of the oscillator increases in consequence. Here,

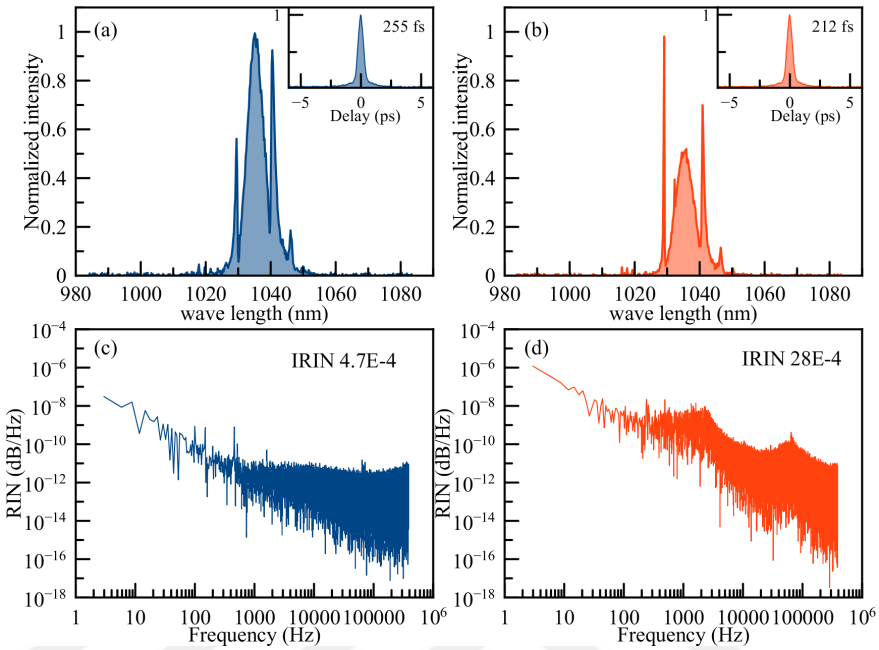

Figure 6.2: Effect of nonlinearity on a pulse and dispersive wave interaction: (a) and (b) show the optical spectrum and (c) and (d) show the RIN spectrum of two pulses that coexist in the oscillator at the same pump power with slightly different pulse durations and energies.

annihilation (such as a transition from state (1) to state (2)) or creation (such as a transition from state (2) to state (3)) of solitons resulted in the transition of the old soliton state in to a new soliton state with moderate noise level until the power is increased high enough to provide the needed energy for every soliton to stabilize.

Irrespective of the level of pump power it is formed, the integrated RIN noise level of every solitonic state shows similar dependence on pump power as shown in Fig. 6.3 (b). Every soliton state begins with moderate noise level before it goes to a most stable solution and then becomes most unstable at the critical points. The number of solitons in the new solitons state cannot be justified only with quantization of soliton energy. In our experiment, this process repeats itself up to maximum pump available power. Fig. 6.3(c) shows two types of stabilizing soliton states. States indicated by (1) and (2) lose their stability with increasing intensity of the dispersive waves after the most stable point. And the ones indicated by (3) and (4) which move towards the stable point when a fraction

of the pulse energy goes to dispersive wave increases, then it starts to decrease up to the most stable point. As the pump power increases further, the intensity of DW increases till transition to a new state is happened as usual. This shows that interaction of soliton pulses is determined by the energy they have in addition to its relative phase and separation.

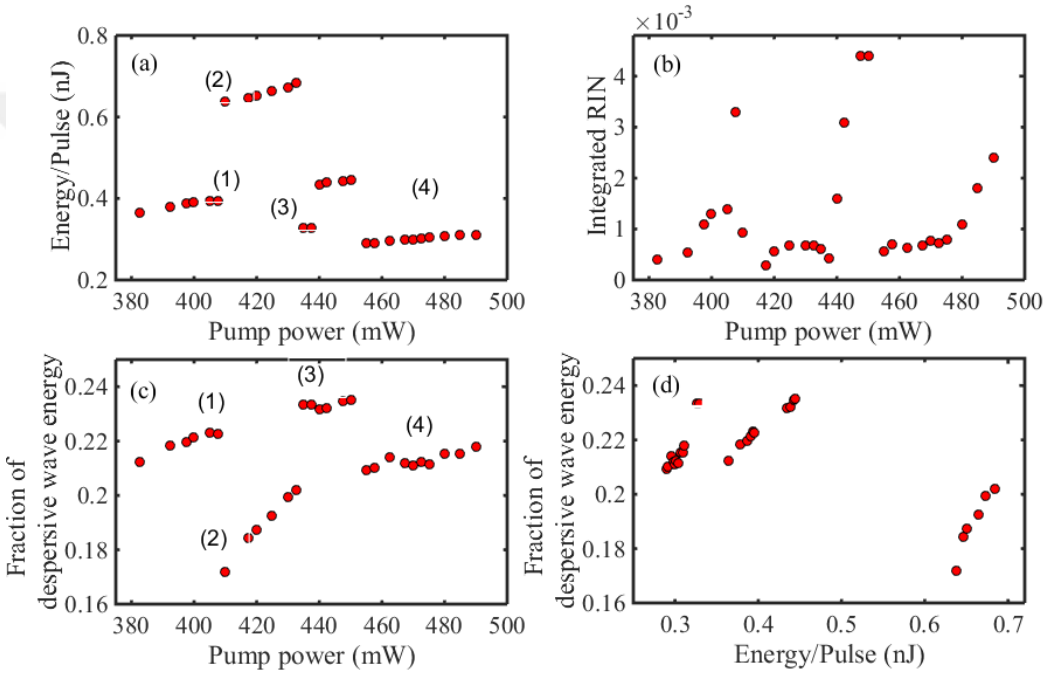

Figure 6.3: Pulse and dispersive wave interaction: Shows relationship between energy/pulse (a), Integrated RIN (b) and a fraction of energy going to dispersive waves (c) as the pump power is scanned.

Interaction of these pulses can be considered as effective attractive or repulsive forces created by some kind of potential which traps the temporal position of the pulse as shown by the intensity distribution of the autocorrelation signal on Fig. 6.4. As the pump power varied between 180 mW to 380 mW the state transformed from single to double at 190 mW and then to four at 210 mW. A significant change of temporal position on the 1st and 3rd AC signal peaks was observed between 210 - 255 mW. And then a different bunch with four solitons emerge. Similarly effective attractive and repulsive forces interplay before a three soliton state emerge at a pump power of 380 mW.

The transition mechanism involves a strong interaction of solitons. One case is

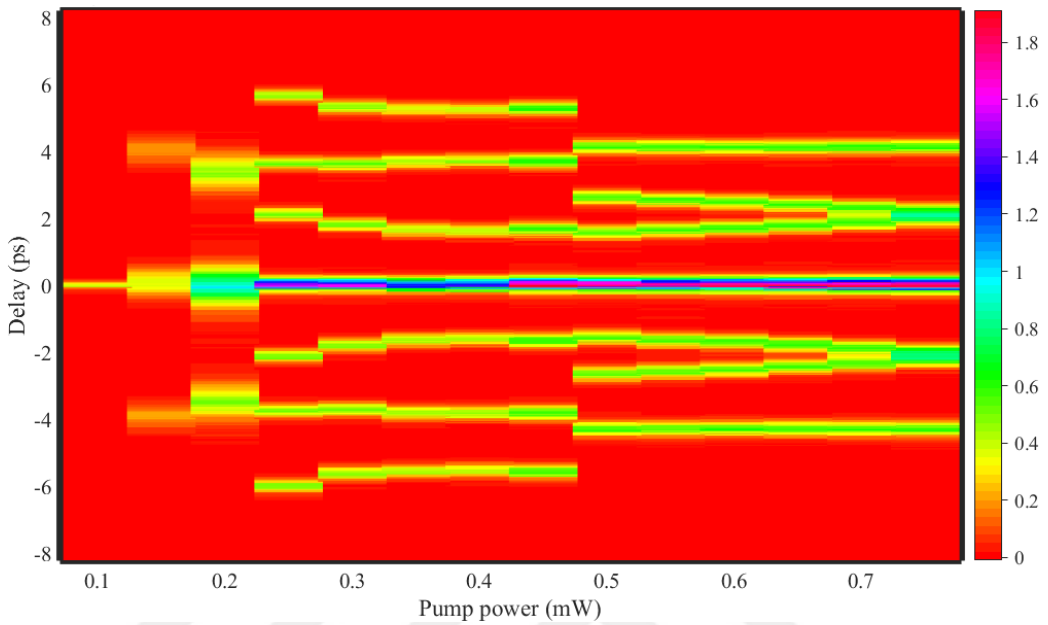

Figure 6.4: Temporal dynamics of soliton state transition: Autocorrelation signal intensity distribution of states that are generated as the pump power is scanned from 180 mW to 380 mW. It is taken in intervals of 15 mW.

through energy exchange between pulses (breather solution), a case for the state transition from state (1) to state (2) in Fig. 6.3. Fig. 6.5 shows autocorrelation, optical and RIN spectrum of a soliton state whose solitons are undergoing energy exchange or competition repeatedly (the same case happens at the last stage of Fig. 6.4). The state contains 6 solitons with stable and clearly resolved autocorrelation peaks at a pump power of 400 mW. When this pump power was increased to 405 mW the solitons start to attract each other and recombination of autocorrelation peaks happen. The state starts switching back and forth between Fig. 6.5 (a) and Fig. 6.5 (b). Such a process modulates the signal power with a modulation frequency shown as a peak on the RIN spectrum. This increases the intensity noise of the oscillator by a factor of five. Further increase 407.5 mW intensifies the interaction and annihilation of optical solitons take place and the soliton changes to a new relatively stable state with three solitons at a pump power of 410 mW. Three solitons are annihilated in the process due to noise induced soliton interaction [131,135,151]. Note that: further transition mechanisms are discussed in Appendix A.

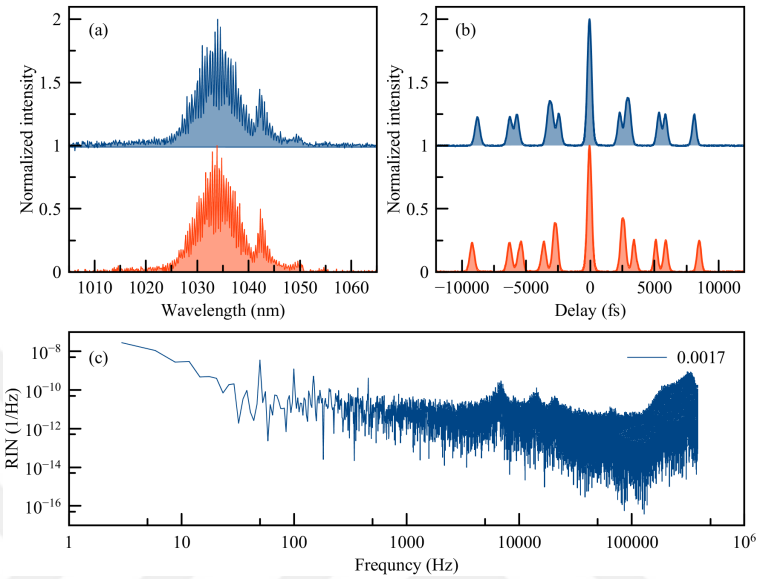

Figure 6.5: Energy exchange: Autocorrelation, optical spectrum and corresponding RIN spectrum of a soliton state with energy exchanging solitons inside a cluster.

In order to support and better understand our results, we have done numerical simulations based on solving the generalized Schrödinger equation with the details of numerical methods given on [47]. Our result shows the intensity noise or pulse energy fluctuating in the cavity is affected by the relative strength of spectral sidebands and the main soliton which can be controlled by the level of pump power or nonlinearity similar to our experimental results. As shown in Fig 6.6, the intensity of the sidebands increase with increasing pump power and at some critical point the pulse structure starts to switch between two single pulse lasing states periodically per round trip. Increasing the pump power further creates periodically breathing solutions, as shown on Fig. B.5, before the dynamics become chaotic. The pulse energy fluctuates before it jumps to another state. Similar results can be obtained by scanning the nonlinearity of components as is provided on Fig. A.5.

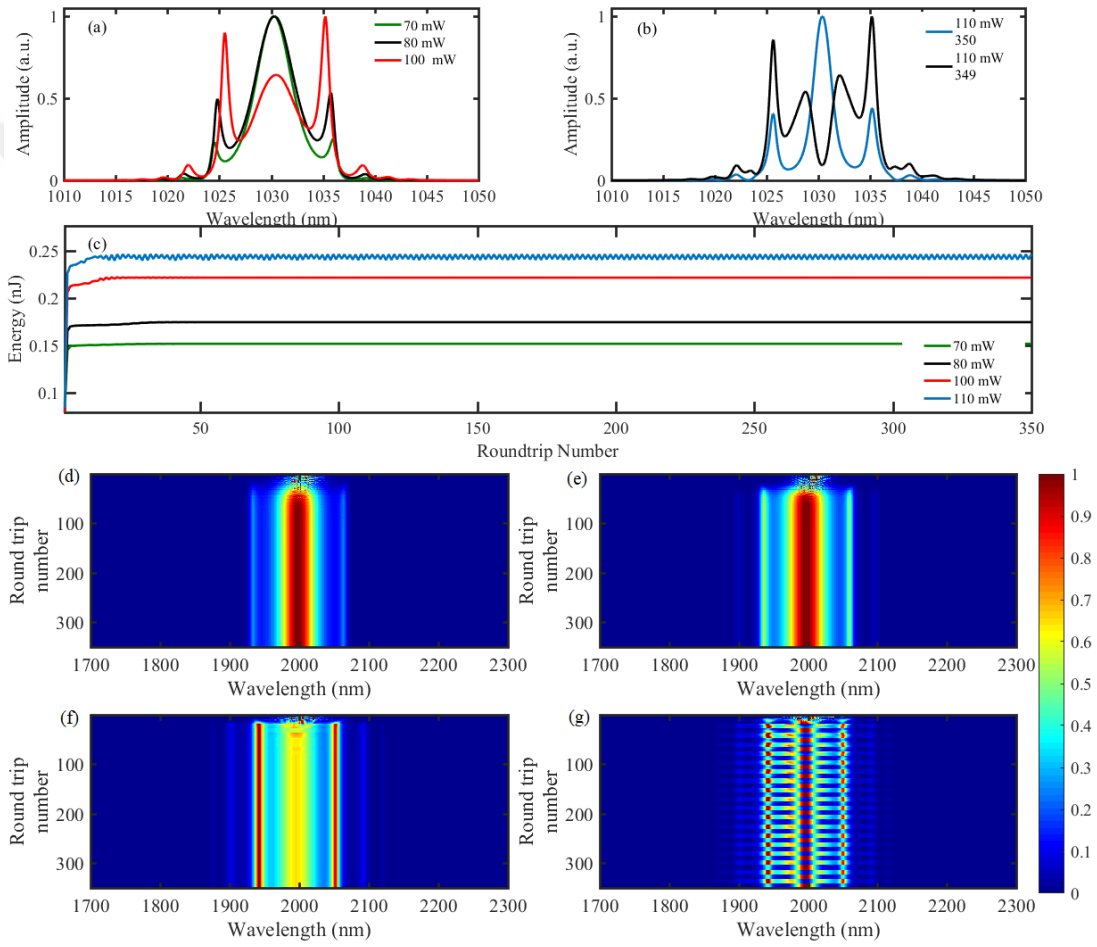

Figure 6.6: Simulation results: (a) and (b) Evolution of the optical pulse spectrum at the end of 350 cavity round trips for the indicated level of pumping powers. (c) Pulse energy evolution in the cavity at different pumping powers. Evolution dynamics of the optical spectra over hundreds of cavity roundtrips are shown in (d)(g) for the power levels indicated in (c).

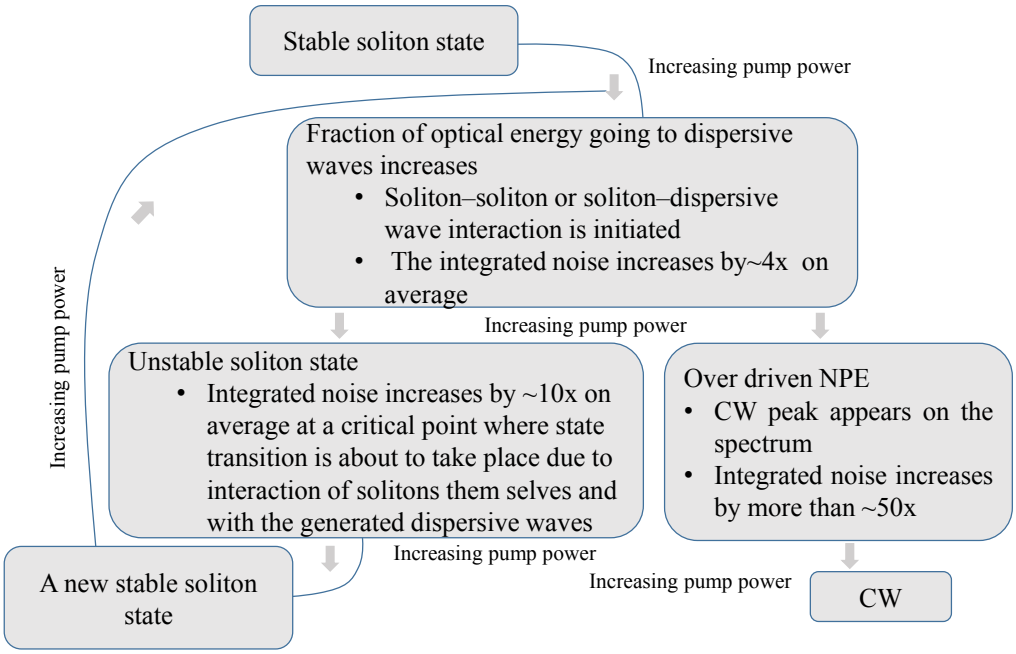

Figure 6.7: Summary: Mechanisms of soliton state transformation as pump power or nonlinearity in the cavity is scanned.

6.3 Conclusion

We have discussed the experimental formation and disappearance mechanism of DM solitons inside a fiber oscillator as depicted in Fig 6.7. The measured noise level (integrated RIN) of almost all soliton-like states showed similar a dependence on the pump power. Energy per pulse and the relative intensity of generated dispersive wave increase before a transformation takes place. Every transition point is characterized by (and its arrival can be predicted by) relatively higher noise level, which is likely due to the long-range soliton-soliton and the short-range soliton-dispersive wave interactions, in addition to inherent bifurcations arising a result of the boundary conditions imposed by the laser cavity. This elevated intrinsic noise induces an irreversible formation or annihilation of DM solitons in the oscillator. Considering the laser system as a heat bath and pump power as a temperature [142], this critical phenomenon is similar to the first-order phase transitions in statistical mechanics.

Chapter 7

Direct control of mode-locking states of a fiber laser

Parts of this chapter, primarily, Section 7.1 and Section 7.2.1, have been published in [1] and reproduced here with permission from the publisher.

7.1 Introduction

The technological importance of passively mode-locked fiber lasers is well recognized [34, 157]. In addition, mode-locking is of fundamental importance, since it is inherently nonlinear [158–160] and constitutes a non-equilibrium steady state [161]. The same nonlinearity that makes mode-locking possible ultimately limits laser performance. In response, researchers have devised numerous ways to manage nonlinearity. Prior to the seminal paper of Ippen, *et al.*, in 1993 [162], which introduced dispersion management to laser cavities, mode-locked fiber lasers could hardly generate several-hundred femtosecond pulses with energies of tens of picojoules. Dispersion management weakens nonlinearity by increasing the average pulse duration. An alternative is to increase the mode area of the fibers [163, 164]. Use of microstructured rod-type fibers has allowed much

higher powers to be accessed [164]. However, reduction of nonlinearities is limited both in theory, because the instabilities are never eliminated, merely pushed to higher powers, and often at the cost of generation of longer pulses and in practice, because, *e.g.*, there are practical limits to mode size. A complementary approach involves management of nonlinear effects directly [28], ranging from use of negative (self-defocussing) nonlinearities [28, 165] to identification of nonlinearity-resilient pulse propagation schemes. Milestones include demonstration of the wave-breaking-free laser [106] in 2003, the similariton laser in 2004 [52], the all-normal dispersion laser [166] in 2008, supporting dissipative solitons [103], and the soliton-similariton laser [47] in 2010, which is the only laser to date that has two types of nonlinear waves propagating in the cavity [**?**]. While these developments have led to superior laser performance and unravelled new laser physics, there is currently no possibility of detailed control over the mode-locking states that the lasers support.

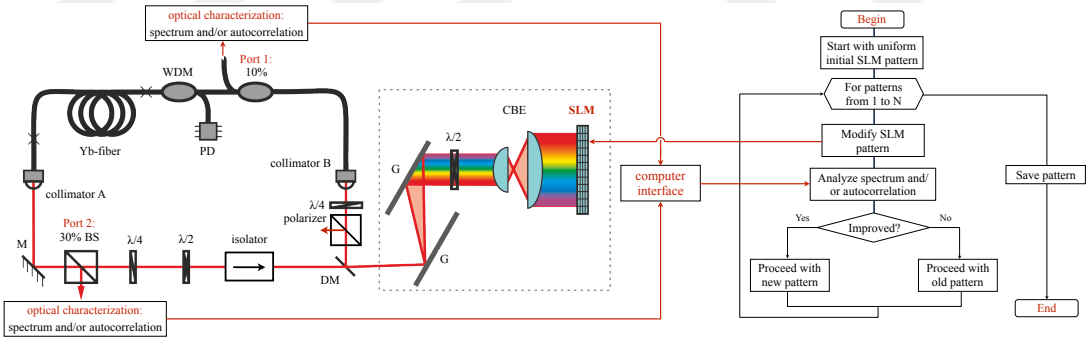

Figure 7.1: Experimental setup: Schematics of the experimental setup comprising of Yb-doped fiber, wavelength division multiplier (WDM), pump diode (PD), 10%-coupler, collimators A and B, 30% non-polarizing beamsplitter (BS), $\lambda/2$- and $\lambda/4$-waveplates, polarizing isolator for unidirectional operation, and dispersive delay line with diffraction gratings (G), mirrors (M), D-shaped mirror (DM), cylindrical beam expander (CBE) and spatial light modulator (SLM). The SLM is controlled by a computer algorithm, which takes into account measured optical spectrum or autocorrelation data. Main elements of the quasi-realtime control algorithm are also shown. Adapted from [1] with permission.

Here, we report on direct control of the mode-locking states, nonlinear restructuring of each state, reversible and irreversible transitions between them, Generation of arbitrary wave forms from a given soliton states or dissipative solution, manipulation of pulse positions in a train of pulses and blue or red shifting

of pulse spectral components based on algorithmic modulation or reshaping of the pulse in the spectral domain directly inside the cavity. To this end, we use a spatial light modulator (SLM) positioned in the Fourier plane of a zero dispersive delay line in a fiber laser cavity. Use of fixed spectral filters to influence mode-locking goes back to 1980s [167]. There are recent demonstrations of SLM-based spectral filtering using amplitude modulation in picosecond fiber lasers [168, 169]. Here we explore pulse dynamic and fully adjustable control on mode locking states through amplitude and phase modulation on Fourier domain. We now show that we can initiate or halt mode-locking, steer the mode-locking state to more favourable, but difficult-to-reach states, prevent cw breakthrough instability, automatically improve pulse shape, generate pulses as short as 40 fs, steer between different cavity solutions, generation of different wave forms, tweezing and manipulation of temporal position of pulses with in a bunch or bound multi-pulse states and blue and red shifting of spectral components with in the optical spectrum. Such applications enable the laser cavity to be a source of arbitrary optical wave forms for coherent quantum control of biological, chemical, magnetic or physical nano scale processes, fundamental studies of dissipative cavity solutions and its relation to other nonlinear far-from-thermodynamic equilibrium processes in nature [31, 170–173].

7.2 Experimental result

7.2.1 Adaptive filtering through amplitude modulation of spectral combs

In order to demonstrate our approach, we have replicated the first wave-breaking-free laser [106] and then modified it to include the SLM. We have chosen this laser, since it offered an additional challenge. Even though mode-locked operation, once adjusted, was robust, finding that state required laborious adjustment of the waveplates and pump power to limit a persistent CW peak, which could not be completely eliminated. Could we suppress this peak using the SLM only?

Schematics of the experimental setup is shown in Fig. 7.1. The repetition rate is approximately 40 MHz. The cavity comprises of ∼2.3 m-long passive fiber corresponding to the lead fibers of two collimators, a 10%-coupler for monitoring and a wavelength division multiplexer (WDM) for pump delivery. The gain fiber is 30 cm-long Yb-doped fiber (Yb1200-4/125, nLIGHT, Inc.). The 980-nm pump diode provides maximum 600-mW power, ∼500 mW of which can be delivered to the gain fiber following losses at pump protection filters and the WDM. The lead fiber of the collimator after the gain fiber is ∼10 cm. After the fiber section, the beam traverses a 30%-beam-splitter, followed by a quarter and a half waveplate, a polarizing beam-splitter, which converts polarization rotation into amplitude modulation, a dispersive delay line and a final quarter waveplate that converts the beam into elliptical polarization before coupling back into the fiber section. Total cavity dispersion was set to $+4000$ fs^2.

The SLM (Pluto, Holoeye, Inc.) was incorporated by replacing the end mirror of the dispersive delay line. The beam incident on the SLM matrix is spectrally spread along the horizontal direction with a resolution 25 pixels/nm. Each column of pixels of the SLM matrix imparts a relative phase delay that can electronically be adjusted over the $0 - 2\pi$ range. The beam is optionally expanded by a cylindrical beam expander (expansion ratio of 1:3.2) to better fill the SLM aperture. The grating pair partially acts as a linear polarizer and it is followed by another polarizer. By including a half-wave plate between the SLM and the grating pair, we convert the spectral phase modulation imparted by the SLM to amplitude modulation. The modulation depth is adjustable through the half-wave plate. The lowest and highest transmission are set to $\sim$ 20% and 64%, respectively. The lower value is set conservatively by the losses that the laser can comfortably tolerate. The upper limit is determined by the losses of the SLM matrix. Transmittance of each spectral element can be independently adjusted to 180 equal levels. Despite the losses of the SLM, typical power after gain fiber is 180 mW and power coupled back into the fiber section is 13 mW at pump power of 400 mW. This is close to the typical efficiency for similar lasers, implying that the presence of the SLM does not contract the accessible phase space of the laser's operation too much.

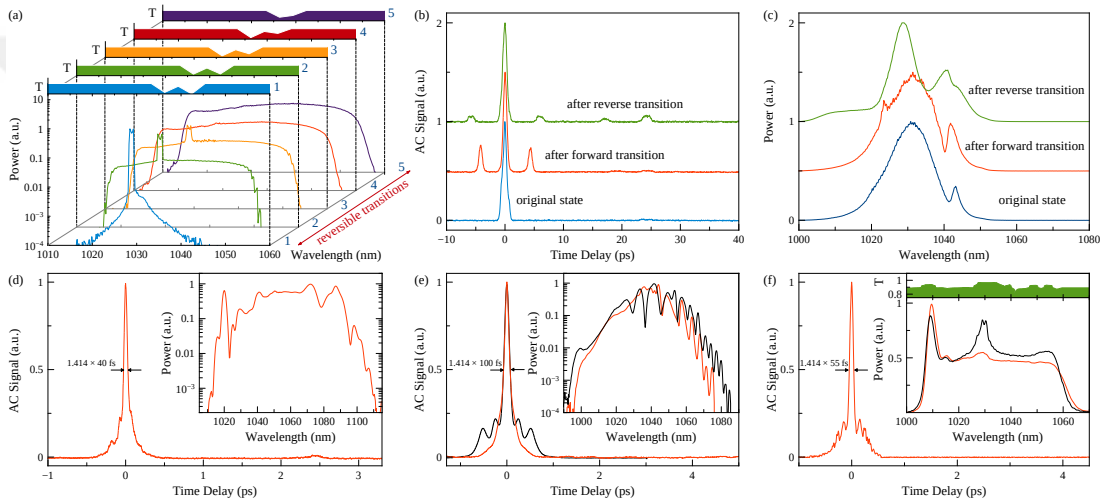

Figure 7.2: Experimental results for amplitude modulation: Control of mode-locking states using the SLM: (a) Optical spectra corresponding to reversible transitions from CW to mode-locking with CW peak to pure mode-locking. The corresponding spectral filters applied by the SLM are shown at the top of each panel. (b) Autocorrelations and (c) optical spectra corresponding to repeatable irreversible transitions. (d) Autocorrelation trace of 40 fs-long pulses. Inset shows corresponding optical spectrum. (e) Autocorrelation traces showing SLM-based pedestal removal; inset shows corresponding optical spectra. Black (red) lines before (after) filtering. (f) Elimination of undesired, characteristic spectral structure for a wave-breaking-free laser operating near its stability limit in terms of pulse energy. Autocorrelation trace is shown. Inset shows spectra before filtering (black line) and after filtering (red line) along with the filter transmission pattern. Adapted from [1] with permission.

The fundamental capability of the SLM to transform a pulse is the same as in its well-known usage outside the cavity [174, 175]. However, because of being placed inside the cavity, its role is completely different. The SLM becomes another cavity element that transforms the pulse nonlinearly and dispersively with the major advantage of this transformation being dynamically reconfigurable. Nevertheless, it is also constrained and cannot be made to impart an arbitrary transformation, because it must comply with the stringent requirement that all changes must balance each other at the end of each round-trip [28, 176].

For simple tasks, such as disruption of mode-locking or preliminary and crude shaping of prominent features in the spectrum, one can guess the required spectral transmission profile after having acquired some experience. For a more complex operation, the necessary spectral transformation profile is not easy to determine. We have developed an iterative computer algorithm (Fig. 7.1), to which we can specify various goals, such as reduction of autocorrelation width, maximization of the autocorrelation's peak or maximization of FWHM (or root-mean-square, *e.g.*) of the spectrum. This iterative procedure is capable of testing a large number (order of thousands) of transmission profiles in order to maximize a merit function, which is supposed to characterize the desired outcome. For experimental measurement and confirmation, either the optical spectrum or autocorrelation can be used. Overall, this configuration constitutes a quasi-realtime feedback loop between the laser, the SLM and the controlling computer.

For the sake of simplicity, we now describe a specific implementation of the optimization algorithm that maximizes the FWHM of the spectral bandwidth. Other variants, such as disruption of mode-locking (requiring minimization of the spectral FWHM), elimination of a specific feature (by calculating the merit over a limited portion of the spectrum) or maximization of another merit (such as the autocorrelation width) are implemented similarly. Using a single numerical value as merit has obvious limitations, but it allows us to vastly simplify the algorithm and increase the iteration speed. The iterative process itself is primitive, but robust and effective (albeit with some restrictions, discussed below): It scans the spectrum from one edge to the other, experimenting with different phase values for each spectral element. The transmission values are varied by scanning the

phase value within from $-\pi/16$ to $+\pi/16$ with steps of $\pi/96$ around its previous value. If any change results in an increase of the spectral bandwidth, the value of that spectral element is updated. In other to minimize erroneous updates due to naturally occurring fluctuations, the FWHM values are first averaged over 5 measurements, and total measurement takes 50-70 ms. The SLM matrix itself can be updated within 20 ms. Thus, a full readout and reconfiguration cycle lasts about 100 ms. While this is relatively fast, typically thousands of iterations are made. Each optimization ranged from mere seconds or several minutes (for simple tasks) to as much as 3 hours for an exhaustive search. We note that both the algorithm and the data acquisition setup described here constitute a first demonstration and can certainly be vastly improved by sophisticated algorithms, such as those used in [177].

We first demonstrate the ability to initiate or halt mode-locking, followed by suppression of an instability and finally detailed shaping of the spectrum (Fig. 7.2). We have found that a transmission profile with a local dip at the central wavelength of the laser, surrounded by two neighboring, deeper minima (state 1 of Fig. 7.2a), is highly effective in disrupting mode-locking with only $\sim 10\%$ of reduction in transmittance at those wavelengths, even though the waveplates were adjusted for self-starting mode-locking. In order to put this value into perspective, we note that the same cavity could tolerate much higher losses (up to 90% was observed) in certain waveplate settings [106], when losses were spectrally uniform. We repeatedly confirmed that mode-locking immediately restarted after the SLM was set to uniform transmission (or some other profile, such as state 5 of Fig. 7.2a). Halting, restarting of mode-locking could be repeated indefinitely at other mode-locking states that the laser exhibited at different pump power and waveplate settings. Similarly, when the laser is in a non-self-starting mode-locking state, mode-locking can be initiated by applying a narrow filter, which is gradually broadened and then removed.

We show that one can suppress a commonly encountered instability, namely, formation of a CW peak accompanying a mode-locked spectrum (state 2 in Fig. 7.2a) when the intra-cavity energy exceeds the level a single pulse can hold. Further increases in nonlinearity lead to a bifurcation; most commonly the pulse

breaks up into multiple pulses, less commonly, transitions into a noise-like state or into a multi-wavelength state [160]. Even before such a bifurcation, the presence of a CW peak leads to order-of-magnitude increase in intensity fluctuations of the laser [122]. To illustrate this, we adjust the pump power and waveplate settings for a self-starting mode-locked state with an accompanying CW state to be formed when the SLM is set to a flat transmittance profile. We show that by selectively reducing transmission of its central wavelength, the CW peak can be reduced (state 3 of Fig. 7.2a), highly suppressed (state 4) and even completely eliminated (state 5) by selectively inducing attenuation on intended spectral comb or component.

The transitions shown in Figure 2(a) are completely reversible and indefinitely repeatable. By switching the profile of the SLM, we can transition among all 5 states reliably and in either direction. From the physics point of view [130], irreversible transitions are most interesting. We can indeed induce irreversible transitions using the SLM controllably and repeatedly: By turning the pump off and on, the laser always is placed in the same original state, so the experiment can be repeated indefinitely many times. Upon execution of an SLM pattern sequence, the laser transitions to a different state. However, upon application of the time-reversed sequence, unlike the reversible transitions in Fig. 7.2(a), the laser ends up at different mode-locking states at each realization due to fluctuations (noise) present in the system (Fig. 7.2(b) and 7.2(c)). This setup is ideally suited to test emerging theories about non-equilibrium systems [178].

A legitimate concern is whether the SLM introduces spurious optical phase, deteriorating the pulse quality or excess intensity noise, both of which may not be discernible from the optical spectrum. To check against the former, we dechirped spectra outside of the cavity using a grating compressor for various cases. We were able to obtain pulses as short as 40 fs, assuming a Gaussian deconvolution factor when we optimized for minimum autocorrelation width (Fig. 7.2(d)). Given the spectral width of 50 nm, the time-bandwidth product is 0.56, which is within 25% of the transform limit. The pedestal is likely due to residual third-order dispersion (TOD) and excess nonlinear phase shift. The second possibility is addressed by close-up RF spectrum around the fundamental repetition frequency, which shows

at least 90-dB (limited by measurement) suppression of sidebands. Thus, there is no evidence of adverse effects on pulse shape or excess noise due to the SLM.

Finally, we demonstrate use of the SLM for advanced pulse shaping. Our purpose here is to demonstrate the potential, rather than optimize this specific laser's output. Thus, we only provide generic examples. We first focus on cleaning up the pedestal for an intentionally chosen, highly structured spectrum (Fig. 7.2(e)). In our experience, such a spectrum corresponds to the edge of stability of mode-locking. The SLM profile we converge to is a simple narrow (6 nm-wide) band-stop filter (centred around 1030 nm), which transforms the laser to another, less modulated spectrum. This example succinctly demonstrates that the nonlinearity and periodicity of the cavity means that even a small spectral modulation with a profile that no human would likely guess can have large consequences.

As discussed above, our self-imposed target was to duplicate the hard-to-find mode-locking state that is characteristic of the original wave-breaking-free laser laser. We duplicate this state as recorded from Port 2 (Fig. 7.2(f); note the similarity to Fig. 7.2 of [106]). We focus on suppression of the pesky structure at the center, which contains about $\sim 20\%$ of the total energy. The structure on the blue edge is a characteristic feature of this mode-locking state, akin to similar structures on all-normal-dispersion lasers [166]. As such, one should not attempt to eliminate it; otherwise the mode-locking state changes completely. This time, our algorithm converges to a more complex profile (top panel of the inset of Fig. 7.2(f)), which leads to excellent suppression of this feature, resulting in a spectral width of 50 nm. The corresponding dechirped pulse duration is 55 fs, assuming a Gaussian pulse, where the width and the size of the pedestal is similar to the results in [106]. However, this state is now obtainable using a simple algorithm controlling the SLM. Thus, we have met our original challenge of obtaining a wave-breaking-free laser mode and also eliminating this pesky spectral feature without active human intervention.

7.2.2 Pulse manipulation by dynamic periodic linear spectral phase mask in fiber oscillator

Next, we introduce spectral phase modulation to manipulate the optical temporal structures in a ring cavity, analogous to particle tweezing. Spatial optical manipulation of particles is common practice in laboratories around the world since 1970 [179] due to its important applications. Similarly, tweezing optical solitons in time domain has gained interest due to its applications, such as pulse shaping [175], in data flow management of optical communication [180], spatial and spectral coherent control in nonlinear spectroscopy [181], for managing heat effects in material processing [5], optical switching and manipulation of magnetization [182, 183] etc. The pioneering work for practicing of control of pulse delay with an idea of *"fast and slow"* light was enabled through the effects of *"spectral narrow resonance"* created by radiation induced transparency. That method requires a special propagation medium maintained at cryogenic temperatures and a pulse signal with spectrum narrower than the resonance bandwidth of the atomic transition [180,184]. By that, the researchers were able to induce a delay of tenths of micro seconds between pulses. It should be noticed that nonlinear pulse broadening imposes a trade-off between the signal spectral bandwidth and resonance bandwidth in optical fibers, hence the delay induced by such process is limited [180,185]. Another method is the optical manipulation of pulses by phase modulation of the pumping source, or a carrier radiation, is recently reported in passive resonator [131]. However, such method requires synchronization of the phase modulation applied on the driving field and the cavity repetition rate for tweezing the pulse. Here, we report a method with less degree of complexity that enables manipulation of the temporal position of femtosecond optical solitons inside oscillator by directly applying dynamic periodic phase modulation mask on its own spectrum.

In order to have effective control, we introduce the well-known zero dispersion 4-f pulse shaping configuration [175] to apply the spectral phase modulation. The 600 lines/mm grating is kept in the cavity for dispersion management with the

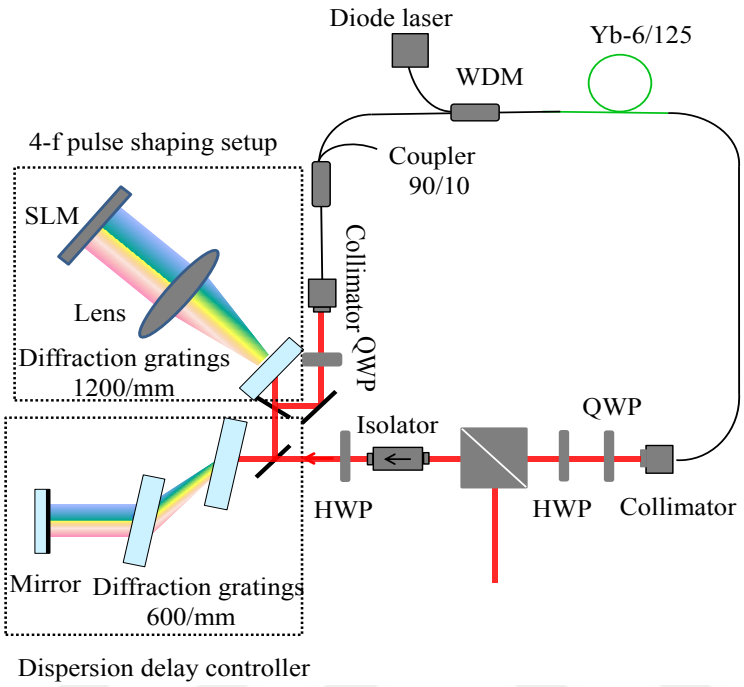

Figure 7.3: Experimental setup for phase modulation: Schematics of dispersion managed fiber oscillator with zero dispersion 4-f pulse shaping configuration used for spectral phase modulation.

position of SLM on Fig. 7.1 replaced by a mirror. A single 1200 lines/mm efficient transmitting grating performs angular dispersion. A cylindrical lens with 100 mm focal length converts the angular dispersion to a spatially separated frequency components on to the surface of the SLM. The whole set up is called zero dispersion in a 4-f configuration. Spatial holographic patterns or phase mask are applied on the SLM to manipulate phase on the Fourier spectral components. This configuration has a resolution of 5.5 nm per 45 pixels and introduces additional 15 percent insertion loss. The cavity net dispersion is intentionally kept at about -9000 fs^2. The cavity in such conditions generates multi-soliton states exhibiting active matter like far-from-equilibrium thermodynamics governed by long and short range interactions.

On the SLM, a blazed grating at fixed period with varying phase between 0 and 2π is applied to manipulate certain arbitrary soliton state. The laser stays mode-locked while these patterns on the SLM are varied along a direction perpendicular to the propagation of pulses such that it provides both discretely

and continuously varying phase with time on the spectral components in Fourier domain. Physically, the applied pattern imposes a linear phase variation in the frequency domain, which is equivalent to a temporal shift of the waveform in the time domain by an amount proportional to the slope of the linear phase variation. Since the SLM has a finite diffraction efficiency, two collinear beams are produced, one that has not been altered by the SLM and the other that was altered. The altered one is temporally shifted with respect to the unmodified one, which is similar to adding a temporally delayed replicate of a pulse.

It has been recently reported that solitons can be attracted towards local phase maxima [131]. The pattern is scanned until some of the solitons in the cluster start responding to phase gradient on the mask. Moving the mask patterns slightly further from this point we able to decrease pulse separation by 5.2 ps (the case for Fig. 7.3(a) and 7.3(b)), turn a stable state (the case for Fig. 7.3(c) and 7.3(d)) into an oscillatory state with a temporal separation of 1.65, which is similar to particle motion under a harmonic-oscillator-like potential. We have been able to induce creation and removal of additional pulses in addition to changing a stable state into an unstable gas like soliton states and vice versa. What makes this more surprising is that the mode locking is intentionally chosen to be not a self-starting one. The observed dissipative temporal structures maintain their existence not only by taking energy from the pump source but also supported by the frequency shifts resulted from induced phase gradient [48, 58].

A phase gradient on spectral combs is generated as the patterns on the SLM move. This creates a blue or red shift on spectral components depending on the increase or decrease of the phase gradient with time. Fig 7.4 shows a 310 THz frequency shift of relatively stronger spectral component. Such a purely electronically controlled shift may find applications in selective excitation of certain energy levels in fluorescence spectroscopy or microscopy, and in nonlinear harmonic generation [131, 186–188].

Similar results were observed when the pattern on the SLM was slowly varied at a constant speed. As the speed increases spontaneous symmetry breaking and

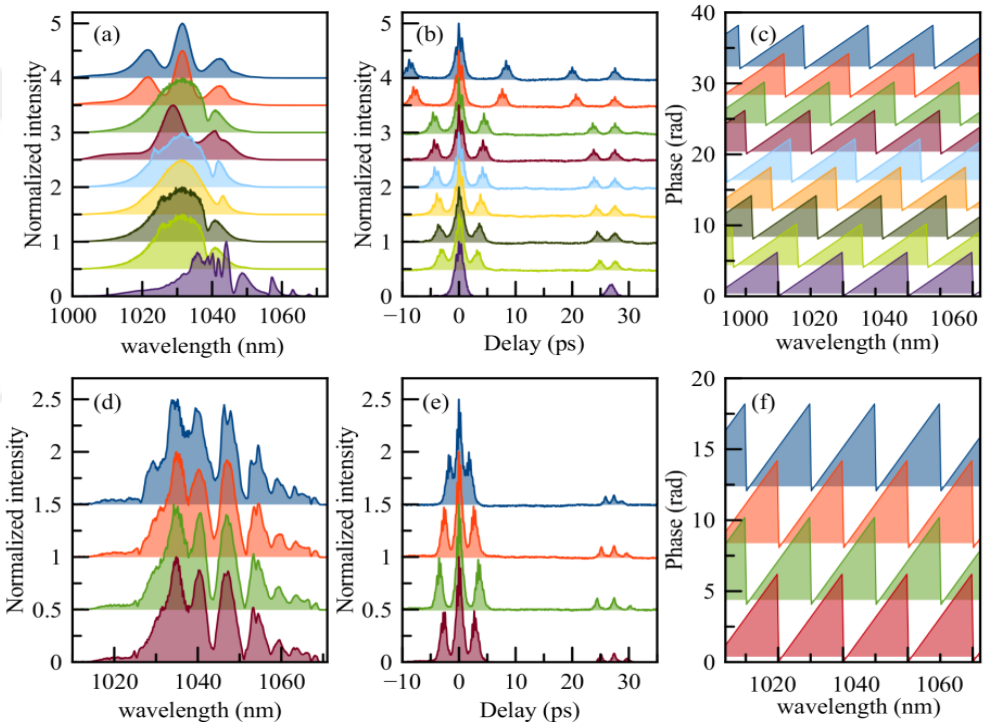

Figure 7.4: Temporal tweezing of soliton: (a) Optical spectra and (b) corresponding autocorrelation measurements of the soliton state as the blazed grating pattern (c) on the SLM is scanned in discrete steps horizontally or perpendicular to the propagation direction. (d) Optical spectra and (e) corresponding autocorrelation signal of controllably changed into oscillatory soliton pulse state from a stable state by discreetly applying periodic phase mask patterns (f) for respective states indicated by the same color.

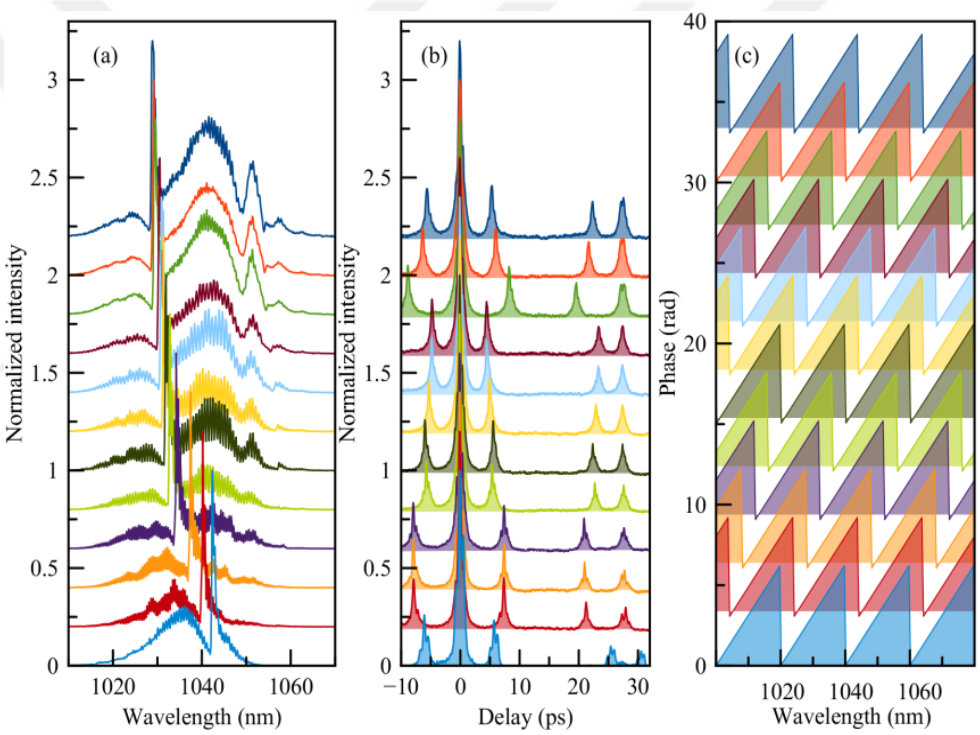

Figure 7.5: Frequency shifting: (a) Optical spectra and (b) corresponding autocorrelation signal of soliton state as the blazed grating pattern indicated by (c) on the SLM is scanned in discrete steps horizontally or perpendicular to the propagation direction. The direction of motion of the patterns determines the sign of phase gradient.

self-reorganization of temporal structures happened similar to other natural phenomena such as oscillatory chemical reaction or environment dependent change in colour of chameleon skin [189]. The oscillator solution varies rapidly and when the pattern on the SLM stop moving, the laser remains in a single solution. This controlled temporal structuring of lasing states could have potential applications in information storage and processing [**?**]. The fact that a single solution remains in the steady state when a uniformly distributed constant phase pattern on the SLM moves with constant speed indicates that the results are not as a result of Doppler shift.

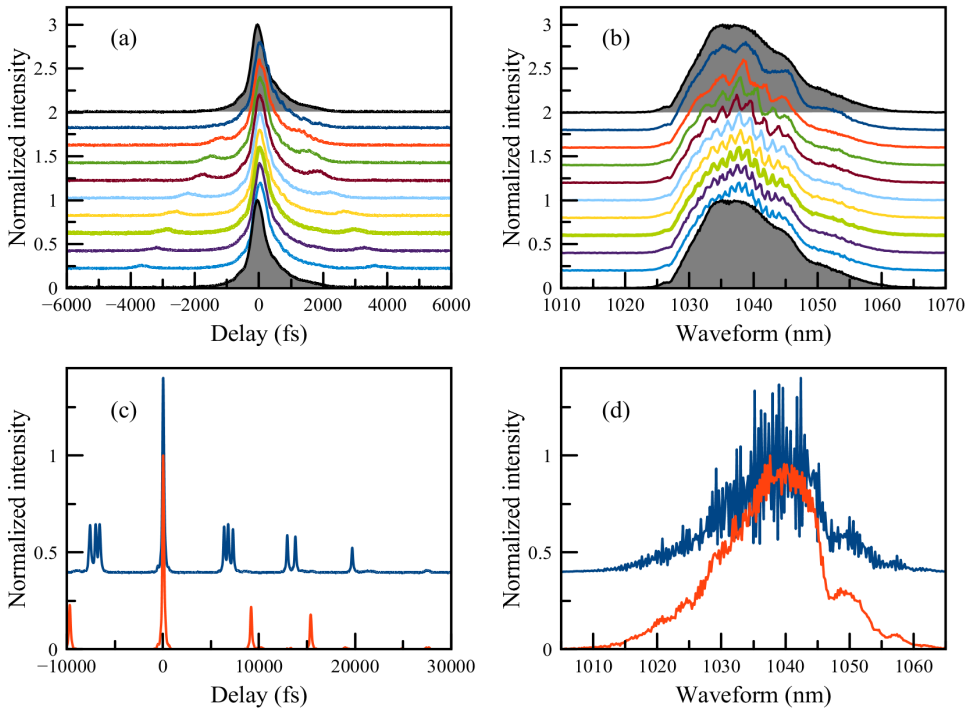

Figure 7.6: pulse splitting: Traces in (a) and (b) are the autocorrelations and corresponding optical spectra of the soliton states as the period of holographic blazed gritting on the SLM is varied. (c) and (d) show the autocorrelation and corresponding optical spectra with (blue, blazed gritting of period 1) and without the (red) linear phase modulation.

Pulse splitting is another interesting process that can be done with the same or similar procedure. Highly varied, even arbitrary wave forms have been generated outside laser cavities for applications like coherent control of quantum dynamics

[181], manipulation of chemical reaction, nonlinear spectroscopy [189] and all-optical magnetization switching [190]. The result in Fig. 7.5 (a and b) is obtained when period of holographic grating are varied (from 5, 8, 10, 12, 15, 18, 20, 22, 25, 28, 30, 32, 35 discretely). A dwarf pulse is split and controllably pushed away from the main soliton as the period is increasingly scanned. As this dwarf pulse is pushed away it is strangled by the periodic boundary condition of the cavity dynamics. Although the range of the different waveforms that can be generated here are clearly limitedin our caase, Fig. 7.5(c and d) demonstrates the possibilities of control.

7.2.3 Conclusion

In conclusion, we have demonstrated adaptive selection, controlled transitions between and individual restructuring of mode-locking states using an intra-cavity SLM, generation of pulses as short as 40 fs with ease, manipulation of pulse shape and positions including tweezing of soliton states and blue as well as red shifting of stronger spectral components on optical spectrum of a pulse. The demonstrations reported here provide merely a glimpse of what is possible. Clearly, various practical applications can be imagined, such as improving laser performance, automated mode-locking [177], generation of an arbitrary optical waveform. We are deeply motivated to use this capability to experimentally investigate bifurcations, reversible and irreversible transitions, by selecting, steering, even competing for various mode-locking states. Such studies can explore collective dynamics of dissipative soliton molecules [103], Casimir-like pulse-to-pulse interactions [191], and ultimately test emerging theories about far-from-equilibrium physics [130, 178], where there is an acute lack of experimental systems that are well controlled.

We also note that an intra-cavity SLM may not be desirable for non-scientific applications due to its cost and complexity. However, one can first determine spectral amplitude and phase profile that addresses a specific need using SLM, after which a custom dielectric filter with a corresponding profile can replace the SLM.

Chapter 8

Conclusion and future perspectives

The basic premise of this thesis is to take a fresh look at the rich dynamics of mode-locked lasers from two perspectives, simultaneously and for the first time, to our knowledge. Namely, that the nonlinear dynamics of mode-locking of lasers is rich and particularly so in the case of fiber lasers is well known. Furthermore, it was shown that exploiting the rich and strong nonlinear dynamics can lead to better laser performance, in addition to the fundamental interest in the topic, was probably argued for the first time in the Ph.D. of Dr. F. Ö. Ilday, the advisor for the present thesis. However, to date, there has been little appreciation and no detailed study that provides a general perspective including both the far-from-equilibrium dynamics of mode-locking and the nonlinear dynamics of mode-locking. Previous efforts, led by the group of Dr. B. Fischer from Technion, Israel, have mostly focussed on equilibrium and near-equilibrium dynamics. It is beyond the scope of this thesis, also, to provide a comprehensive nonlinear and far-from-equilibrium perspective, but it is our hope that the results presented here will, first highlight the importance of and potential for new understanding of this perspective and also provide an important starting point for the studies surely to follow. We believe that such explorations will be interesting not for laser physics per se, but, possibly even more importantly, mode-locked lasers will come to be

recognized as versatile tools for highly quantitative studies of far-from-equilibrium phenomena in general.

Below, we will recapitulate the main results of this thesis before presenting our perspective for future studies. We first demonstrated an impressive performance by generating 1.2-nJ and 62-fs linear-chirp-free pulses from a custom-designed fiber oscillator simply by exploiting the nonlinear interplay between SPM and TOD, thereby achieving energetic pulses without requiring external compression (Chapter 3). The inclusion of a second DDL enabled us to tune TOD without affecting the net GVD. Given that there are DDLs with very low insertion loss suggests that we can even avoids the tradeoff in laser efficiency. These results constitute a step forward in the design of custom oscillators, where the designer can manipulate dynamics to reach a particular, preplanned output. Further efforts can incorporate additional dynamics such as intra-cavity extreme nonlinear broadening for generation of ultrashort pulses, intra-cavity Cherenkov radiation generation for broadband spectral tunability and even intra-cavity harmonic wave generation, among others.

An oscillator with two gain segments was used to manage the nonlinearity map, i.e., both its strength and its distribution throughout the cavity (Chapter 4). We have shown that the pulse evolution can experience an effective negative nonlinearity from the complex interplay of gain filtering, dispersion, SPM, four-wave mixing, inverse four-wave mixing, and frequency chirp on the pulse, even though all of the optical segments making up the cavity have strictly positive nonlinearity coefficients. This idea can be exploited to push both the energy and pulse duration limits of fiber laser systems in the future.

Next, we explored the characteristics of amplitude modulation on the pump source and how it is transferred to the signal power inside the oscillator. Our investigations covered all the major regimes of mode-locking, revealing qualitatively similar characteristics, despite large quantitative differences. Complex interactions between optical pulses were observed at certain critical points. Increasing the pumping, i.e., effective nonlinearity, beyond these critical points

resulted in phase transitions to new pulsing states, which were typically multiple-pulsing states. Amplitude modulation near these critical points cause the laser system to favor certain pulsing states among other, nominally coexisting, mode-locked "macrostates". Understanding the selection criterion of such phenomena will definitely shade light on understanding the basic thermodynamics of self-organization not only in the laser system under study, but possibly in a large class of similar nonlinear systems and in testing emerging theories on non-equilibrium systems [130, 178] and various motif information processing systems [192–195].

In chapter 7, an intra-cavity spatial light modulator was used to further manipulate the pulse amplitude and phase dynamics. We have demonstrated an adaptive selection of, controlled transitions between and individual restructuring of mode-locking states. Generation of pulses as short as 40 fs were achieved with ease, and manipulation of pulse shape and positions including tweezing of soliton states and blue as well as red shifting of stronger spectral components on optical spectrum of the pulse. The demonstrations reported here provide merely a glimpse of what is possible. Clearly, various practical applications can be imagined, such as improving laser performance, automated mode-locking [177], generation of an arbitrary optical waveform. We are deeply motivated to use this capability to experimentally investigate bifurcations, reversible and irreversible transitions, by selecting, steering, even triggering competition among various mode-locking states. Such studies can shed light on nonlinear and collective dynamics of dissipative soliton molecules [103], pulse-to-pulse interactions [191].

A particularly interesting proposition is the so-called dissipative adaptation theory forwarded by Dr. Jeremy England, et al. from MIT. Based on the idea that a biological system is a physical system that has a fluctuating structure and functionality, they proposed this theory, which was supported by thermodynamic analysis of a chemical system. However, there is no experimental test to date. We note that those systems are much harder to analyze experimentally, than the mode-locked lasers discussed in this thesis. As we mentioned earlier, when the nonlinearity is strong enough, i.e., when there is sufficient pump power, a laser oscillator can support a number of coexisting mode-locking macrostates that can be driven with the external source so that the system oscillates or rapidly switches

between these macrostates. For instance, Fig. 8.1 shows the autocorrelation signal of certain accessible macrostates at a pump power of 530 mW, driven by an external sinusoidal modulation with 0.1 percent modulation depth and at a frequency of 100 Hz. The grouping is done by choosing three states which have almost the same or similar cavity life time. The average time spent in each group, the corresponding average measured output power after the gain fiber, calculated dissipated energy relative to the first group (group (a)), and repetition rate are provided in Table 8.1. From these data, one can roughly state that the system spends more of its time in the macrostates that dissipate more energy, which is consistent with dissipative adaptation. However, we believe a lot has to be done along this direction to connect quantitatively to this theory, but this is a promising first result. In particular, it is important to measure how much of the driving energy is dissipated by each available macrostate. Nevertheless, we believe that this system is likely a more practical platform than the chemical systems to test this theory [73, 178].

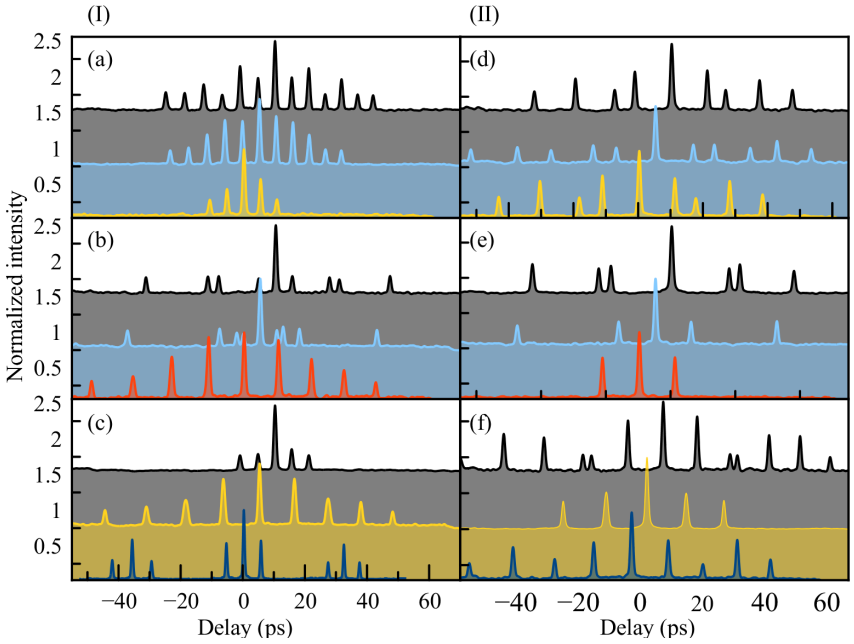

Figure 8.1: Driven dissipative adaptation: Autocorrelation function of optical soliton states undergoing dissipative adaptation inside fiber oscillator with an external driving signal with 0.1 percent modulation depth at a frequency of 100 Hz.

Table 8.1: Averaged parameters of the mode locking macrostates indicated on Figure 8.1

State	Time(s)	Average power (mW)	$\Delta E(pJ)$	Rep. rate (MHz)
(a)	–	103.30	–	49
(b)	0.96	103.26	0.7	49
(c)	0.68	103.98	0.5	49
(d)	2.2	102.01	5.8	49
(e)	1.9	103.08	6.4	49
(f)	120.4	102.52	15.8	49

Shortage of reasonably well controlled and sufficiently quantitative experimental platform for studies in far-from-equilibrium physics is broadly appreciated [196], which renders testing of theories developed in the field difficult and slows down progress. Dissipative soliton dynamics in mode-locked lasers is a rich and promising phenomenon in this regard, particularly because measurements of laser parameters, such as power, pulse duration, and especially dynamic phenomena, such as fluctuations, transitions are relatively easy in comparison to far-from-equilibrium phenomena in the nanoscale or biological systems. Furthermore, various optical techniques exist for control of laser systems, such as the external pump modulation and the intra-cavity spatial light modulators, used for the first time in this thesis for controlled transitions between mode-locking states. The challenges are also numerous and include the necessity to adopt non-equilibrium principles and terminology developed originally for chemical and biological systems to laser physics. We believe that the present thesis has taken a first step in this direction. The author of this thesis is strongly motivated to continue his studies along this direction.

Bibliography

[1] R. Iegorov, T. Teamir, G. Makey, and F. Ö. Ilday, "Direct control of mode-locking states of a fiber laser," *Optica*, vol. 3, no. 12, pp. 1312–1315, 2016.

[2] A. H. Zewail, "Femtochemistry. past, present, and future," *Pure Applied Chemistry*, vol. 72, no. 12, pp. 2219–2231, 2000.

[3] Th. Udem, R. Holzwarth and T. W. Hänsch, "Optical frequency metrology," *Nature*, vol. 416, no. 6877, pp. 233–237, 2002.

[4] K. Sugioka and Y. Cheng, "Optical frequency metrology," *Light: Science & Applications*, vol. 3, pp. e149 1–12, 2014.

[5] C. Kerse, H. Kalaycoglu, P. Elahi, B. Cetin, D. K. Kesim, Ö. Akcaalan, S. Yavas, M. D. Ask, B. Öktem, H. Hoogland, R. Holzwarth and F.Ö.Ilday, "Ablation-cooled material removal with ultrafast bursts of pulses," *Nature*, vol. 537, no. 7618, pp. 84–88, 2016.

[6] M. Wegener, "Extreme nonlinear optics," *Springer-Verlag Berlin Heidelberg*, vol. 1st, 2005.

[7] P. B. Corkum, F. Krausz, "Attosecond science," *Nature Physics*, vol. 3, no. 6, pp. 381–387, 2007.

[8] H. W. Mocker and R. J. Collins, "Mode competition and self-locking effects in a q-switched ruby laser," *Applied Physics Letters*, vol. 7, no. 10, pp. 270 – 273, 1965.

[9] A. Demaria, D. Stetser and H. Heynau, "Self mode-locking of lasers with saturable absorbers," *Applied Physics Letters*, vol. 8, no. 7, pp. 174–176, 1966.

[10] U. Keller, K. Weingarten, F. Kartner, D. Kopf, B. Braun, I. Jung, R. Fluck, C. Honninger, N. Matuschek, and J. Au, "Semiconductor saturable absorber mirrors (sesams) for femtosecond to nanosecond pulse generation in solid-state lasers," *IEEE Journal of Selected Topics in Quantum Electronics*, vol. 2, no. 3, pp. 435–453, 1996.

[11] F. Wang, A. Rozhin, V. Scardaci, Z. Sun, F. Hennrich, I. White, W. Milne, A. Ferrari, "Wideband-tuneable, nanotube mode-locked, fibre laser," *Nature Nanotechnology*, vol. 3, no. 12, pp. 738 – 742, 2008.

[12] W. Liu, L. Pang, H. Han, W. Tian, H. Chen, M. Lei, P. Yan, Z. Wei, "70-fs mode-locked erbium-doped fiber laser with topological insulator," *Scientific Reports*, vol. 5, no. 19997, pp. 1–7, 2016.

[13] D. Spence, P. Kean, W. Sibbett, "60-fsec pulse generation from a self-mode-locked Ti:sapphire laser," *Optics Letters*, vol. 16, no. 1, pp. 42–44, 1991.

[14] T. Sogawa, Y. Arakawa1, M. Tanaka1 and H. Sakaki, "Observation of a short optical pulse (<1.3 ps) from a gain switched quantum well laser," *Applied Physics Letters*, vol. 53, no. 1580, pp. 1580–1582, 1988.

[15] V. Matsas, T. Newson, D. Richardson and D. Payne, "Self-starting passively mode-locked fibre ring soliton laser exploiting nonlinear polarisation rotation," *IEEE Electronics Letters*, vol. 28, no. 15, pp. 1391–1393, 1992.

[16] M. Fermann, F. Haberl, M. Hofer, H. Hochreiter, "Nonlinear amplifying loop mirror," *Optics Letters*, vol. 15, no. 13, pp. 752 – 754, 1990.

[17] N. Tarasov, A. M. Perego, D. V. Churkin, K. Staliunas and S. K. Turitsyn, "Mode-locking via dissipative faraday instability," *Nature Communication*, vol. 7, no. 12441, pp. 1–4, 2016.

[18] M. Yu, Y. okawachi, A. Griffith, M. Lipson, A. Gaeta, "Mode-locked mid-infrared frequency combs in a silicon microresonator," *Optica*, vol. 3, no. 8, pp. 854–860, 2016.

[19] T. Nagy and G. Steinmeyer, "A closer look at ultra-intense lasers," *Nature Photonics*, vol. 10, no. 8, pp. 502–504, 2016.

[20] L. Leuzzi, C. Conti, V. Folli, L. Angelani, and G. Ruocco, "Phase diagram and complexity of mode-locked lasers: from order to disorder," *Physical Review Letters*, vol. 102, no. 8, pp. 083901 1–4, 083901 2009.

[21] J. Klein and J. D. Kafka, "The Ti:sapphire laser: The flexible research tool," *Nature Photonics*, vol. 4, no. 5, p. 289, 2010.

[22] F. Ö. Ilday, J. Buckley, L. Kuznetsova, and F. W. Wise, "Generation of 36-femtosecond pulses from a ytterbium fiber laser," *Optics Express*, vol. 11, no. 26, pp. 3550–3554, 2003.

[23] X. Zhou, D. Yoshitomi, Y. Kobayashi, K. Torizuka, "Generation of 28-fs pulses from a mode-locked ytterbium fiber oscillator," *Optics Express*, vol. 16, no. 10, pp. 7055–7059, 2008.

[24] J. R. Buckley, S. W. Clark, F. W. Wise, "Generation of ten-cycle pulses from an ytterbium fiber laser with cubic phase compensation," *Optics Letters*, vol. 31, no. 9, pp. 1340–1342, 2006.

[25] A. Chong, H. Liu, B. Nie, B. Bale, S. Wabnitz, W. Renninger, M. Dantus, "Pulse generation without gain-bandwidth limitation in a laser with self-similar evolution," *Optics Express*, vol. 20, no. 13, pp. 14213–14220, 2012.

[26] L. J. Qian, X. Liu, F. W. Wise, "Femtosecond kerr-lens mode locking with negative nonlinear phase shifts," *Optics Express*, vol. 24, no. 3, pp. 166–168, 1999.

[27] T. Eidam, J. Rothhardt, F. Stutzki, F. Jansen, S. Hädrich, H. Carstens, C. Jauregui, J. Limpert, A. Tünnermann, "Fiber chirped-pulse amplification system emitting 3.8 GW peak power," *Optics Express*, vol. 19, no. 1, pp. 255–260, 2011.

[28] F. Ö. Ilday, F. W. Wise, "Nonlinearity management: a route to high-energy soliton fiber lasers," *Optics Express*, vol. 19, no. 3, pp. 470–476, 2002.

[29] R. DeSalvo, D. Hagan, M. Bahae, G. Stegeman, E. Stryland, and H. Vanherzeele, "Self-focusing and self-defocusing by cascaded second-order effects in ktp," *Optics Letters*, vol. 17, no. 1, pp. 28–30, 1992.

[30] M. Bache, J. Moses, and F. W. Wise, "Fiber chirped-pulse amplification system emitting 3.8 gw peak power," *Journal of Optical society of America B*, vol. 24, no. 10, pp. 255–260, 2007.

[31] J. Dudley, F. Dias, M. Erkintalo, and G. Genty, "Instabilities, breathers and rogue waves in optics," *Nature Photonics*, vol. 8, no. 10, pp. 755–764, 2014.

[32] N. J. Zabusky and M. D. Kruskal, "Interaction of "solitons" in a collisionless plasma and the recurrence of initial states," *Physics Review Letters*, vol. 15, no. 6, pp. 240–243, 1965.

[33] J. Denschlag, J. Simsarian, D. Feder, C. W. Clark, L. Collins, J. Cubizolles, L. Deng, E. W. Hagley, K. Helmerson, and W. P. Reinhardt, "Generating solitons by phase engineering of a Bose-Einstein condensate," *Science*, vol. 287, no. 5450, pp. 97–101, 2000.

[34] C. Xu and F. Wise, "Recent advances in fibre lasers for nonlinear microscopy," *Nature Photonics*, vol. 8, no. 11, pp. 875–882, 2013.

[35] L. Wright, D. Christodoulides, and F. Wise1, "Controllable spatiotemporal nonlinear effects in multimode fibres," *Nature Photonics*, vol. 9, no. 5, pp. 306–310, 2015.

[36] A. Runege, N. Broderick, AND M. Erkintalo, "Observation of soliton explosions in a passively mode-locked fiber laser," *Optica*, vol. 2, no. 1, pp. 36–39, 2015.

[37] K. Kao and G. Hockham, "Dielectric-fibre surface waveguides for optical frequencies," *IEE Proceedings Journal of Optoelectronics*, vol. 113, no. 7, pp. 191–197, 1966.

[38] E. Mattia and S. Otto, "Supramolecular systems chemistry," *Nature Nanotechnology*, vol. 10, no. 2, pp. 111–119, 2015.

[39] D. A. Egolf, "Far from equilibrium," *Science*, vol. 290, no. 5574, pp. 1813–1815, 2002.

[40] D. Kondepudi and I. Prigogine, "Modern thermodynamics from heat engines to dissipative structures," *John Wiley and Sons, Chichester UK*, 2015.

[41] H. Sugiura, M. Ito, T. Okuaki, Y. Mori, H. Kitahata, and M. Takinoue, "Pulse-density modulation control of chemical oscillation far from equilibrium in a droplet open-reactor system," *Nature Communications*, vol. 7, no. 10212, pp. 1–8, 2016.

[42] S. Semenov, L. Kraft, A. Ainla, M. Zhao, M. Baghbanzadeh, V. Campbell, K. Kang, J. Fox, and G. M. Whitesides, "Autocatalytic, bistable, oscillatory networks of biologically relevant organic reactions," *Nature*, vol. 537, no. 7622, pp. 656–660, 2016.

[43] A. Aliprandi, M. Mauro, and L. Cola, "Controlling and imaging biomimetic self-assembly," *Nature Chemistry*, vol. 8, no. 1, pp. 10–15, 2015.

[44] T. M. Scanlon, K. K. Caylor, S. A. Levin, and I. Rodriguez-Iturbe, "Positive feedbacks promote power-law clustering of Kalahari vegetation," *Nature*, vol. 449, no. 7159, pp. 209–212, 2007.

[45] C. D. Nadell, K. Drescher, and K. R. Foster, "Spatial structure, cooperation and competition in biofilms," *Nature Review Microbiology*, vol. 14, no. 9, pp. 589–600, 2016.

[46] K. Ruiz-Mirazo, C. Briones, and A. de la Escosura, "Prebiotic systems chemistry: New perspectives for the origins of life," *Chemistry Review*, vol. 114, no. 1, pp. 285–366, 2016.

[47] B. Öktem, C. Ülgüdür, and F. Ö. Ilday, "Soliton-similariton fibre laser," *Nature Photonics*, vol. 4, no. 5, pp. 307–311, 2010.

[48] G. P. Agrawal, "Nonlinear fiber optics," *Academic Press*, vol. 4th, no. 7, pp. 4997–5007, 2007.

[49] S. K. Turitsyn, B. G. Bale, M. P. Fedoruk, "Dispersion-managed solitons in fibre systems and lasers," *Physics Reports*, vol. 521, no. 4, pp. 135–203, 2012.

[50] V. E. Zakharov and A. B. Shabat, "Exact theory of two-dimensional self-focusing and one-dimensional self-modulation of waves in nonlinear media," *Soviet Physics JETP*, vol. 34, no. 1, pp. 62–69, 1972.

[51] V. I. Kruglov, A. C. Peacock, J. D. Harvey and J. M. Dudley, "Self-similar propagation of parabolic pulses in normal-dispersion fiber amplifiers," *Journal of Optical society of America B*, vol. 19, no. 3, pp. 461–469, 2007.

[52] F. Ö. Ilday, J. R. Buckley, W. G. Clark, and F. W. Wise, "Self-similar evolution of parabolic pulses in a laser," *Physical Review Letters*, vol. 92, no. 21, pp. 461–469, 2004.

[53] J. M. Dudley, "Ultrafast optics: Nonlinear attraction," *Nature Photonics*, vol. 4, no. 5, pp. 272 – 274, 2010.

[54] J. M. Dudley, C. Finot, D. J. Richardson and G. Millot, "Self-similarity in ultrafast nonlinear optics," *Nature Physics*, vol. 3, no. 9, pp. 597 – 603, 2007.

[55] E. Koros and M. Orban, "Uncatalysed oscillatory chemical reactions," *Nature*, vol. 273, no. 21, pp. 371–372, 1978.

[56] A. F. Taylor and M. R. Tinsley, "Chemical self-organization: A path to patterns," *Nature Chemistry*, vol. 1, no. 5, pp. 340–341, 2009.

[57] N. Akhmediev and A. Ankiewicz, "Dissipative solitons in the complex Ginzburg-Landau and Swift-Hohenberg Equations," *Lecture Notes Physics*, vol. 661, pp. 1–17, 2005.

[58] M. Tlidi, K. Staliunas, K. Panajotov, A. G. Vladimirov, and M. G. Clerc, "Localized structures in dissipative media: from optics to plant ecology," *Philosophical Transitions of The Royal Society A*, vol. 372, pp. 1–5, 2014.

[59] J. Soto-Crespo, N. Akhmediev, and A. Ankiewicz, "Pulsating, creeping, and erupting solitons in dissipative systems," *Physical Review Letters*, vol. 85, no. 14, pp. 2937–2940, 2000.

[60] C. Phillips, A. Mayer, A. Klenner, and U. Keller, "Femtosecond mode locking based on adiabatic excitation of quadratic solitons," *Optica*, vol. 2, no. 8, pp. 667–674, 2015.

[61] S. Chouli and P. Grelu, "Soliton rains in a fiber laser: An experimental study," *Physical Review Letters A*, vol. 81, no. 6, pp. 063829 1–6, 2010.

[62] J. Soto-Crespo, N. Akhmediev, and A. C. Town, "Continuous-wave versus pulse regime in a passively mode-locked laser with a fast saturable absorber," *Journal Optics society Am B.*, vol. 19, no. 2, pp. 234–242, 2002.

[63] S. Chouli and P. Grelu, "Mechanism of intrinsic wavelength tuning and sideband asymmetry in a passively mode-locked soliton fiber ring laser," *Journal of Optical society of America B*, vol. 17, no. 1, pp. 28–32, 2000.

[64] G. Herink, B. Jalali, C. Ropers and D. R. Solli, "Resolving the build-up of femtosecond mode-locking with single-shot spectroscopy at 90MHz frame rate," *Nature Photonics*, vol. 10, no. 5, pp. 321–326, 2016.

[65] O. Gat, A. Gordon, and B. Fischer, "Solution of a statistical mechanics model for pulse formation in lasers," *Physical Review E*, vol. 70, no. 4, pp. 046108 1–10, 2004.

[66] J. Elgin, "Spectral modulation and the growth of resonant modes associated with periodically amplified solitons," *Optics Letters*, vol. 18, no. 10, pp. 787–789, 1993.

[67] N. Akhmediev and M. Karlsson, "Cherenkov radiation emitted by solitons in optical fibers," *Physical Review A*, vol. 51, no. 3, pp. 2602–2604, 1995.

[68] S. Roy, S. K. Bhadra, and G. P. Agrawal, "Dispersive waves emitted by solitons perturbed by third-order dispersion inside optical fibers," *Physical Review A*, vol. 79, pp. 023824 1–6, 2009.

[69] A. Melloni, M. Frasca, A. Garavaglia, A. Tonini, and M. Martinelli, "Direct electrostriction measurement in optical fibers," *Optics Letters*, vol. 23, no. 9, pp. 691–693, 1998.

[70] S. J. Kelly, "Characteristic sideband instability of periodically amplified average soliton," *Electronics Letters*, vol. 28, no. 8, pp. 787–789, 1992.

[71] A. N. Pilipetskii, E. A. Golovchenko, and C. R. Menyuk, "Acoustic effect in passively mode-locked fiber ring lasers," *Optics Letters*, vol. 20, no. 8, pp. 907–909, 1995.

[72] K Laland, et al., "Does evolutionary theory need a rethink?," *Nature*, vol. 514, no. 7521, pp. 161–164, 2014.

[73] N. Perunov, R. Marsland, and J. L. England, "Statistical physics of adaptation," *Physical Review X*, vol. 6, no. 2, pp. 021036 1–12, 2016.

[74] G. E. Crooks, "Entropy production fluctuation theorem and the nonequilibrium work relation for free energy differences," *Physical Review E*, vol. 60, no. 3, pp. 2721 1–6, 1999.

[75] N. Dogru, M. Ozyazici, "Relative intensity noise of mode-locked fiber grating external cavity semiconductor lasers," *Optics and Laser Technology*, vol. 35, no. 3, pp. 163–168, 2003.

[76] W. Yue, Y. Wang, C. Xiong, Z. Wang, and Q. Qiu, "Intensity noise of erbium-doped fiber laser based on full quantum theory," *Journal of Optical society of America B*, vol. 30, no. 2, pp. 275–281, 2013.

[77] A. M. Weiner, "Ultrafast optical pulse shaping a tutorial review," *Optics Communication*, vol. 284, no. 15, pp. 3669–3692, 2011.

[78] T. Oksenhendler and N. Forget, "Pulse-shaping techniques theory and experimental implementations for femtosecond pulses," *INTECH Open Access Publisher*, vol. 503, pp. 3669–3692, 2010.

[79] O. E. Martinez, "Grating and prism compressors in the case of finite beam size," *Journal of Optical society of America B*, vol. 3, no. 7, pp. 929–9342, 1986.

[80] M. Wollenhaupt, A. Prkelt, C. Tudoran, D. Liese and T. Baumert, "Quantum control and quantum control landscapes using intense shaped femtosecond pulses," *Journal of Modern Optics*, vol. 52, no. 16, pp. 2187–2195, 2006.

[81] I. Barmes, A. Ruehl, "Generation of pulse sequences with periodic spectral phase masks," *arXiv:1401.3163 [Physics.optics]*, vol. 52, pp. 1–5, 2014.

[82] J. D. McMullen, "Chirped-pulse compression in strongly dispersive media," *Applied Optics*, vol. 18, no. 5, pp. 1575–1578, 1979.

[83] E. B. Treacy, "Optical pulse compression with diffraction gratings," *IEEE Journal of Quantum Electronics*, vol. 5, no. 9, pp. 454–458, 1969.

[84] R. Fork, O. Martinez, and J. Gordon, "Negative dispersion using pairs of prisms," *Optics Letters*, vol. 9, no. 5, pp. 150–152, 1984.

[85] V. Chauhan, J. Cohen, P. Vaughan, P. Bowlan, and R. Trebino, "Distortion-free single prism/grating ultrashort laser pulse compressor," *IEEE Journal of Quantum Electronics*, vol. 46, no. 12, pp. 1726–1731, 2010.

[86] R. Szipocs, K. Ferencz, C. Spielmann, and F. Krausz, "Chirped multilayer coatings for broadband dispersion control in femtosecond lasers," *Optics Letters*, vol. 19, no. 3, pp. 201–203, 1994.

[87] A. Gomes, A. Gouveia, J. Taylor, "Optical fibre-grating pulse compressors," *Optical and Quantum Electronics*, vol. 20, no. 2, pp. 95–112, 1988.

[88] P. Colman, C. Husko, S. Combrie, I. Sagnes, C. W. Wong and A. De Rossi, "Temporal solitons and pulse compression in photonic crystal waveguides," *Nature Photonics*, vol. 4, no. 12, pp. 862–868, 2010.

[89] R. Iegorov, T. Teamir, G. Makey, and F. Ø. Ilday, "Direct control of mode-locking states of a fiber laser," *Optica*, vol. 3, no. 12, pp. 1312–1315, 2016.

[90] N. Karasawa, L. Li, A. Suguro, H. Shigekawa, R. Morita and M. Yamashita, "Optical pulse compression to 5.0 fs by use of only a spatial light modulator for phase compensation," *Journal of Optical society of America B*, vol. 18, no. 11, pp. 1742–1746, 2001.

[91] S. Huang, H. Zhou, J. Yang, J. Mcmillan, A. Matsko, M. Yu, D. Kwong, L. Maleki, and C. W. Wong, "Modelocked ultrashort pulse generation from on-chip normal dispersion microresonators," *Physical Review Letters*, vol. 114, no. 5, pp. 053901 1–5, 2015.

[92] R. Schiek, "Time-resolved switching characteristic of the nonlinear directional coupler under consideration of susceptibility dispersion," *IEEE Journal of Quantum Electronics*, vol. 27, no. 9, pp. 2150–2158, 1991.

[93] I. Gabitov, P. Lushnikov, "Nonlinearity management in a dispersion-managed system," *Optics Letters*, vol. 27, no. 2, pp. 113–115, 2002.

[94] L. Berge, V. Mezentsev, J. Rasmussen, P. Christiansen, and Yu. Gaididei, "Self-guiding light in layered nonlinear media," *Optics Letters*, vol. 25, no. 14, pp. 1037–1039, 2000.

[95] I. Towers and B. Malomed, "Stable (2+1)-dimensional solitons in a layered medium with sign-alternating kerr nonlinearity," *Journal of Optical society of America B*, vol. 19, no. 3, pp. 537–543, 2002.

[96] M. Centurion, M. Porter, P. Kevrekidis, and D. Psaltis, "Nonlinearity management in optics: Experiment, theory, and simulation," *Physical Review Letters*, vol. 97, no. 3, pp. 033903 1–4, 2006.

[97] S. Palomba, S. Zhang, Y.Park, G. Bartal, X. Yin and X. Zhang, "Optical negative refraction by four-wave mixing in thin metallic nanostructures," *Nature Materials*, vol. 11, no. 1, pp. 34–38, 2012.

[98] S. K. Turitsyn, A. E. Bednyakova, M. P. Fedoruk, S. B. Papernyi, and W. L. Clements, "Inverse four-wave mixing and self-parametric amplification in optical fibre," *Nature Photonics*, vol. 9, no. 9, pp. 608–614, 2015.

[99] A. Chong, H. Liu, B. Nie, B. G. Bale, S. Wabnitz, W. H. Renninger, M. Dantus and F. Wise, "Pulse generation without gain-bandwidth limitation in a laser with self-similar evolution," *Optics Express*, vol. 20, no. 13, pp. 14213–14220, 2012.

[100] B. G. Bale and S. Wabnitz, "Strong spectral filtering for a mode-locked similariton fiber laser," *Optics Express*, vol. 35, no. 14, pp. 2466–2468, 2010.

[101] A. Chong, J. Buckley, W. Renninger, and F. Wise, "All-normal-dispersion femtosecond fiber laser," *Optics Express*, vol. 14, no. 21, pp. 10095–10100, 2006.

[102] W. H. Renninger, A. Chong, and F. W. Wise, "Pulse shaping and evolution in normal-dispersion mode-locked fiber lasers," *IEEE Journal of Selected Topics in Quantum Electronics*, vol. 18, no. 1, pp. 389–397, 2012.

[103] P. Grelu, N. Akhmediev, "Dissipative solitons for mode-locked lasers," *Nature Photonics*, vol. 6, no. 2, pp. 84–92, 2012.

[104] A. Suda and T. Takeda, "Effects of nonlinear chirp on the self-phase modulation of ultrashort optical pulses," *Applied Sciences*, vol. 2, no. 4, pp. 549–557, 2012.

[105] D. N. Schimpf, E. Seise, J. Limpert, and A. Tünnermann, "Self-phase modulation compensated by positive dispersion in chirped-pulse systems," *Applied Science*, vol. 17, no. 7, pp. 4997–5007, 2009.

[106] F. Ö. Ilday, J. R. Buckley, F. W. Wise, and W. G. Clark, "Generation of 50-fs, 5-nJ pulses at 1.03 μm from a wave-breaking-free fiber laser," *Optics Letters*, vol. 28, no. 18, pp. 1365–1367, 2003.

[107] J. Buckley, F. Wise, F. Ö. Ilday, T. Sosnowski, "Femtosecond fiber lasers with pulse energies above 10 nj," *Optics Letters*, vol. 30, no. 14, pp. 1888–1890, 2005.

[108] W. J. Tomlinson, R. H. Stolen, and A. M. Johnson, "Optical wave breaking of pulses in nonlinear optical fibers," *Optics Letters*, vol. 10, no. 9, pp. 457–459, 1985.

[109] F. W. Wise, A. Chong, and W. H. Renninger, "High-energy femtosecond fiber lasers based on pulse propagation at normal dispersion," *Laser Photonics Review*, vol. 2, no. 2, pp. 58–73, 2008.

[110] F. C. Finot, L. Provost, P. Petropoulos and D. J. Richardsoni, "Parabolic pulse through passive nonlinear pulse reshaping in a normally dispersive two segment fiber device," *Optics Express*, vol. 15, no. 3, pp. 852–864, 2007.

[111] S. Boscolo, A. I. Latkin, and S. K. Turitsyn, "Passive nonlinear pulse shaping in normally dispersive fiber systems," *IEEE Journal of Quantum Electronics*, vol. 44, no. 10, pp. 1196–1202, 2008.

[112] W. H. Renninger, A. Chong, and F. W. Wise, "Dissipative solitons in normal-dispersion fiber lasers," *Physical Review A*, vol. 77, no. 023814, pp. 10095–10100, 2008.

[113] T. Shinbrot, F. Muzzio, "Noise to order," *Nature*, vol. 410, no. 6825, pp. 251–258, 2001.

[114] M. Cross, H. Greenside, "Pattern formation and dynamics in nonequilibrium systems," *Cambridge University Press, Cambridge UK*, vol. 410, pp. 1–500, 2009.

[115] J. P. Crutchfeld, "Between order and chaos," *Nature Physics*, vol. 8, no. 1, pp. 17–24, 2012.

[116] A. Picozzi, J. Garnier, T. Hansson, P. Suret, S. Randoux, G. Millot, D. Christodoulides, "Optical wave turbulence: towards a unified nonequilibrium thermodynamic formulation of statistical nonlinear optics," *Physics Reports*, vol. 542, no. 1, pp. 1–132, 2014.

[117] H. A. Haus, "Mode locking of lasers," *IEEE Journal of Selected Topics in Quantum Electronics*, vol. 6, no. 6, pp. 1173–1185, 2006.

[118] M. E. Fermann, I. Hartl, "Ultrafast fibre lasers," *Nature Photonics*, vol. 7, no. 11, pp. 868–874, 2013.

[119] C. Jauregui, J. Limpert, A. Tunnermann, "High-power fibre lasers," *Nature Photonics*, vol. 7, no. 11, pp. 861–867, 2013.

[120] N. Newbury, W. Swann, "Low-noise fiber-laser frequency combs," *Journal of Optical society of America B*, vol. 24, no. 8, pp. 1756–1770, 2007.

[121] C. Lee, T. Schibli, "Intrinsic power oscillations generated by the backaction of continuum on solitons and its implications on the transfer functions of a mode-locked laser," *Physical Review Letters*, vol. 112, no. 22, pp. 223903 1–4, 2014.

[122] L. Budunoğlu, C. Ulgudur, B. Oktem, F. Ö. Ilday, "Intensity noise of mode-locked fiber lasers," *Optics Letters*, vol. 34, no. 16, pp. 2516–2518, 2009.

[123] K. Croussore, D. Kilper, M. Raja, "Polarization-resolved intensity noise in erbium-ytterbium codoped fiber lasers," *Journal of Optical society of America B*, vol. 21, no. 5, pp. 865–870, 2004.

[124] E. Ronnekleiv, M. Zervas, J. Kringlebotn, "Corrections to modeling of polarization mode competition in fiber DFB lasers," *IEEE Journal of Quantum Electronics*, vol. 35, no. 7, pp. 1097–1100, 1999.

[125] T. Ralph, C. Harb, H. Bachor, "Intensity noise of injection locked laser: quantum theory using a linearized input-output method," *Physical Review A*, vol. 54, no. 5, pp. 4359–4369, 1996.

[126] K. Gurel, P. Elahi, L. Budunoglu, C. Senel, P. Paltani, F. Ö. Ilday, "Prediction of pulse-to-pulse intensity fluctuation characteristics of high power ultrafast fiber amplifiers," *Applied Physics Letters*, vol. 105, pp. 011111 1–4, 2014.

[127] T. Mulder, R. Scott, B. Kolner, "Amplitude and envelope phase noise of a mode locked laser predicted from its noise transfer function and the pump noise power spectrum," *Optics Express*, vol. 16, no. 18, pp. 14186–14191, 2008.

[128] K. Wu, J. Wong, P. Shum, S. Fu, C. Ouyang, H. Wang, E. Kelleher, A. Chernov, E. Obraztsova, J. Chen, "Noise conversion from pump to the passively mode-locked fiber lasers at 1.5 μm," *Optics Letters*, vol. 37, no. 11, pp. 1901–1903, 2012.

[129] J. Mcferran, W. Swann, B. Washburn, N. Newbury, "Suppression of pump-induced frequency noise in fiber-laser frequency combs leading to sub-radian f_{ceo} phase excursions," *Applied Physics B*, vol. 86, no. 2, pp. 219–227, 2007.

[130] C. Jarzynski, "Equalities and inequalities: Irreviewersibility and the second law of thermodynamics at the nanoscale," *Journal Physics Condensed Matter*, vol. 86, pp. 329–351, 2011.

[131] J. Jang, M. Erkintalo, S. Murdoch, S. Coen, "Ultraweak long-range interactions of solitons observed over astronomical distances," *Nature Photonics*, vol. 7, no. 8, pp. 657–663, 2013.

[132] D. Tang, L. Zhao, X. Wu, H. Zhang, "Soliton modulation instability in fiber lasers," *Physical Review A*, vol. 80, no. 2, pp. 023806 1–6, 2009.

[133] K. J. Weingarten, B. Braun, U. Keller, "*In situ* small-signal gain of solid-state lasers determined from relaxation oscillation frequency measurements," *Optics Letters*, vol. 19, no. 15, pp. 1140–1142, 1994.

[134] E. Turitsyna, S. Smirnov, S. Sugavanam, N. Tarasov, X. Shu, S. Babin, E. Podivilov, D. Churkin, G. Falkovich, S. Turitsyn, "The laminar-turbulent transition in a fibre laser," *Nature Photonics*, vol. 7, no. 10, pp. 783–786, 2013.

[135] C. Rotschild, B. Alfassi, O. Cohen, M. Segev, "Long-range interactions between optical solitons," *Nature Physics*, vol. 2, no. 11, pp. 769–774, 2006.

[136] E. Ding, E. Shlizerman, J. Kutz, "Modeling multipulsing transition in ring cavity lasers with proper orthogonal decomposition," *Physical Review A*, vol. 82, no. 2, pp. 023823 1–10, 2010.

[137] F. Li, P. Wai, J. Kutz, "Geometrical description of the onset of multipulsing in mode-locked laser cavities," *Journal of Optical society of America B*, vol. 27, no. 10, pp. 2068–207, 2010.

[138] S. De, G. Loas, A. Amili, M. Alouini, F. Bretenaker, "Theoretical and experimental analysis of intensity noise correlations in an optically pumped, dual-frequency Nd:YAG laser," *Journal of Optical society of America B*, vol. 30, no. 11, pp. 2830–2839, 2013.

[139] M. Guasoni, J. Fatome, S. Wabnitz, "Intensity noise-driven nonlinear fiber polarization scrambler," *Optics Letters*, vol. 39, no. 18, pp. 5309–5312, 2014.

[140] V. Tsatourian, S. Sergeyev, C. Mou, A. Rozhin, V. Mikhailov, B. Rabin, P. Westbrook, S. Turitsyn, "Polarisation dynamics of vector soliton molecules in mode locked fibre laser," *Scientific Reports*, vol. 3, no. 3154, pp. 1–8, 2013.

[141] D. Tang, L. Zhao, B. Zhao, A. Liu, "Mechanism of multisoliton formation and soliton energy quantization in passively mode-locked fiber lasers," *Physical Review A*, vol. 72, no. 4, pp. 043816 1–9, 2007.

[142] D. Tang, W. Man, H. Tam, and P. Drummond, "Observation of bound states of solitons in a passively mode-locked fiber soliton laser," *Physical Review A*, vol. 66, no. 3, pp. 033806 1–3, 2002.

[143] P. Grelu, and N. Akhmediev, "Stable subpicosecond soliton fiber laser passively mode-locked by gigahertz acoustic resonance in photonic crystal fiber core," *Optics Letters*, vol. 2, no. 4, pp. 339–342, 2015.

[144] M. Pang, W. He, X. Jiang, and P. Russell, "All-optical bit storage in a fibre laser by optomechanically bound states of solitons," *Nature Photonics*, vol. 10, no. 7, pp. 454–458, 2016.

[145] W. Chang, J. M. Soto-Crespo, P. Vouzas, and N. Akhmediev, "Extreme soliton pulsations in dissipative systems," *Physical Review E*, vol. 92, no. 2, pp. 1–8, 2015.

[146] J. L. England, "Dissipative adaptation in driven self-assembly," *Nature Nanotechnology*, vol. 10, no. 11, pp. 919–923, 2015.

[147] M. Erkintalo, K. Luo, J. K. Jang, S. Coen, S. G. Murdoch, "Bunching of temporal cavity solitons *via* forward Brillouin scattering," *New Journal of Physics*, vol. 17, no. 115009, pp. 657–663, 2015.

[148] G. Stegeman, M. Segev, "Optical spatial solitons and their interactions: Universality and diversity," *Science*, vol. 2, no. 5444, pp. 1518–1523, 1999.

[149] F. Leo, S. Coen, P. Kockaert, S. Gorza, P. Emplit and M. Haelterman, "Temporal cavity solitons in one-dimensional kerr media as bits in an all-optical buffer," *Nature Photonics*, vol. 4, no. 7, pp. 471–476, 2010.

[150] J. P. Gordon, "Dispersive perturbations of solitons of the nonlinear schrödinger equation," *Journal of Optical society of America B*, vol. 9, no. 1, pp. 91–97, 1992.

[151] B. Vodonos, R. Weill, A. Gordon, A. Bekker, V. Smulakovsky, O. Gat and B. Fischer, "Formation and annihilation of laser light pulse quanta in a thermodynamic-like pathway," *Physical Review Letters*, vol. 93, no. 15, pp. 153901 1–4, 2004.

[152] J. Soto-Crespo, M. Grapinet, P. Grelu, and N. Akhmediev, "Bifurcations and multiple-period soliton pulsations in a passively mode-locked fiber laser," *Physical Review E*, vol. 70, no. 6, pp. 066612 1–11, 2004.

[153] A. Hause, F. Mitschke, "Higher-order equilibria of temporal soliton molecules in dispersion-managed fibers," *Physical Review A*, vol. 88, no. 6, pp. 063843 1–10, 2013.

[154] A. Hause, H. Hartwig, M. Böhm, and F. Mitschke, "Interaction of an optical soliton with a dispersive wave," *Physical Review Letters*, vol. 97, no. 21, pp. 213902 1–4, 2005.

[155] X. Liu, "Hysteresis phenomena and multipulse formation of a dissipative system in a passively mode-locked fiber laser," *Physical Review A*, vol. 81, no. 2, pp. 023811 1–6, 023811 2010.

[156] R. Weill, A. Bekker, V. Smulakovsky, B. Fischer, and O. Gat, "Spectral sidebands and multi-pulse formation in passively mode locked lasers," *Physical Review A*, vol. 83, no. 4, pp. 043831 1–6, 043831 2011.

[157] M. E. Fermann and I. Hartl, "Ultrafast fibre lasers," *Nature Photonics*, vol. 7, no. 11, pp. 868–874, 2013.

[158] S. Wang, A. Docherty, B. S. Marks, and C. R. Menyuk, "Boundary tracking algorithms for determining the stability of mode-locked pulses," *Journal of Optical society of America B*, vol. 31, no. 11, pp. 2914–2930, 2014.

[159] B. G. Bale, K. Kieu, J. N. Kutz, and F. Wise, "Transition dynamics for multi-pulsing in mode-locked lasers," *Optics Express*, vol. 17, no. 25, pp. 23137–23146, 2009.

[160] J. S. Feehan, F. Ö. Ilday, W. S. Brocklesby, and J. H. V. Price, "Simulations and experiments showing the origin of multi-wavelength mode-locking in femtosecond, yb-fiber lasers," *Journal of Optical society of America B*, vol. 33, no. 18, pp. 1668–1676, 2016.

[161] A. Gordon and B. Fischer, "Phase transition theory of many-mode ordering and pulse formation in lasers," *Physical Review Letters*, vol. 89, no. 10, pp. 103901 1–4, 2002.

[162] K. Tamura, E. P. Ippen, H. A. Haus, and L. E. Nelson, "77-fs pulse genration from a stretched-pulse mode-locked all-fiber ring laser," *Optics Letters*, vol. 18, no. 13, pp. 1080–1082, 1993.

[163] M. E. Fermann, "Single-mode excitation of multimode fibers with ultrashort pulses," *Optics Letters*, vol. 23, no. 1, pp. 52–54, 1998.

[164] M. Baumgartl, C. Lecaplain, A. Hideur, J. Limpert, and A. Tünnermann, "66 W average power from a microjoule-class sub-100 fs fiber oscillator," *Optics Letters*, vol. 37, no. 10, pp. 1640–1642, 2012.

[165] C. R. Phillips, A. S. Mayer, A. Klenner, and U. Keller, "Femtosecond mode locking based on adiabatic excitation of quadratic solitons," *Optica*, vol. 2, no. 8, pp. 667–674, 2015.

[166] W. Renninger, A. Chong, and F. Wise, "Dissipative solitons in normal-dispersion fiber lasers," *Physical Review A*, vol. 77, no. 2, pp. 023814 1–4, 2008.

[167] K. L. Schehrer, E. S. Fry, and G. T. Bennett, "Colliding pulse mode-locked dye laser stabilization using an intracavity spectral filter," *Applied Optics*, vol. 27, no. 10, pp. 1908–1910, 1988.

[168] S. Boscolo, C. Finot, H. Karakuzu, and P. Petropoulos, "Pulse shaping in mode-locked fiber lasers by in-cavity spectral filter," *Optics Letters*, vol. 39, no. 3, pp. 438–441, 2014.

[169] J. Peng, S. Boscolo, "Filter-based dispersion-managed versatile ultrafast fibre laser," *Scientific Reports*, vol. 6, no. 25995, 2016.

[170] T. C. Weinacht, J. Ahn and P. H. Bucksbaum, "Controlling the shape of a quantum wavefunction," *Nature*, vol. 397, no. 6716, pp. 233–235, 1999.

[171] M. Aeschlimann, M. Bauer, D. Bayer, T. Brixner, F. Garcia de Abajo, W. Pfeiffer, M. Rohmer, C. Spindler and F. Steeb, "Adaptive subwavelength control of nano-optical fields," *Nature*, vol. 446, no. 7133, pp. 301–304, 2007.

[172] N. Forget, "Ultrashort optical pulses shaping up," *Nature Photonics*, vol. 4, no. 3, pp. 154–155, 2010.

[173] L. G. Wright, Z. Liu, D. A. Nolan, M.-J. Li, D. N. Christodoulides, and F. W. Wise, "Self-organized instability in graded-index multimode fibres," *Nature Photonics*, vol. 10, no. 12, pp. 771–776, 2016.

[174] D. Yelin, D. Meshulach, and Y. Silberberg, "Adaptive femtosecond pulse compression," *Optics Letters*, vol. 22, no. 23, pp. 1793–1795, 1997.

[175] A. M. Weiner, "Femtosecond pulse shaping using spatial light modulators," *Review of Scientific Instruments*, vol. 71, no. 5, pp. 1929–1960, 2000.

[176] H. A. Haus, "Mode-locking of lasers," *IEEE Journal of Selected Topics in Quantum Electronics*, vol. 71, pp. 1173–1185, 2000.

[177] U. Andral, R. S. Fodil, F. Amrani, F. Billard, E. Hertz, and P. Grelu, "Fiber laser mode locked through an evolutionary algorithm," *Optica*, vol. 2, no. 4, pp. 275–278, 2015.

[178] J. L. England, "Dissipative adaptation in driven self-assembly," *Nature Nanotechnology*, vol. 10, no. 11, pp. 919–923, 2015.

[179] A. Ashkin, "Acceleration and trapping of particles by radiation pressure," *Physical Review Letters*, vol. 24, no. 4, pp. 156–159, 1969.

[180] L. Thevenaz, "Slow and fast light in optical fibres," *Nature Photonics*, vol. 2, no. 8, pp. 474–481, 2006.

[181] I. Barmes, S. Witte and K. S. Eikema, "Spatial and spectral coherent control with frequency combs," *Nature Photonics*, vol. 7, no. 1, pp. 38–42, 2013.

[182] M. Baldo and V. Stojanovic, "Optical switching: Excitonic interconnects," *Nature Photonics*, vol. 3, no. 10, pp. 558–560, 2009.

[183] T. Volz, A. Reinhard, M. Winger, A. Badolato, K. J. Hennessy, E. L. Hu and A. Imamoglu, "Ultrafast all-optical switching by single photons," *Nature Photonics*, vol. 6, no. 9, pp. 605–609, 2012.

[184] L. V. Hau, S. E. Harris, Z. Dutton, C. H. Behroozi, "Light speed reduction to 17 metres per second in an ultracold atomic gas," *Nature Photonics*, vol. 397, no. 6720, pp. 594–598, 1999.

[185] J. T. Mok, C. M. Sterke, I. C. Littler and B. J. Eggleton, "Dispersionless slow light using gap solitons," *Nature Physics*, vol. 2, no. 11, pp. 775–780, 2006.

[186] H. Hevekerl, J. Tornmalm and J. Widengren, "Fluorescence-based characterization of non-fluorescent transient states of tryptophan prospects for protein conformation and interaction studies," *Scientific Reports*, vol. 6, no. 35052, pp. 1–12, 2016.

[187] G. Wrigge, I. Gerhardt, J. Hwang, G. Zumofen, and V. Sandoghdar, "Efficient coupling of photons to a single molecule and the observation of its resonance fluorescence," *Nature Physics*, vol. 4, no. 1, pp. 60–66, 2008.

[188] C. Reimer, M. Kues, P. Roztocki, B. Wetzel, F. Grazioso, B. E. Little, S. T. Chu, T. Johnston, Y. Bromberg, L. Caspani, D. J. Moss, and R. Morandotti, "Generation of multiphoton entangled quantum states by means of integrated frequency combs," *Science*, vol. 351, no. 6278, pp. 1176–1180, 2016.

[189] A. Assion, T. Baumert, M. Bergt, T. Brixner, B. Kiefer, V. Seyfried, M. Strehle, and G. Gerber, "Control of chemical reactions by feedback-optimized phase-shaped femtosecond laser pulses," *Science*, vol. 282, no. 5390, pp. 919–922, 1998.

[190] S. Alebrand, A. Hassdenteufel, D. Steil, M. Bader, A. Fischer, M. Cinchetti, and M. Aeschlimann, "All-optical magnetization switching using phase shaped ultrashort laser pulses," *Physica Status Solidi A*, vol. 209, no. 12, pp. 2589–2595, 2012.

[191] R. Weill, A. Bekker, V. Smulakovsky, B. Fischer, and O. Gat, "Noise-mediated Casimir-like pulse interaction mechanism in lasers," *Optica*, vol. 3, no. 2, pp. 189–192, 2016.

[192] P. Sartori, L. Granger, C. Lee, Horowitz, "Thermodynamic costs of information processing in sensory adaptation," *arXiv:1404.1027v2 [cond-mat.stat-mech.]*, vol. v2, pp. 1–17, 2014.

[193] G. Lan, P. Sartori, S. Neumann, V. Sourjik, and Y. Tu, "The energy-speed accuracy trade-off in sensory adaptation," *Nature Physics*, vol. 8, no. 5, pp. 422–428, 2012.

[194] A. E. Allahverdyan, Q. A. Wang, "Adaptive machine and its thermodynamic costs," *Physical Review E*, vol. 87, no. 3, pp. 032139 1–14, 2013.

[195] U. Seifert, "Entropy production along a stochastic trajectory and an integral fluctuation theorem," *Physical Review Letters*, vol. 95, no. 4, pp. 040602 1–4, 2005.

[196] Editorial, "Driven by theory," *Nat. Nano.*, vol. 10, no. 11, pp. 909–909, 2015.

[197] W. He, M. Pang, and P. Russell, "Wideband-tunable soliton fiber laser mode-locked at 1.88 Ghz by optoacoustic interactions in solid-core PCF," *Optics Express*, vol. 23, no. 19, pp. 24945–24954, 2015.

[198] S. M. Kelly, "Characteristic sideband instability of periodically amplified average soliton," *Electronics Letters*, vol. 8, no. 8, pp. 806–808, 1992.

[199] A. Kobyakov, M. Sauer, and D. Chowdhury, "Stimulated Brillouin scattering in optical fibers," *Advances in Optics and Photonics*, vol. 2, no. 1, pp. 1–59, 2010.

Appendix A

Supplementary information for chapter 6

A.1 Additional processes that can occur at a critical point

A.1.1 Vibrating pulse

Interaction of solitons can create a harmonic oscillator like potential which form oscillating temporal separation between pulses in a bunch as shown in Fig. B.1. The pulses vibrate in a limited temporal position. The RIN of this system increases by a factor of four when the pulses get closer than when they were at a maximum separation.

Oscilloscope trace of the spatio-temporal dynamics of two soliton states is shown on Fig B.1. It shows the intensity distribution of pulse power along the cavity taken in 35 s with 12 Ghz photodiode and a 2.5 GHz oscilloscope. The laser was operating at its third harmonics with a repetition rate of 148.4 MHz. There are three bunch of pulses per cavity round trip. In the first dynamics the

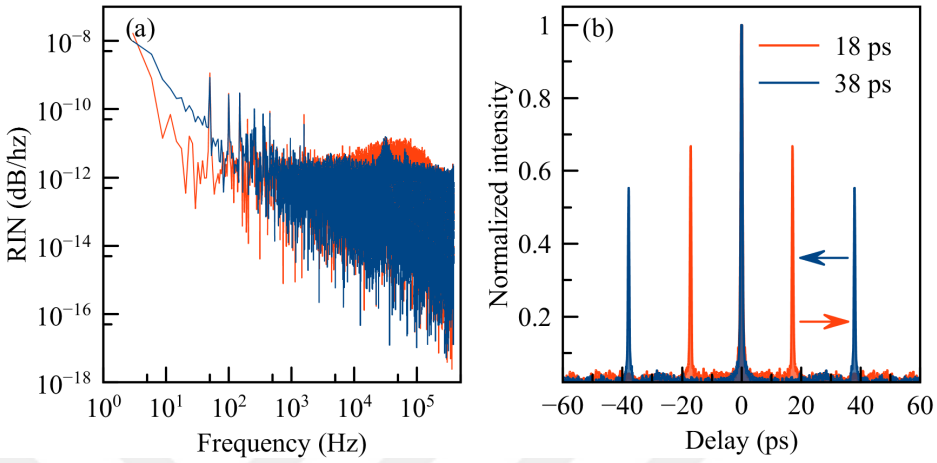

Figure A.1: Vibrating pulse: pulse vibration like harmonic oscillator can happen at critical points.

three bunches were at a fixed position relative to each other. As the pump power is increased these bunches could not maintain their relative temporal position due to interaction. As the intensity of side bands gets stronger the pulses in the cavity experience alternating effective attractive and repulsive forces between each other as can be seen from Fig. B.1(b) and corresponding long range interaction is indicated on Fig. B.2. Such jittering of the temporal position can be fundamentally limiting quality of performance especially in telecommunication and information processing application. Unlike the results of ref. [197], the RIN is associated with the intensity of side band rather than the operating harmonics of the repetition rate.

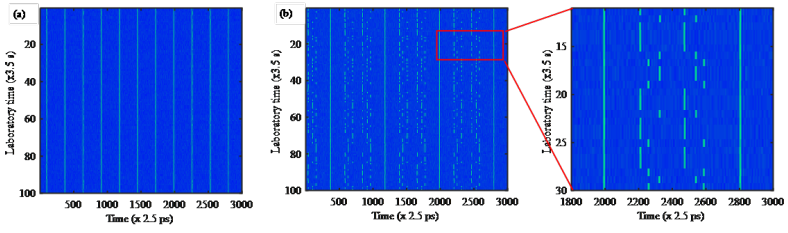

Figure A.2: Spatiotemporal dynamics of the two states indicated in Fig. B.1 (red and blue), which indicates that the role of stronger dispersive wave on the long and short range stability of the pulses in the cavity.

A.1.2 Dynamic variation of pulse-to-pulse separation and energy exchange between bound pulses

Formation of solitons with varying temporal separation as shown on Fig. B.3 is another interaction induced by the force created due to intracavity interactions [147] that causes particular state transition, which is from state (2) to state (3) on Fig. 6.3(a). As the pump power increases state (2) was stabilized at around pump power of 425 mW. At pump power 430 mW interaction characterized by none-symmetrical autocorrelation peaks happened. The asymmetry in the AC signal is due to temporal shape difference of the soliton cluster at time t and another time t + τ. The soliton and dispersive wave interaction causes modulation on the signal power with modulation frequency shown on the noise spectrum in Fig. B.3(d). Eventhough this was explained in terms of interfering forward signal and backward scattered brillouin stocks waves in [153, 198, 199], The presence of isolator in the oscillator and the fact that every solitonic state showed similar behaviour further supported the mechanism in chapter 6. Further increase of the pump power to 432.5 mW intensifies the interaction and increases the noise level of the oscillator as well. At 435 mW the noisy three soliton state was transformed in to 7 relatively stable soliton state. Four more solitons are created in the process.

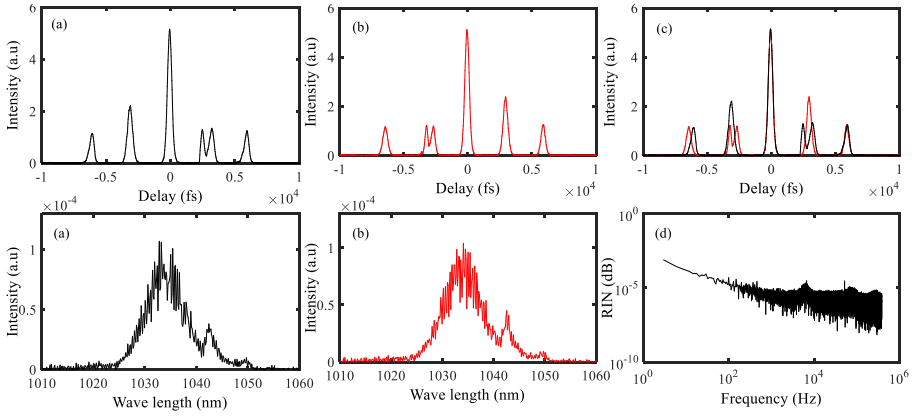

Figure A.3: Autocorrelation, optical spectrum and corresponding RIN spectrum of a soliton state with dynamically varying temporal separation which is the transition mechanism between state (2) and state (3) on Fig 6.3(a).

Fig. B.4 shows another interaction in DM soliton system. At 370 mW a resonance peak at a frequency of 110 KHz on the RIN spectrum appears due to the interaction of very close pulses on the last autocorrelation peak. Points on this peak (inside the red ellipse on Fig. A.4(a)) were moving very fast over a very small range. This motion of the indicated autocorrelation points was not due to averaging of points in measurement of our instrumentation since the motion was very clearly visible relative to other points on the autocorrelation. This interaction increases the integrated RIN by factor of 4 from average integrated RIN of a stable soliton state. When the pump power was increased to 375 mW the system start to oscillate between Fig. A.4(a) and B.4(b). There appears oscillation between the separation of second and third peaks indicated on the onset of Fig. A.4(c). These autocorrelation peaks (2nd and 3rd) start to attract and repel each other. Another resonance peak at 131 KHz appears when the two peaks are close to each other and it disappears immediately after this point go back to the largest separation point. We claim that this resonance peak is due to soliton-soliton interaction. Soliton and soliton collision can generate dispersive waves and the back action of a generated dispersive wave on the solitons electric field creates power oscillation [121] which increases the integrated RIN of the whole state by more than 6.5 fold. The oscillation of this peaks increases till pump power reaches 385 mW. Further increments of pump power merges the 2nd and 3rd autocorrelation peaks and the system stabilized in to a state indicated by Fig. A.4(d). No resonance appears on the RIN spectrum and the integrated RIN decreased by factor of 8 (value for non-interacting states).

Figure A.5 shows numerical simulation result of dynamics of a single soliton cavity solution changed to a breather solution with bifurcation period of two (red on Fig. A.5(b)) and then the bifurcation period increased to 24 (blue on Fig. A.5(b)) before the soliton state is transformed in to new one as a result of increase in nonlinearity on the gain segment. The new soliton state will follow similar dynamics with increasing nonlinearity or pump power. When the number of solitons in the state is more than two, Pulse interaction will create additional complexity to the cavity stability dynamics, which is similar to what was discussed in chapter 6.

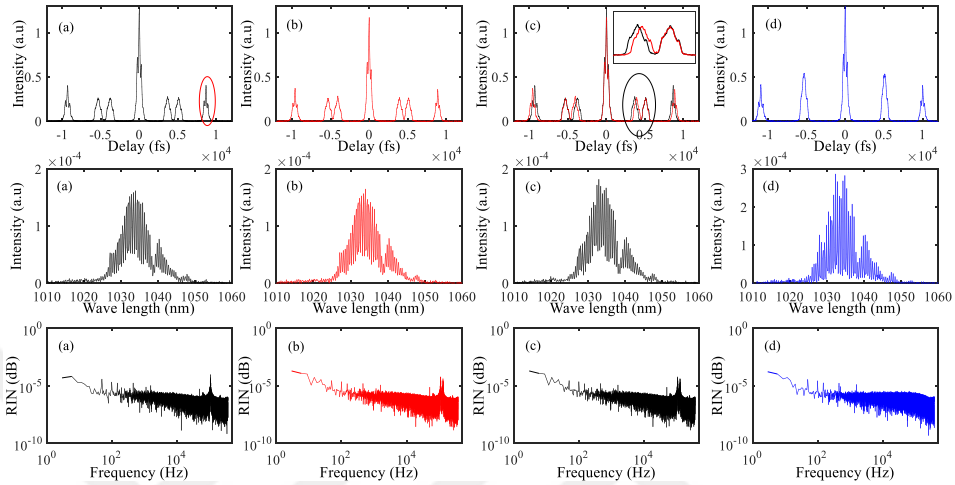

Figure A.4: Autocorrelation, optical spectrum and corresponding RIN spectrum of a soliton state with energy exchange between very close solitons and with oscillating temporal separations inside a cluster.

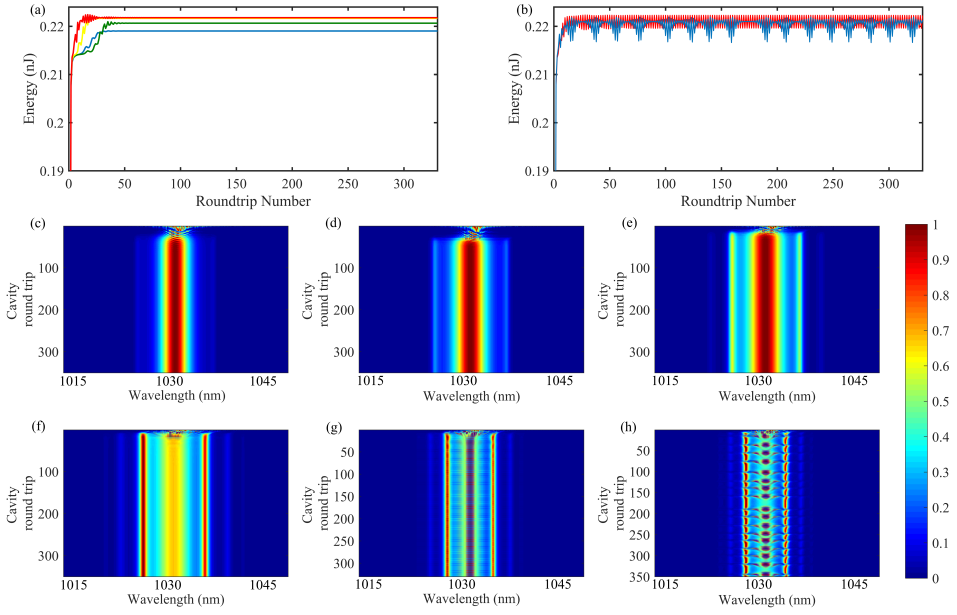

Figure A.5: Characteristics of pulse energy evolution per cavity round trip as nonlinearity of a gain cavity segment is scanned (a and b). Corresponding optical spectrum evolution (c-f for (a) and (g) for (b red) and (h) for (b blue)) of a single soliton.

A.2 Bound soliton states

The sum of two soliton pulses with temporal separation of τ and relative phase difference of θ can be mathematically described in time domain as

$$f(t) = a(t) + a(t-\tau) \tag{A.1}$$

In frequency domain, it will be

$$f(\nu) = a(\nu) + a(\nu)\exp(i(2\pi\nu\tau))\exp(i\theta) \tag{A.2}$$

$$f(\nu) = a(\nu)[1 + \exp(i(2\pi\nu\tau - \theta)] \tag{A.3}$$

$$f(\nu) = 2a(\nu)\cos[\pi\nu\tau - \frac{\theta}{2}]\exp(\pi\nu\tau - \frac{\theta}{2}) \tag{A.4}$$

Thus, the spectral intensity will be proportional to

$$s(\nu) \propto 4 \mid a(\nu) \mid^2 \cos^2[\pi\nu\tau - \frac{\theta}{2}] \tag{A.5}$$

The same approach can be extended to three pulses

$$f(t) = a(t) + a(t-\tau_1) + a(t-\tau_2) \tag{A.6}$$

In frequency domain

$$f(\nu) = a(\nu) + a(\nu)\exp(i(2\pi\nu\tau_1))\exp(i\theta_1) + a(\nu)\exp(i(2\pi\nu\tau_2))\exp(i\theta_2) \tag{A.7}$$

$$f(\nu) = a(\nu) + a(\nu)\exp(i(2\pi\nu\tau_1))\exp(i\theta_1) + a(\nu)\exp(i(2\pi\nu\tau_2))\exp(i\theta_2) \tag{A.8}$$

Considering the same pulse separation one can simplify the above equation to

$$f(\nu) = a(\nu)\exp(i(2\pi\nu\tau_1 - \frac{\theta_2}{2}))[2\cos(2\pi\nu\tau_1 - \frac{\theta_2}{2}) + \exp(i(\theta_1 - \frac{\theta_2}{2}))] \tag{A.9}$$

The spectral intensity will be

$$s(\nu) \propto \mid a(\nu) \mid^2 [4\cos^2(2\pi\nu\tau_1 - \frac{\theta_2}{2}) + 4\cos(2\pi\nu\tau_1 - \frac{\theta_2}{2}) * \cos(\theta_1 - \frac{\theta_2}{2})] \tag{A.10}$$

The cosine forms of eqn. B.5 and B.10 produces modulation on the spectral amplitude (| $a(\upsilon)$ |) The following figures show autocorrelation signal and optical spectrum simulation result of multi pulses with different intensity, temporal separation, relative intensity and relative phase.

The effect of a relative phase difference between two soliton pulses is evident on the symmetry of peaks (see the central part) on the optical spectrum (compare Fig. A.6(a) and Fig. A.6(b) or Fig. A.6(c) and Fig. A.6(d)). The relative intensity difference between the two pulses have effect on the modulation depth of the spectrum. If a state jumps from a soliton state indicated by Fig. A.6(a) to Fig. A.6(c) then energy exchange is taking place and a finger print on the optical spectrum will be evident. This can be seen on central part of the optical spectrum. There will be further evidence on the intensity of the autocorrelation peaks if the energy exchange is not a total energy exchange.

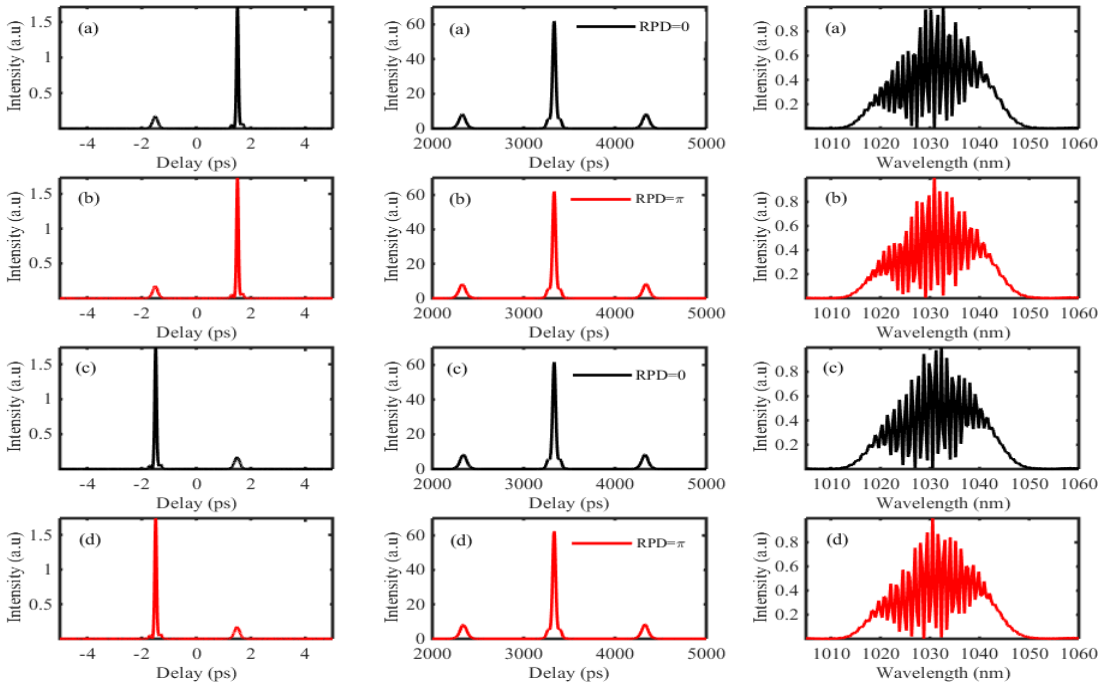

Figure A.6: Effect of relative phase: Real time temporal profile, autocorrelation and optical spectrum of two soliton pulses with separation of and relative phase difference indicated on the legends.

Relative phase difference is evident on the symmetry of peaks on the spectrum

((compare Fig. A.7(a) and Fig. A.7(b), compare Fig. A.7(d) and Fig. A.7(d) or black and red graphs in general). No information about relative phase difference can be found on the autocorrelation information. Variation in intensity creates shape and modulation depth defence on optical spectrum. Energy exchange between peaks will create a shape change both in autocorrelation and optical spectrum (compare Fig. A.8(a) and Fig. A.8(c) for energy exchange between the first and third soliton pulses). Hopping of phase is evident on the symmetry of the spectrum. If the symmetry of optical spectrum is progressively changing, it implies that the relative phase between pulses is changing. The above simulation results support the forwarded experimental result explanations in chapter 6.

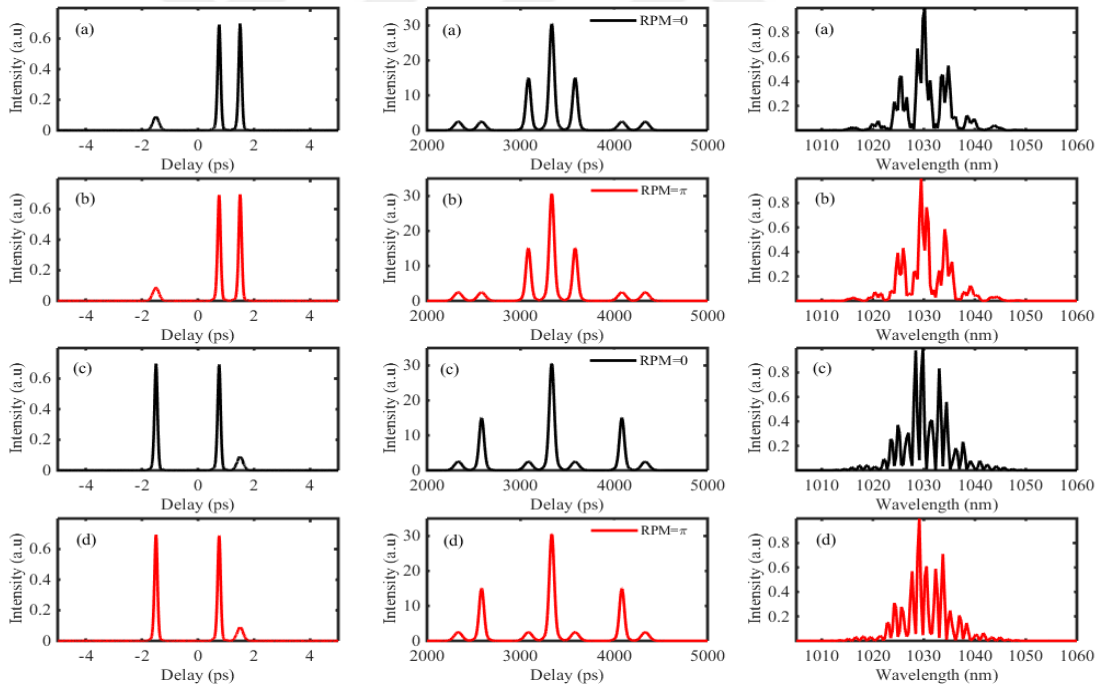

Figure A.7: Effect of relative intensity on the shape of AC signal: Real time temporal profile, autocorrelation and optical spectrum of three soliton pulses with separation of 0.750 ps and 2.25 ps and relative phase difference indicated on the legends.

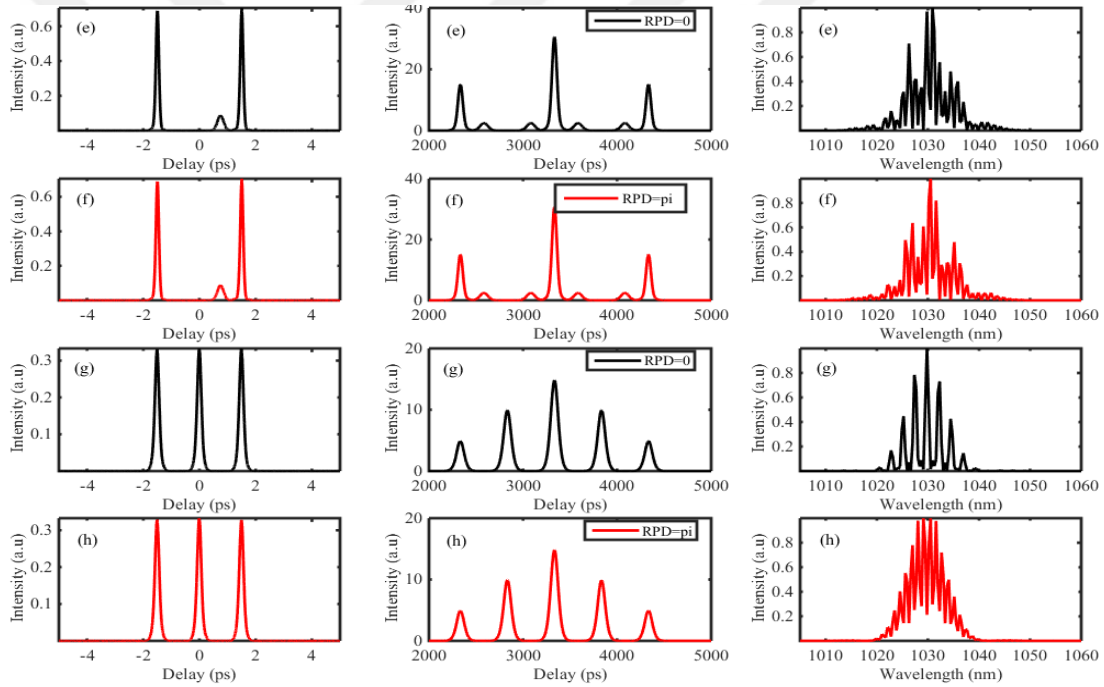

Figure A.8: Real time temporal profile, autocorrelation and optical spectrum of three soliton pulses with separation of 0.750 ps and 2.25 ps and relative phase difference indicated on the legends.